MIT Open Access Articles

Search for Higgs boson pairs decaying to WW*WW*, WW*##, and #### in proton-proton collisions at √# = 13 TeV

Search for Higgs boson pairs decaying to WW*WW*, WW*ττ, and ττττ in proton-proton collisions at $\sqrt{s} = 13$ TeV

The CMS collaboration

E-mail: cms-publication-committee-chair@cern.ch

ABSTRACT: The results of a search for Higgs boson pair (HH) production in the WW*WW*, WW*ττ, and ττττ decay modes are presented. The search uses $138\,\mathrm{fb}^{-1}$ of proton-proton collision data recorded by the CMS experiment at the LHC at a center-of-mass energy of 13 TeV from 2016 to 2018. Analyzed events contain two, three, or four reconstructed leptons, including electrons, muons, and hadronically decaying tau leptons. No evidence for a signal is found in the data. Upper limits are set on the cross section for nonresonant HH production, as well as resonant production in which a new heavy particle decays to a pair of Higgs bosons. For nonresonant production, the observed (expected) upper limit on the cross section at 95% confidence level (CL) is 21.3 (19.4) times the standard model (SM) prediction. The observed (expected) ratio of the trilinear Higgs boson self-coupling to its value in the SM is constrained to be within the interval −6.9 to 11.1 (−6.9 to 11.7) at 95% CL, and limits are set on a variety of new-physics models using an effective field theory approach. The observed (expected) limits on the cross section for resonant HH production range from 0.18 to 0.90 (0.08 to 1.06) pb at 95% CL for new heavy-particle masses in the range 250–1000 GeV.

Contents

1 Introduction

Since the discovery of the Higgs (H) boson [1–3], many of its properties have already been measured with high precision [4–6]. One important property that remains largely unknown is the H boson self-coupling. A precise measurement of this coupling is necessary to determine the shape of the Higgs potential, and thus verify that the mechanism breaking the electroweak gauge symmetry is indeed the Higgs mechanism [7–12] of the standard model (SM) [13–15]. The SM predicts the existence of both trilinear and quartic H boson self-couplings. Due to the very low predicted cross section for triple H boson production, the SM quartic self-coupling will not be experimentally accessible at the CERN LHC, even with the full integrated luminosity of $3000\,\mathrm{fb}^{-1}$ scheduled to be delivered after the high-luminosity LHC upgrade [16, 17]. The strength of the trilinear self-coupling, however, can be determined using measurements of H boson pair (HH) production.

In the SM, most HH pairs are produced in two types of processes. The Feynman diagrams for the dominant "gluon fusion" (ggHH) process at leading order (LO) in perturbative quantum chromodynamics (QCD) are shown in figure 1. The left "triangle" diagram
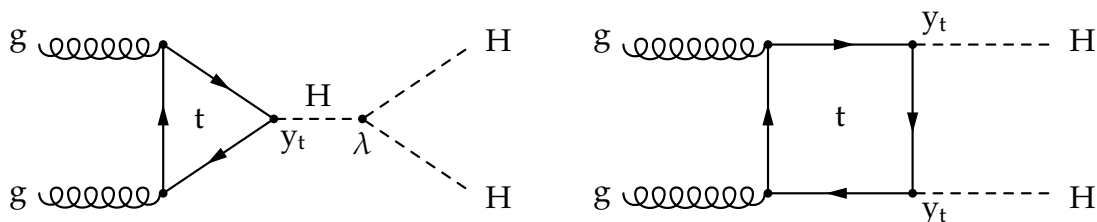
Figure 1. Leading order Feynman diagrams for SM nonresonant HH production via gluon fusion, including the "triangle" diagram (left) and the "box" diagram (right).

amplitude varies proportionally to the H boson self-coupling (λ) and the Yukawa coupling of the top quark (y_t), while the right "box" diagram amplitude is insensitive to λ and varies as y_t^2. The triangle and box diagrams interfere destructively, so the ggHH cross section exhibits a strong dependence on both λ and y_t. The ggHH cross section in the SM has been computed to be $31.1^{+2.1}_{-7.2}$ fb at next-to-next-to-LO (NNLO) accuracy in QCD using the FT_{approx} scheme, in which the true top quark mass is used for the real radiation matrix elements, while the virtual part is computed using an infinite top quark mass [18]. The predicted SM cross section for the subdominant "vector boson fusion" (qqHH) process is 1.73 ± 0.04 fb at next-to-NNLO accuracy in QCD [19].

Deviations of the coupling strength modifiers $\kappa_\lambda = \lambda/\lambda^{SM}$ and $\kappa_t = y_t/y_t^{SM}$ from unity would affect both the rate of HH production and kinematic distributions of the HH signal. The HH invariant mass (m_{HH}) is particularly sensitive to changes in κ_λ and κ_t, as these couplings affect the triangle and box diagram amplitudes differently. Because SM ggHH and qqHH production do not include a heavy resonant particle, and typically result in a broad m_{HH} distribution, they are referred to as "nonresonant". Changes in κ_λ and κ_t also influence the rate of single Higgs boson production and the Higgs boson decay branching fractions [20, 21].

The presence of undiscovered particles or interactions, predicted by a variety of theoretical models beyond the SM, may alter the HH production rate as well as observable kinematic distributions. Such particles could give rise to loop diagrams similar to the one shown on the left of figure 1. These diagrams may significantly enhance the HH production rate, as they occur at the same loop level as HH production in the SM. Since no particles beyond those predicted by the SM have been observed so far, their mass may be at the TeV scale or higher, well above the scale of electroweak symmetry breaking. Loop contributions of such heavy particles can be approximated as contact interactions with the H boson using an effective field theory (EFT) approach [22, 23]. Following ref. [24], the contact interactions relevant for HH production are parametrized by the couplings c_g, c_{2g}, and c_2, referring to the interactions between two gluons and one H boson, two gluons and two H bosons, and two top quarks and two H bosons, respectively. The corresponding Feynman diagrams for ggHH production are shown in figure 2. The LO diagrams for qqHH production contain no gluons or top quarks, so the impacts of c_g, c_{2g}, and c_2 are only considered in the ggHH signal in this publication.
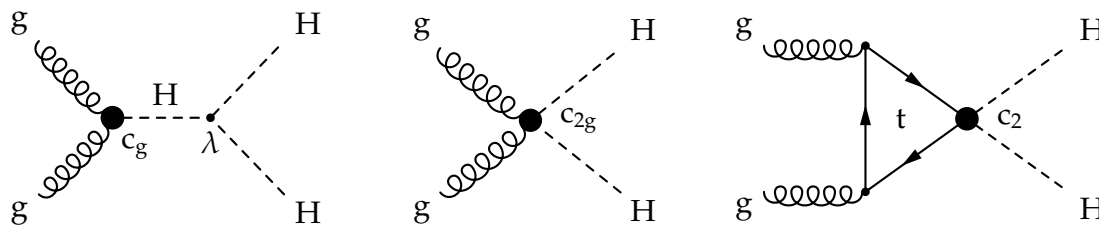
Figure 2. Leading order Feynman diagrams for nonresonant HH production via gluon fusion in an EFT approach, where loop-mediated contact interactions between (left) two gluons and one H boson, (middle) two gluons and two H bosons, and (right) two top quarks and two H bosons are parametrized by three effective couplings: c_g, c_{2g}, and c_2.
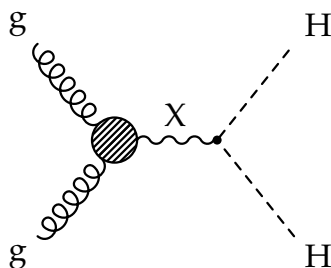

Figure 3. Leading order Feynman diagram for resonant HH production.

An excess of HH signal events may also result from decays of new heavy particles, denoted as X, into pairs of H bosons. Various theoretical models of new physics postulate such decays, in particular two-Higgs-doublet models [25, 26], composite-Higgs models [27, 28], Higgs portal models [29, 30], and models inspired by warped extra dimensions [31]. In the last class of models, the new heavy particles may have spin 0 ("radions") or spin 2 ("gravitons") [32]. In this paper, the resulting "resonant" HH production is sought for mass values of X from 250 to 1000 GeV, and the width of X is assumed to be negligible compared to the experimental resolution in m_{HH}. This would create a peak in the reconstructed m_{HH} distribution around the mass m_X of the resonance. The Feynman diagram for this process is shown in figure 3. For resonance masses above 1 TeV the strongest constraints are given by searches for HH production targeting H boson decays to bottom quarks [33–35], as the selection and reconstruction efficiency for hadronic decays increases, in particular in the trigger, and relevant backgrounds decrease with energy. For leptonic decay modes, the selection and reconstruction efficiency in general is high and as such do not increase notably for high masses above 1 TeV.

Phenomenological studies of the prospects for discovering HH signal in the WW^*WW^* decay mode are documented in refs. [36–40], where the symbol $*$ denotes virtual particles. The ATLAS Collaboration published results of a search for nonresonant and resonant HH pairs decaying to WW^*WW^* based on $36\,\mathrm{fb}^{-1}$ of proton-proton (pp) collision data recorded at $\sqrt{s} = 13\,\mathrm{TeV}$ [41], placing an upper limit of 160 times the SM predicted cross section for nonresonant HH production at 95% confidence level (CL). Searches for HH production in pp collisions at $\sqrt{s} = 7$, 8, and 13 TeV have previously been performed by

the CMS and ATLAS Collaborations in the decay modes bb$\gamma\gamma$ [42, 43], bbbb [33, 44–47], bb$\tau\tau$ [35, 48, 49], bbWW* [34, 50–52], and WW$^*\gamma\gamma$ [53]. Limits on HH production obtained from a combination of some of these analyses have been published by the CMS and ATLAS Collaborations [54, 55].

Searches targeting the bb$\tau\tau$ [48], bbbb [45, 46], and bb$\gamma\gamma$ [42] final states in CMS, and bb$\tau\tau$ [35] and bb$\gamma\gamma$ [43] in ATLAS, provide the strongest constraints on nonresonant HH production to date, with observed (expected) 95% CL upper limits ranging from 3.3 to 9.9 (3.9 to 7.8) times the SM predicted cross section. The corresponding lower bounds on κ_λ vary from -1.5 to -3.3 (-2.4 to -5.0 expected), with upper bounds between 6.7 and 9.4 (7.7 to 12.0 expected). The ATLAS bb$\gamma\gamma$ analysis places a 95% CL upper limit of 0.64 pb on resonant HH production with a mass around 250 GeV (where 0.39 pb was expected) [43], while the ATLAS resonant bbbb search constrains higher mass hypotheses most strongly, with observed and expected limits around 0.01 pb at 1 TeV [33]. The ATLAS bb$\tau\tau$ performs best for many mass points in between [35]. The only published HH search using an EFT approach comes from CMS in the bb$\gamma\gamma$ final state, with 95% CL upper limits on the HH production cross section ranging from 0.1 to 0.6 pb, depending on the EFT scenario [42].

This paper presents the first search for H boson pairs decaying to WW*WW*, WW$^*\tau\tau$, and $\tau\tau\tau\tau$. Both nonresonant and resonant HH production in final states with multiple reconstructed leptons, i.e., electrons (e), muons (μ), or hadronically decaying tau leptons (τ_h) are covered. The search is based on LHC pp collision data recorded by the CMS experiment at a center-of-mass energy of 13 TeV, corresponding to an integrated luminosity of 138 fb^{-1}. Signal candidate events are subdivided into seven mutually exclusive "search categories" based on ℓ (e, μ) and τ_h multiplicity: two same-sign ℓ with fewer than two τ_h (2ℓss), three ℓ with no τ_h (3ℓ), four ℓ (4ℓ), three ℓ with one additional τ_h (3$\ell+1\tau_h$), two ℓ with two τ_h (2$\ell+2\tau_h$), one ℓ with three τ_h (1$\ell+3\tau_h$), or four τ_h with no ℓ (4τ_h). In final states with a total of four ℓ and τ_h, the charge sum of all ℓ and τ_h candidates is required to be zero. The seven search categories target HH signal events in which the H boson pair decays into WW*WW*, WW$^*\tau\tau$, or $\tau\tau\tau\tau$. Multivariate analysis (MVA) methods are used to distinguish the HH signal from backgrounds.

The paper is structured as follows. A brief overview of the CMS detector is given in section 2. Section 3 lists the data sets and simulation samples used. The reconstruction of e, μ, τ_h, and jets, along with various kinematic observables, is detailed in section 4. This is followed by a description, in section 5, of the event selection criteria defining the seven search categories. The multivariate methods used to distinguish the HH signal from backgrounds are detailed in section 6. The estimation of these backgrounds is described in section 7, followed by an outline of the relevant systematic uncertainties in section 8. The statistical procedure used to extract limits on the HH production rate in the SM, as well as constraints on SM coupling strengths, EFT benchmark scenarios, and resonant HH production rates are presented in section 9. The paper concludes with a summary in section 10.

2 The CMS detector

The central feature of the CMS apparatus is a superconducting solenoid of 6 m internal diameter, providing a magnetic field of 3.8 T. Within the solenoid volume are a silicon pixel and strip tracker, a lead tungstate crystal electromagnetic calorimeter (ECAL), and a brass and scintillator hadron calorimeter (HCAL), each composed of one barrel and two endcap sections. The silicon tracker measures charged particles within the pseudorapidity range $|\eta| < 2.5$ for data recorded in 2016, and within the range $|\eta| < 3.0$ for data recorded in 2017 and 2018. The ECAL is a fine-grained hermetic calorimeter with quasi-projective geometry, and is divided into a barrel region covering $|\eta| < 1.5$, and two endcaps that extend to $|\eta| = 3.0$. The HCAL barrel and endcaps similarly cover the region $|\eta| < 3.0$. Forward calorimeters extend beyond these endcaps to $|\eta| = 5.0$. Muons are detected within the range $|\eta| < 2.4$ by gas-ionization detectors embedded in the steel flux-return yoke outside the solenoid. Collision events of interest are selected using a two-tiered trigger system. The level-1 trigger, composed of custom hardware processors, uses information from the calorimeters and muon detectors to select less than 100 kHz of events from a 40 MHz base event rate, within a fixed latency of 4 μs [56]. The second tier, known as the high-level trigger, is a processor farm which runs a version of the full event reconstruction software optimized for fast processing, and reduces the event rate to around 1 kHz before data storage [57]. A more detailed description of the CMS detector, together with a definition of the coordinate system used and the most relevant kinematic variables, can be found in ref. [58].

3 Data samples and Monte Carlo simulation

The analyzed pp collision data correspond to an integrated luminosity of 138 fb^{-1}, collected by the CMS detector over three years: 36 fb^{-1} in 2016, 42 fb^{-1} in 2017, and 60 fb^{-1} in 2018 [59–61]. This analysis uses triggers requiring one or more reconstructed e, μ, or τ_{h} candidates to be associated with the same collision vertex. The exact triggers and their thresholds varied slightly from year to year because of changes in luminosity and detector conditions, as well as improvements to the trigger algorithms. The transverse momentum (p_{T}) thresholds imposed by the trigger on the "leading" (highest p_{T}), "subleading" (second-highest p_{T}), and third e, μ, or τ_{h}, and the corresponding η requirements for each year are shown in table 1. All triggers include identification and isolation requirements on the e, μ, and τ_{h} candidates [57]. When combined, the triggers achieve an efficiency of 95–100% for simulated SM HH signal events in each of the seven search categories.

Monte Carlo (MC) simulated samples are used to model HH signal events and a wide range of SM background processes that produce final states with e, μ, or τ_{h}. Background MC samples include processes producing a single W or Z boson, two bosons (WW, WZ, ZZ, Wγ, and Zγ), three bosons (WWW, WWZ, WZZ, ZZZ, and WZγ), a single H boson (via gluon fusion, vector boson fusion, or associated production with a W or Z boson), a single top quark, a top quark-antiquark pair (t$\bar{\mathrm{t}}$), and top quarks associated with one or more bosons (t$\bar{\mathrm{t}}$W, t$\bar{\mathrm{t}}$Z, t$\bar{\mathrm{t}}$H, tHq, and tHW). All MC samples were generated using either

Trigger	Selection requirements for reconstructed e, μ, and τ_h objects
Single e	$p_T(e) > 27\text{–}35\,\text{GeV}$
Single μ	$p_T(\mu) > 22\text{–}27\,\text{GeV}$
Double e	$p_T(e) > 23,\ 12\,\text{GeV}$
e + μ	$p_T(e) > 23\,\text{GeV},\ p_T(\mu) > 8\,\text{GeV}$
μ + e	$p_T(\mu) > 23\,\text{GeV},\ p_T(e) > 8\text{–}12\,\text{GeV}$
Double μ	$p_T(\mu) > 17,\ 8\,\text{GeV}$
e + τ_h	$p_T(e) > 24\,\text{GeV},\ p_T(\tau_h) > 20\text{–}30\,\text{GeV},\ |\eta(e, \tau_h)| < 2.1$
μ + τ_h	$p_T(\mu) > 19\text{–}20\,\text{GeV},\ p_T(\tau_h) > 20\text{–}27\,\text{GeV},\ |\eta(\mu, \tau_h)| < 2.1$
Double τ_h	$p_T(\tau_h) > 35\text{–}40\,\text{GeV},\ |\eta(\tau_h)| < 2.1$
Triple e	$p_T(e) > 16,\ 12,\ 8\,\text{GeV}$
Two e + μ	$p_T(e) > 12,\ 12\,\text{GeV},\ p_T(\mu) > 8\,\text{GeV}$
Two μ + e	$p_T(\mu) > 9,\ 9\,\text{GeV},\ p_T(e) > 9\,\text{GeV}$
Triple μ	$p_T(\mu) > 12,\ 10,\ 5\,\text{GeV}$

Table 1. Selection requirements on p_T and η of reconstructed electrons (e), muons (μ), and hadronically decaying tau leptons (τ_h) applied by the triggers used in this analysis. The trigger p_T thresholds for leading, subleading, and third e, μ, or τ_h are separated by commas. For trigger thresholds that varied over time, the range of variation is indicated.

MADGRAPH5_aMC@NLO v2 [62, 63], POWHEG v2 [64–66], MCFM v7 [67–69], or PYTHIA v8.2 [70]. All samples that include a H boson were produced for a H boson mass of 125 GeV. Specific details of the simulated processes are summarized in table 2.

The parton distribution functions (PDFs) of the proton are modeled using the NNPDF3.0 and NNPDF3.1 PDF sets [85–89]. Parton shower, hadronization processes, and τ decays are modeled by PYTHIA, using the tunes CP5, CUETP8M1, CUETP8M2, or CUETP8M2T4 [90–92], depending on the process and the data-taking period that is being modeled. The matching of matrix elements to parton showers is performed using the MLM scheme [93] for the LO samples and the FxFx scheme [94] for the NLO samples. The interactions of particles with the CMS detector material was simulated in detail using GEANT4 [95]. Simulated events were reconstructed using the same procedure as in data. The response of the trigger is included in the simulation. Additional pp interactions (pileup) were generated with PYTHIA and overlaid on all MC events, with event weights used to match the collision multiplicity to the distribution inferred from data. Residual differences between data and simulation are rectified by applying corrections to simulated events.

A variety of HH signal samples were generated at LO and NLO accuracy in QCD to simulate nonresonant HH production, covering the ggHH and qqHH production processes, with the H bosons decaying to either WW*, ZZ*, or ττ. The NLO samples are used to extract the rate of the HH signal from the data, while LO samples with a larger number of simulated events are used to train machine learning algorithms. Separate ggHH samples are produced for SM HH production and for a total of twelve EFT benchmark (BM) scenarios in the Higgs Effective Field Theory (HEFT) approach [24]. These benchmarks, along with

Process	MC generator (order)	Cross section order
ggHH	MadGraph5_aMC@NLO v2 (LO) [71, 72]	NNLO FT$_{approx}$
	powheg v2 (NLO) [73–75]	
qqHH	MadGraph5_aMC@NLO v2 (LO)	N3LO
Single H boson production		
(via gluon fusion)	powheg v2 (NLO) [76]	N3LO QCD, NLO EW
(via vector boson fusion)	powheg v2 (NLO) [77]	NNLO QCD, NLO EW
(with a W or a Z boson)	powheg v2 (NLO) [78]	NNLO QCD, NLO EW
(with a pair of top quarks)	MadGraph5_aMC@NLO v2 (NLO)	NLO QCD, NLO EW
(with a single top quark)	MadGraph5_aMC@NLO v2 (LO)	NLO
W	MadGraph5_aMC@NLO v2 (LO)	NNLO
Z	MadGraph5_aMC@NLO v2 (LO)	NNLO QCD, NLO EW
WW (double-parton interaction)	pythia v8.2 (LO)	LO
(same-sign pair)	MadGraph5_aMC@NLO v2 (LO)	LO
(opposite-sign pair)	powheg v2 (NLO) [79, 80]	NNLO
WZ	MadGraph5_aMC@NLO v2 (NLO)	NNLO
ZZ (quark-initiated)	powheg v2 (NLO) [79, 80]	NNLO
(gluon-initiated)	mcfm v7 (LO) [81]	NLO
$W\gamma$, $Z\gamma$, $WZ\gamma$, $t\gamma$, $t\bar{t}\gamma$	MadGraph5_aMC@NLO v2 (NLO)	NLO
WWW, WWZ, WZZ, ZZZ	MadGraph5_aMC@NLO v2 (NLO)	NLO
Single top	powheg v2 (NLO) [82]	NLO
(with a W boson)	powheg v2 (NLO) [83]	NLO
(with a Z boson)	MadGraph5_aMC@NLO v2 (NLO)	NLO
$t\bar{t}$	powheg v2 (NLO) [84]	NNLO
$t\bar{t}t\bar{t}$	MadGraph5_aMC@NLO v2 (NLO)	NLO
$t\bar{t}$W	MadGraph5_aMC@NLO v2	NLO QCD, NLO EW
	(NLO QCD, NLO EW)	
$t\bar{t}$Z	MadGraph5_aMC@NLO v2 (NLO)	NLO QCD, NLO EW
$t\bar{t}$WW, $t\bar{t}$WZ, $t\bar{t}$ZZ	MadGraph5_aMC@NLO v2 (LO)	LO

Table 2. The MC generators that are used to simulate HH signal and background processes. The order of MC simulation and cross section calculation both refer to the perturbative expansion in QCD. Additional higher order electroweak (EW) corrections, if present, are indicated separately.

the seven benchmarks from ref. [96], represent different combinations of κ_λ, κ_t, c_g, c_{2g}, and c_2 HEFT parameter values, and are chosen to probe distinct classes of HH kinematic configurations. These benchmarks are referred to as JHEP04 BM1-12, and JHEP03 BM1-7, respectively. The benchmark JHEP04 BM8 is complemented by a modified version of this benchmark, published in ref. [97], denoted as JHEP04 BM8a. The parameter values of these twenty BM scenarios are shown in table 3. The values of the c_g and c_{2g} couplings published in ref. [96] have been scaled by factors of 1.5 and -3, respectively, to convert them to the convention introduced for these couplings in ref. [24]. In order to increase the number of simulated events and to model kinematic configurations not explicitly generated, such as JHEP03 BM1-7, the ggHH samples are merged and the events in the merged samples are reweighted, using the procedure documented in ref. [98], to match the distributions in m_{HH} and $|\cos\theta^*|$ computed at NLO accuracy and published in ref. [97]. This procedure is applied to the LO and NLO ggHH samples separately. The symbol $\cos\theta^*$ denotes the cosine of the polar angle of one H with respect to the beam axis in the HH rest frame. The qqHH samples are produced only for SM HH production.

Benchmark	κ_λ	κ_t	c_2	c_g	c_{2g}
JHEP04 BM1	7.5	1.0	−1.0	0.0	0.0
JHEP04 BM2	1.0	1.0	0.5	−0.8	0.6
JHEP04 BM3	1.0	1.0	−1.5	0.0	−0.8
JHEP04 BM4	−3.5	1.5	−3.0	0.0	0.0
JHEP04 BM5	1.0	1.0	0.0	0.8	−1.0
JHEP04 BM6	2.4	1.0	0.0	0.2	−0.2
JHEP04 BM7	5.0	1.0	0.0	0.2	−0.2
JHEP04 BM8	15.0	1.0	0.0	−1.0	1.0
JHEP04 BM8a	1.0	1.0	0.5	4/15	0.0
JHEP04 BM9	1.0	1.0	1.0	−0.6	0.6
JHEP04 BM10	10.0	1.5	−1.0	0.0	0.0
JHEP04 BM11	2.4	1.0	0.0	1.0	−1.0
JHEP04 BM12	15.0	1.0	1.0	0.0	0.0
JHEP03 BM1	3.94	0.94	−1/3	0.75	−1
JHEP03 BM2	6.84	0.61	1/3	0	1
JHEP03 BM3	2.21	1.05	−1/3	0.75	−1.5
JHEP03 BM4	2.79	0.61	1/3	−0.75	−0.5
JHEP03 BM5	3.95	1.17	−1/3	0.25	1.5
JHEP03 BM6	5.68	0.83	1/3	−0.75	−1
JHEP03 BM7	−0.10	0.94	1	0.25	0.5
SM	1.0	1.0	0.0	0.0	0.0

Table 3. Parameter values for κ_λ, κ_t, c_2, c_g, and c_{2g} in MC samples modeling twenty benchmark scenarios in the EFT approach, plus SM HH production.

Resonant HH production was simulated at LO for both spin-0 (radion) and spin-2 (graviton) scenarios with m_X values of 250, 260, 270, 280, 300, 320, 350, 400, 450, 500, 550, 600, 650, 700, 750, 800, 850, 900, and 1000 GeV.

4 Event reconstruction

The CMS particle-flow (PF) algorithm [99] aims to reconstruct and identify each individual particle in an event, using an optimized combination of information from the various elements of the CMS detector. The particles are subsequently classified into five mutually exclusive types: electrons, muons, photons, and charged and neutral hadrons. These particles are then combined to reconstruct hadronic τ decays, jets, and the missing transverse momentum in the event.

The candidate vertex with the largest value of summed physics-object p_T^2 is taken to be the primary pp interaction vertex. The physics objects used for this determination are the jets, clustered using the infrared and collinear safe anti-k_T algorithm [100, 101], with the tracks assigned to candidate vertices as inputs, and the associated missing transverse momentum, taken as the negative vector sum of the p_T of those jets.

Electrons are reconstructed within the geometric acceptance of the tracking detectors ($|\eta| < 2.5$) by combining information from the tracker and the ECAL [102]. They are

initially identified using an MVA classifier which distinguishes real electrons from hadrons, along with requirements that the track be associated with the collision vertex, and limits on hadronic energy deposits separated by $\Delta R < 0.4$ from the electrons (their "isolation"). The angular separation between two particles is defined as $\Delta R = \sqrt{(\eta_1 - \eta_2)^2 + (\phi_1 - \phi_2)^2}$, where the symbol ϕ refers to the azimuthal angle of the particle. Electrons passing this initial selection are referred to as "loose". In this analysis, events with electrons originating from hadron decays ("nonprompt"), or with hadrons misidentified as electrons, constitute the largest source of background. This motivates the use of an additional MVA classifier, which is trained to select "prompt" electrons from W, Z, and τ lepton decays, and to reject nonprompt or misidentified electrons. This MVA classifier was previously used for measurements of $t\bar{t}H$ production in events with multiple leptons [103]. It combines observables comparing measurements of the electron energy and direction in the tracker and the ECAL, the compactness of the electron cluster, the bremsstrahlung emitted along the electron trajectory, and the electron isolation. Two levels of thresholds on the output of this MVA classifier are used in the analysis, referred to as the "tight" and "medium" electron selections for the more and less restrictive thresholds, respectively. The tight selection has an average efficiency of 60% for electrons from SM HH decays. Only the electrons passing the tight selections are used to reconstruct signal candidate events, while data events with electrons passing the medium selections and failing the tight selections are used to estimate the contribution of misidentified- and nonprompt-electron backgrounds in each search category. Compared to ref. [103], this analysis uses lower thresholds on the MVA classifier output for the medium and tight electron selections, in order to increase the efficiency in particular for low-p_T electrons, which frequently appear in the HH signal events studied in this analysis. Electrons from photon conversions in the tracker are suppressed by requiring that the track is missing no hits in the innermost layers of the silicon tracker, and is not matched to a reconstructed conversion vertex. In the 2ℓss category, further electron selection criteria are applied, which require agreement among three independent measurements of the electron charge, including the Gaussian sum filter and Kalman filter track curvatures, as well as the ECAL supercluster position [104]. The remaining charge misidentification rate is measured to be less than 0.1% for $|\eta| < 1.479$, and under 0.4% for $|\eta| > 1.479$. The charge quality requirement reduces the electron identification efficiency by about 4%.

Muons are reconstructed by extrapolating tracks in the silicon tracker to hits in the gas-ionization muon detectors embedded in the steel flux-return yoke outside the solenoid [105]. To pass the initial loose identification requirement for this analysis, muons must satisfy criteria related to isolation and track proximity to the primary interaction vertex, as well as track quality observables and matching between the tracker and muon chambers. Additional requirements on the prompt vs. nonprompt muon identification MVA classifier from ref. [103] serve to select muons passing a tight selection for signal candidate events, and a medium selection for nonprompt background estimation. Inputs to this MVA classifier include energy deposits close to the muon in the ECAL and HCAL, the hits and track segments reconstructed in the muon detectors located outside the solenoid, the quality of

the spatial matching between the track segments reconstructed in the silicon tracker and in the muon detectors, and the isolation of the muon with respect to other particles. Again, lower selection thresholds on the MVA classifier output compared to ref. [103] bring higher efficiency for the HH signal, amounting to 80% per muon in simulated SM HH events for the tight selection. In the 2ℓss channel, the uncertainty in the curvature of the muon track is required to be less than 20% to ensure a high-quality charge measurement [103]. This requirement reduces the muon identification efficiency by about 2%.

Hadronic decays of tau leptons are identified using the "hadrons-plus-strips" algorithm [106]. This algorithm classifies individual hadronic decay modes of the τ by combining charged hadrons from the PF reconstruction with neutral pions. The latter are reconstructed by clustering electrons and photons into rectangular strips, which are narrow in η but wide in the ϕ direction. The spread in ϕ accounts for photons originating from neutral pion decays that convert into electron-positron ($e^- e^+$) pairs while traversing the silicon tracker. The e^- and e^+ are bent in opposite directions in ϕ by the magnetic field, and may further emit bremsstrahlung photons before reaching the ECAL. The decay modes considered in this analysis produce one charged pion or kaon plus up to two neutral pions (collectively referred to as "one-prong" τ_h), or three charged pions or kaons plus zero or one neutral pion (referred to as "three-prong" τ_h). The DEEPTAU algorithm [107] distinguishes true τ_h objects from quark and gluon jets, electrons, and muons using a convolutional artificial neural network (NN) [108] with 42 high-level observables as input, together with low-level information obtained from the silicon tracker, ECAL, HCAL, and the muon detectors. The former include the p_T, η, ϕ, and mass of the τ_h candidate, the reconstructed τ_h decay mode, its isolation with respect to charged and neutral particles, and the estimated distance that the τ lepton traverses between its production and decay. For three-prong τ_h candidates, this distance is determined by reconstructing the decay vertex, while for one-prong τ_h candidates, the transverse impact parameter of the charged pion track with respect to the primary pp interaction vertex is used as an estimate of the distance. The low-level information quantifies the particle activity within two $\eta \times \phi$ grids, centered on the direction of the τ_h candidate: an inner grid of size 0.2×0.2, filled with 0.02×0.02 cells, and an outer grid of size 0.5×0.5 (partially overlapping with the inner grid), with 0.05×0.05 cells. Selected τ_h candidates in this analysis must have $p_T > 20\,\text{GeV}$ and $|\eta| < 2.3$, and are subjected to two levels of thresholds on the NN output that separates τ_h from quark and gluon jets, referred to as the tight and medium τ_h selections, respectively.

Hadronic jets (j) are reconstructed with the anti-k_T algorithm using the particles reconstructed with the PF algorithm as input, and serve to identify $H \to WW^* \to jj\ell\nu$ decays in this analysis. Jets reconstructed with size parameters of 0.4 ("small-radius jets") and 0.8 ("large-radius jets") are both used: two small-radius jets to reconstruct the two quarks from low-p_T W boson decays, or a single large-radius jet to reconstruct high-p_T W boson decays, where the quarks are collimated. Overlap between small-radius jets and electrons, muons, and τ_h is resolved by discarding those small-radius jets that contain one or more PF particles matched to an electron, a muon, or a constituent of a τ_h passing the medium selection criteria. In case of large-radius jets, electrons and muons passing

the loose selection are removed from the collection of PF particles used as input to the jet reconstruction, so that leptons produced in $H \to WW^* \to jj\ell\nu$ decays of Lorentz-boosted H bosons are not clustered into those jets.

The effect of pileup on the reconstruction of large-radius jets is mitigated by applying the pileup per particle identification algorithm (PUPPI) [109, 110] to the collection of particles used as input to the jet reconstruction. For small-radius jets, the effect of pileup is reduced by removing charged particles identified with pileup vertices from the jet reconstruction, and applying corrections to the jet energy to account for neutral particles from pileup.

After calibration, the jet energy resolution at the central rapidities amounts to 15–20% at 30 GeV, 10% at 100 GeV, and 5% at 1 TeV [111]. This analysis only considers jets reconstructed in the region $|\eta| < 2.4$. Small-radius jets must have $p_T > 25$ GeV, while large-radius jets must have $p_T > 170$ GeV. Additional criteria requiring that each large-radius jet contain exactly two identifiable, energetic subjets are applied to specifically select those from boosted hadronic W boson decays [112].

Events containing small-radius jets identified with the hadronization of bottom quarks (b jets) are vetoed in this analysis. The DEEPJET algorithm [113] exploits observables related to the long lifetime of b hadrons and the higher particle multiplicity and mass of b jets compared to light quark and gluon jets. Both "loose" and "medium" b jet selections on the DEEPJET output are employed in this analysis, corresponding to b jet selection efficiencies of 84 and 70%, while the misidentification rates for light-quark or gluon jets are 11 and 1.1%, respectively.

The missing transverse momentum vector $\vec{p}_T^{\,\mathrm{miss}}$ is computed as the negative vector p_T sum of all the particles reconstructed by the PF algorithm in an event, and its magnitude is denoted as p_T^{miss} [114]. The $\vec{p}_T^{\,\mathrm{miss}}$ is modified to account for corrections to the energy scale of the reconstructed jets in the event. A linear discriminant, denoted as $p_T^{\mathrm{miss,LD}}$, is employed to remove background events in which the reconstructed p_T^{miss} arises from resolution effects. The discriminant is defined by the relation $p_T^{\mathrm{miss,LD}} = 0.6 p_T^{\mathrm{miss}} + 0.4 H_T^{\mathrm{miss}}$, where H_T^{miss} corresponds to the magnitude of the vector p_T sum of e, μ, and τ_h passing the medium selection criteria, and small-radius jets satisfying the criteria detailed above [115].

5 Event selection

Events are selected with the aim of maximizing the acceptance for HH decays to WW^*WW^*, $WW^*\tau\tau$, and $\tau\tau\tau\tau$, while simultaneously rejecting the large backgrounds from multijet production, single and pair production of W and Z bosons, and $t\bar{t}$ production. To achieve this, each event must contain multiple reconstructed ℓ or τ_h associated with the primary interaction vertex. The ℓ and τ_h may originate from the decay of a W boson or a τ lepton. Seven mutually exclusive search categories, distinguished by the number of reconstructed ℓ and τ_h candidates, are included in the analysis: 2ℓss, 3ℓ, 4ℓ, $3\ell + 1\tau_h$, $2\ell + 2\tau_h$, $1\ell + 3\tau_h$, and $4\tau_h$. Here "ss" indicates a same-sign $\ell\ell$ pair, with two leptons of identical electric charge. The ℓ and τ_h candidates selected in any of the seven search categories must pass the tight selection criteria described in section 4. In addition,

they are required to pass category-specific p_T thresholds motivated by the trigger selection. Further requirements are placed on the sum of ℓ and τ_h charges, and, in two categories, on the discriminant $p_T^{miss,LD}$ and the multiplicity of jets.

The leading and subleading leptons in the 2ℓss category must pass p_T selection thresholds of 25 and 15 GeV, respectively. Events in this category are required to contain two or more small-radius jets, or at least one large-radius jet, targeting hadronic W boson decays. Dielectron events must have $p_T^{miss,LD} > 30$ GeV and $m(\ell\ell) < 81$ GeV or $m(\ell\ell) > 101$ GeV, in order to suppress charge-misidentified $Z \to ee$ background. If the event contains a τ_h, the charge of the τ_h must be opposite to the charge of the leptons. After this selection, the main backgrounds in the 2ℓss category arise from WZ production, from Wγ events in which the photon converts into an e^-e^+ pair and either the e^- or the e^+ is not reconstructed, and from events in which one or both reconstructed leptons are due to a nonprompt ℓ or a misidentified hadron, as shown in table 6. The "other" background given in the table is dominated by same-sign W boson pairs and WWW production. The WW*WW* decay mode accounts for roughly 70% of SM HH signal events selected in the 2ℓss category, with WW$^*\tau\tau$ events accounting for the other 30%.

In the 3ℓ category, the leading, subleading, and third ℓ are required to have p_T values greater than 25, 15, and 10 GeV, respectively, and the sum of their charges must be either $+1$ or -1. At least one small- or large-radius jet must be present, and the $p_T^{miss,LD}$ quantity must be greater than 30 GeV, or 45 GeV if there is at least one same-flavor opposite-sign (SFOS) $\ell\ell$ pair in the event. Again, backgrounds are dominated by WZ production and events with misidentified ℓ. Notable contributions to the "other" background arise from WWW and WWZ production. The signal composition is similar to the 2ℓss category.

The 4ℓ category has identical lepton selection criteria to the 3ℓ category, except that the third ℓ must have $p_T > 15$ GeV, and a fourth ℓ with $p_T > 10$ GeV is required, and the sum of the four lepton charges is required to be equal to zero. In this category and all the remaining categories, there are no selection requirements on jets or $p_T^{miss,LD}$. Almost 70% of signal events come from the WW*WW* decay mode, and about 30% from WW$^*\tau\tau$, while ZZ production accounts for 85% of the background.

Events in the 3$\ell + 1\tau_h$ category are required to satisfy the 3ℓ criteria on the ℓ objects, except that an additional τ_h with $p_T > 20$ GeV and charge opposite to the sum of the ℓ charges is required. Background events in which the reconstructed τ_h fails a loose selection on the NN output of the DEEPTAU algorithm that separates τ_h from electrons, or falls near the ECAL barrel-endcap transition region in $1.460 < |\eta| < 1.558$ are removed. About 70% of signal events come from the WW$^*\tau\tau$ decay mode, while ZZ production and events with at least one misidentified ℓ or τ_h dominate the background.

In the 2$\ell + 2\tau_h$ category, the leading and subleading ℓ are required to pass p_T thresholds of 25 and 15 GeV, while the two τ_h must have $p_T > 20$ GeV. The sum of ℓ plus τ_h charges is required to be zero. Signal contributions are mostly from the WW$^*\tau\tau$ (60%) and $\tau\tau\tau\tau$ (40%) decay modes, while background contributions arise from ZZ production and events with a misidentified ℓ or τ_h candidate.

In the 1$\ell + 3\tau_h$ category, the ℓ is required to satisfy the conditions $|\eta| < 2.1$ and $p_T > 20$ (15) GeV if it is an electron (muon). The leading, subleading, and third τ_h must

have $p_T > 40$, 30, and 20 GeV, respectively, and the sum of τ_h and ℓ charges is required to be zero. Background events containing a Z → ee decay where one electron is misidentified as a τ_h are vetoed by discarding events containing an e-τ_h pair of opposite charge and mass $71 < m(e\tau_h) < 101$ GeV, and in which the τ_h either fails a loose selection on the discriminant that separates τ_h from electrons, or falls into the region $1.460 < |\eta| < 1.558$. Around 80% of HH signal events selected in the $1\ell + 3\tau_h$ category are from $\tau\tau\tau\tau$ and 20% from the WW*$\tau\tau$ decay mode, while the majority of background events stem from ZZ production or contain a misidentified ℓ or τ_h.

The $4\tau_h$ category requires the leading and subleading τ_h to pass p_T thresholds of 40 and 30 GeV, respectively, and the third and fourth τ_h to have $p_T > 20$ GeV. Given the extremely low backgrounds in this category, no charge sum criterion or Z → ee veto is applied. Almost all signal events come from the $\tau\tau\tau\tau$ decay mode, while 55% of the background events contain at least one misidentified τ_h candidate, and the remainder arises from ZZ (30%) and single Higgs boson (15%) production.

In all seven search categories, the background contamination from processes with top quarks is reduced by discarding events with at least one selected small-radius jet passing the medium b jet identification, or at least two passing the loose b jet identification. Leptons originating from low-mass Drell–Yan production, decays of J/ψ and Υ mesons, cascade decays of bottom quarks, and photon conversions are removed by vetoing events containing any pair of loose ℓ with mass $m(\ell\ell) < 12$ GeV. To eliminate overlap with events selected in the ongoing search for HH production in the $b\bar{b}$ZZ, ZZ → 4ℓ decay mode, no event in the 2ℓss, 3ℓ, and 4ℓ categories may contain two SFOS loose $\ell\ell$ pairs with a mass of the four-ℓ system of less than 140 GeV. In addition, to reduce the Z → $\ell\ell$ background, these three categories along with $2\ell + 2\tau_h$ and $3\ell + 1\tau_h$ exclude events where any SFOS loose $\ell\ell$ pair has an invariant mass of 81–101 GeV (Z boson veto).

A summary of the event selection criteria applied in the different categories is given in table 4. Criteria that are common to all seven search categories are given in table 5.

Two control regions (CRs) are used to validate the modeling of the WZ and ZZ backgrounds. These CRs match the signal regions of the 3ℓ and 4ℓ categories, but with the Z boson veto inverted, and are referred to as the "3ℓ WZ" CR and "4ℓ ZZ" CR, respectively.

The number of events selected in the signal regions of each of the seven search categories and in the 3ℓ WZ and 4ℓ ZZ CRs are given in table 6. The contribution expected from nonresonant HH production with event kinematics as predicted by the SM, but 30 times the SM cross section, is given separately for HH decays into WW*WW*, WW*$\tau\tau$, and $\tau\tau\tau\tau$ in the upper three rows of each table. The event yields given in the rows labeled WW*WW* include a small contribution from HH decays into WW*ZZ* and ZZ*ZZ*, and, similarly, the numbers quoted in the rows labeled WW*$\tau\tau$ include a small contribution from HH decays into ZZ*$\tau\tau$.

6 Analysis strategy

The rate of the HH signal is extracted through a binned maximum likelihood (ML) fit to the distributions in the output of boosted decision tree (BDT) classifiers [116], which are

Category	2ℓss	3ℓ	4ℓ
Targeted HH decays	WW*WW*	WW*WW*	WW*WW*
Trigger	Single- and double-lepton	Single-, double- and triple-lepton	Single-, double- and triple-lepton
Lepton p_T	>25 / 15 GeV	>25 / 15 / 10 GeV	>25 / 15 / 15 / 10 GeV
Lepton charge sum	±2, with charge quality requirements applied	±1	0
Dilepton invariant mass	$\|m_{\ell\ell} - m_Z\| > 10$ GeV [†]	$\|m_{\ell\ell} - m_Z\| > 10$ GeV [‡]	$\|m_{\ell\ell} - m_Z\| > 10$ GeV [‡]
Jets	≥2 small-radius jets or ≥1 large-radius jet	≥1 small-radius jet or ≥1 large-radius jet	—
Missing p_T	$p_T^{\mathrm{miss,LD}} > 30$ GeV [§]	$p_T^{\mathrm{miss,LD}} > 30$ GeV [‖]	—

Category	3ℓ + 1τ_h	2ℓ + 2τ_h
Targeted HH decays	WW*ττ	WW*ττ, ττττ
Trigger	Single-, double-, and triple-lepton	Single- and double-lepton
Lepton p_T	>25 / 15 / 10 GeV	>25 / 15 GeV
τ_h p_T	>20 GeV	>20 GeV
Lepton and τ_h charge	ℓ and τ_h charges sum to 0	ℓ and τ_h charges sum to 0
Dilepton invariant mass	$\|m_{\ell\ell} - m_Z\| > 10$ GeV [‡]	$\|m_{\ell\ell} - m_Z\| > 10$ GeV [‡]

Category	1ℓ + 3τ_h	4τ_h
Targeted HH decays	ττττ	ττττ
Trigger	Single-lepton, lepton+τ_h and double-τ_h	Double-τ_h
Lepton η	$\|\eta\| < 2.1$	—
Lepton p_T	>20 GeV (e) or >15 GeV (μ)	—
τ_h p_T	>40 / 30 / 20 GeV	>40 / 30 / 20 / 20 GeV
Lepton and τ_h charge	ℓ and τ_h charges sum to 0	τ_h charges sum to 0
Z → ee veto	$\|m_{e\tau_h} - 86$ GeV$\| > 15$ GeV [¶]	—

[†] Applied to all SFOS $\ell\ell$ pairs and electron pairs with the same charge.

[‡] Applied to all SFOS $\ell\ell$ pairs.

[§] Only applied to events containing two electrons.

[‖] Tightened to $p_T^{\mathrm{miss,LD}} > 45$ GeV if event contains a SFOS $\ell\ell$ pair.

[¶] For τ_h classified as electrons by the DEEPTAU algorithm or with $1.460 < \|\eta\| < 1.558$.

Table 4. Event selection criteria applied in the seven search categories. The p_T thresholds for ℓ and τ_h with the highest, second-, third-, and fourth-highest p_T are separated by slashes. The symbol "—" indicates that no requirement is applied.

Object and event properties	Selection criteria
Lepton and τ_h pseudorapidity	$\|\eta\| < 2.5$ for e, $\|\eta\| < 2.4$ for μ, $\|\eta\| < 2.3$ for τ_h
Dilepton invariant mass	$m_{\ell\ell} > 12$ GeV (all $\ell\ell$ pairs)
Four-lepton invariant mass	$m_{4\ell} > 140$ GeV (any two SFOS $\ell\ell$ pairs)
b jet veto	0 medium and ≤ 1 loose b-tagged small-radius jet

Table 5. Reconstructed object and event selection requirements in all seven search categories. Electrons or muons in the $\ell\ell$ pairs include any leptons passing the loose selection criteria.

trained to discriminate the HH signal from backgrounds, along with kinematic distributions from the two CRs above. The data from each of the three years are fit separately. Three classifiers are trained for each of the seven search categories using a mix of MC simulation

Process	2ℓss	3ℓ	4ℓ
SM HH $\to$ WW*WW* ($\times$ 30)	73 $\pm$ 6	33 $\pm$ 3	2.2 $\pm$ 0.2
SM HH $\to$ WW$^*\tau\tau$ ($\times$ 30)	31 $\pm$ 3	12 $\pm$ 1	0.9 $\pm$ 0.1
SM HH $\to$ $\tau\tau\tau\tau$ ($\times$ 30)	3 $\pm$ 0	1 $\pm$ 0	0.1 $\pm$ 0.0
WZ	1999 $\pm$ 122	1318 $\pm$ 78	0.4 $\pm$ 0.1
ZZ	121 $\pm$ 3	109 $\pm$ 3	53.9 $\pm$ 3.1
Misidentified ℓ	4842 $\pm$ 1327	510 $\pm$ 94	2.2 $\pm$ 1.1
Conversion electrons	804 $\pm$ 174	117 $\pm$ 24	0.7 $\pm$ 0.3
Electron charge misid.	394 $\pm$ 61	—	—
Single Higgs boson	214 $\pm$ 6	61 $\pm$ 1	2.4 $\pm$ 0.3
Other backgrounds	2740 $\pm$ 338	289 $\pm$ 29	4.0 $\pm$ 0.5
Total expected background	11 114 $\pm$ 1387	2404 $\pm$ 128	63.7 $\pm$ 3.3
Data	10 344	2621	62

Process	3ℓ + 1τ_h	2ℓ + 2τ_h	1ℓ + 3τ_h	4τ_h
SM HH $\to$ WW*WW* ($\times$ 30)	0.9 $\pm$ 0.1	0.2 $\pm$ 0.0	0.2 $\pm$ 0.0	0.3 $\pm$ 0.0
SM HH $\to$ WW$^*\tau\tau$ ($\times$ 30)	4.1 $\pm$ 0.3	3.9 $\pm$ 0.4	0.6 $\pm$ 0.1	0.1 $\pm$ 0.0
SM HH $\to$ $\tau\tau\tau\tau$ ($\times$ 30)	0.9 $\pm$ 0.1	2.3 $\pm$ 0.3	2.6 $\pm$ 0.4	1.3 $\pm$ 0.2
WZ	0.2 $\pm$ 0.0	<0.1	<0.1	<0.1
ZZ	24.1 $\pm$ 1.4	18.4 $\pm$ 1.3	1.9 $\pm$ 0.2	0.7 $\pm$ 0.1
Misidentified ℓ and τ_h	23.9 $\pm$ 6.6	31.9 $\pm$ 10.1	2.2 $\pm$ 2.1	2.2 $\pm$ 1.6
Conversion electrons	0.1 $\pm$ 0.0	0.1 $\pm$ 0.1	<0.1	<0.1
Single Higgs boson	3.8 $\pm$ 0.4	2.8 $\pm$ 0.7	0.8 $\pm$ 0.4	0.4 $\pm$ 0.3
Other backgrounds	2.8 $\pm$ 0.4	2.2 $\pm$ 0.8	0.1 $\pm$ 0.1	<0.1
Total expected background	54.9 $\pm$ 6.8	55.4 $\pm$ 10.3	5.0 $\pm$ 2.2	3.4 $\pm$ 1.6
Data	55	55	6	1

Process	3ℓ WZ CR	4ℓ ZZ CR
WZ	12 565 $\pm$ 705	<1
ZZ	765 $\pm$ 47	2000 $\pm$ 108
Misidentified ℓ	804 $\pm$ 211	13 $\pm$ 4
Conversion electrons	106 $\pm$ 21	2 $\pm$ 0
Other backgrounds	625 $\pm$ 76	60 $\pm$ 8
Total expected background	14 866 $\pm$ 742	2074 $\pm$ 108
Data	14 994	2096

Table 6. The number of expected and observed events in each of the seven search categories, and in two CRs, which validate the modeling of the WZ and ZZ backgrounds. The symbol "—" indicates that the background is not relevant for the category. The HH signal represents the sum of the ggHH and qqHH production processes and is normalized to 30 times the event yield expected in the SM, corresponding to a cross section of about 1 pb. The event yields are obtained by performing the event selection and applying appropriate corrections to the simulated events. Quoted uncertainties represent the sum of statistical and systematic components. Uncertainties that are smaller than half the value of the least significant digit have been rounded to zero.

from all three years, targeting nonresonant HH production and resonant HH production from the decay of heavy particles of spin 0 and of spin 2. The binning is chosen with the objective of maximizing the sensitivity for the HH signal, while maintaining sufficient background events in each bin to keep the statistical uncertainty in the background prediction under control. In the two categories with high event yields (2ℓss and 3ℓ) the BDT output binning is chosen such that each bin contains a similar number of expected HH signal events. The four categories containing events with τ_h ($3\ell + 1\tau_h$, $2\ell + 2\tau_h$, $1\ell + 3\tau_h$, and $4\tau_h$) have low event yields and sizable background contributions arising from the misidentification of ℓ and τ_h candidates, which are determined from data and statistically limited. For these categories, we choose the binning for each BDT output distribution such that a similar number of expected background events is contained in each bin. In the 4ℓ category, the fact that the background is dominated by ZZ production, which is modeled by the MC simulation with low statistical uncertainties, allows one to choose the binning in the same way as for the 2ℓss and 3ℓ categories. The number of bins is determined by the condition that the relative statistical uncertainty in the background prediction in each bin does not exceed 15%. Higher bin numbers correspond to a higher BDT output value, and feature a higher signal-to-background ratio. For the SM HH signal, the bins with the highest BDT output values feature a signal-to-background ratio up to 10 times higher than the inclusive ratio in each category.

The inputs to the BDT classifiers differ by search category and include the p_T and η of reconstructed ℓ and τ_h; the angular separation ΔR and invariant mass of $\ell\ell$, $\ell\tau_h$, and $\tau_h\tau_h$ pairs; the ΔR and invariant mass between an ℓ or τ_h candidate and the nearest jet(s); the number of jets in the event; the discriminant $p_T^{\mathrm{miss,LD}}$; the scalar p_T sum of all reconstructed e, μ, τ_h, and jets; the "visible" mass of the Higgs boson pair, given by the mass of the system of reconstructed e, μ, τ_h, and jets; and where applicable, the "full" mass of the HH system, including neutrinos, reconstructed using the algorithm from ref. [117] designed for reconstructing Higgs pair decays into τ leptons. This algorithm targets HH signal events decaying to $\tau\tau\tau\tau$ and thus works best in the $4\tau_h$ and $1\ell + 3\tau_h$ search categories. Distributions in some of the observables used as inputs to the BDT classifiers in the 2ℓss and 3ℓ categories are shown in figure 4.

These observables are complemented by further inputs, which parametrize the BDT as a function of the model parameters: the Higgs boson couplings λ, y_t, c_g, c_{2g}, and c_2 for nonresonant HH production, and the mass of the heavy particle X in resonant HH production. When training the BDT that targets nonresonant HH production, the values for the couplings are chosen according to the twelve EFT benchmark scenarios given in ref. [24] and the SM, indicated by thirteen binary inputs to the BDT. The BDT classifiers used for the analysis of resonant HH production are trained separately for spin-0 and spin-2 on the full set of resonance masses listed in section 3, and the resonance mass is used as an input to the BDT. Each simulated background event is replicated multiple times in the training sample, with different values assigned to the Higgs boson couplings and the mass of the heavy particle X.

The training is performed using simulated samples of signal and background events. The signal events used in the training consist of ggHH events in the HH decay modes
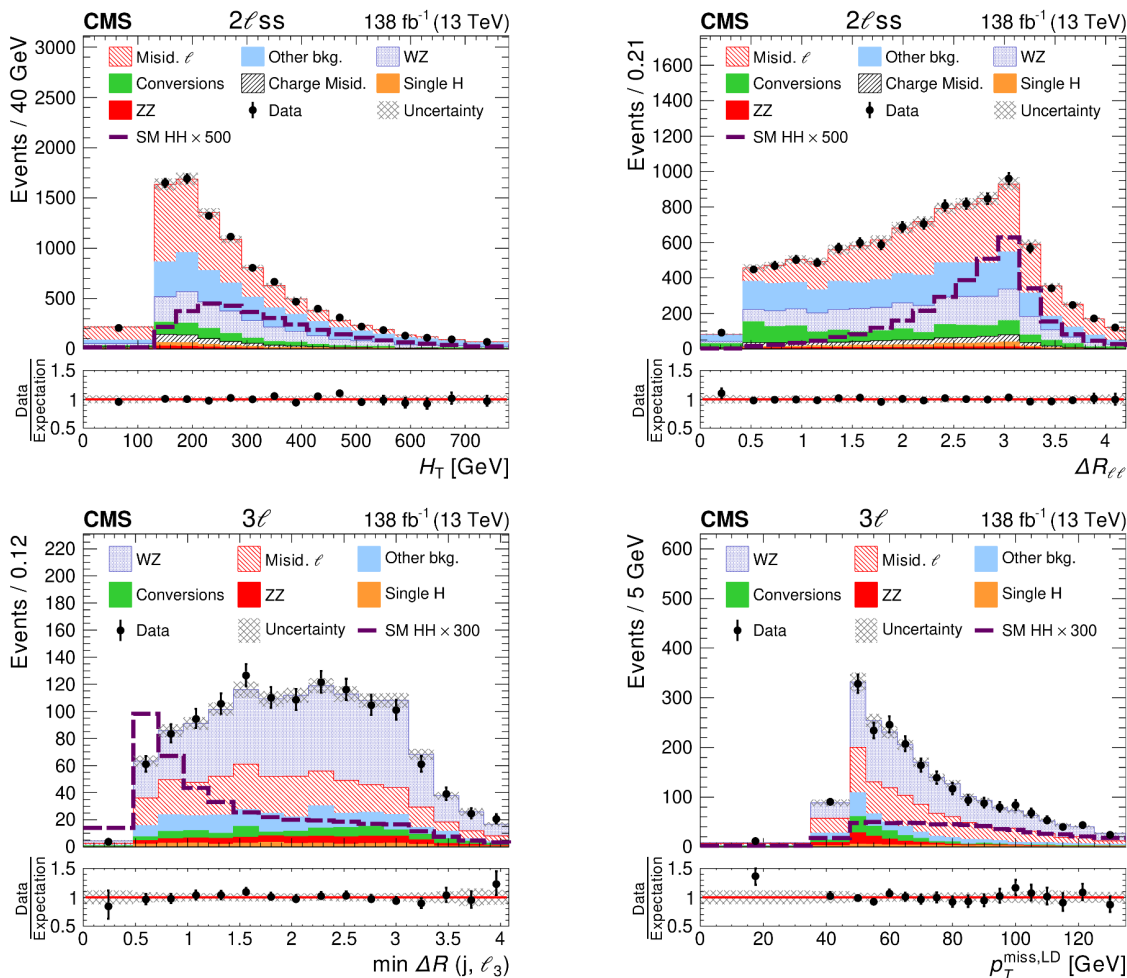
Figure 4. Distributions in a few observables used as inputs to the BDT classifiers in the 2ℓss and 3ℓ categories: the scalar p_T sum, denoted as H_T, of the two reconstructed ℓ and all small-radius jets in the 2ℓss category (upper left); the angular separation ΔR between the two ℓ in the 2ℓss category (upper right); the angular separation between ℓ_3 and the nearest small-radius jet in the 3ℓ category (lower left); and $p_T^{\mathrm{miss,LD}}$ in the 3ℓ category (lower right). The ℓ_3 in the 3ℓ category is defined as the ℓ that is not part of the opposite-sign $\ell\ell$ pair of lowest mass. The normalization and shape of the distributions expected for the different background processes are shown for the values of nuisance parameters obtained from an ML fit in which the HH signal is constrained to be zero. The gray shaded area indicates the sum of statistical and systematic uncertainties on the background prediction obtained from this ML fit.

WW*WW*, WW*$\tau\tau$, and $\tau\tau\tau\tau$. Background contributions arising from the misidentification of ℓ and τ_h candidates and from the mismeasurement of the electron charge are included in the simulation. The signal and background events used in the training are required to pass the event selection criteria for the respective search category, described in section 5. The number of training events is increased by applying the medium ℓ and τ_h identification criteria instead of the tight ones. Weights are applied to background events arising from different sources, such that the relative fractions of different types of back-

grounds in the training match the fractions expected in the signal region of the analysis, i.e. when the tight ℓ and τ_h identification criteria are applied. The MC samples used for the BDT training overlap with the samples used to model signal and background contributions in the analysis. To avoid potential biases, the training samples are split into two samples of equal size, based on even and odd event numbers. The BDTs trained on even events are evaluated on odd events, and vice versa, thereby ensuring that BDTs are not trained and evaluated on the same events. The training is performed using the XGBOOST algorithm [118], interfaced to the SCIKIT-LEARN machine learning library [119]. The parameters of the BDT training (so-called "hyperparameters") are optimized using the particle swarm optimization algorithm described in ref. [120].

7 Background estimation

Background contributions are classified as either "reducible" or "irreducible". In this analysis, three types of reducible backgrounds are considered, arising from misidentified ℓ or τ_h, electron charge misidentification, and electrons from photon conversions. Background events in which all selected ℓ and τ_h come from W, Z, or H boson decays, and are reconstructed with the correct charge, are considered "irreducible". The ℓ/τ_h misidentification and electron charge misidentification backgrounds are both determined from data, while electron conversions and irreducible backgrounds are modeled using MC simulation.

The ℓ/τ_h misidentification background (which includes nonprompt leptons) is the largest reducible background in all search categories. Nonprompt ℓ are either electrons or muons produced in bottom and charm quark decays, or muons that originate from pion and kaon decays. Hadronic jets may also be misidentified as electrons or τ_h. The ℓ/τ_h misidentification background estimate is detailed in section 7.1. The electron charge misidentification background is only relevant for the 2ℓss search category, and is described in section 7.2. The modeling of photon conversion events by the MC simulation has been validated in data as described in refs. [103, 121].

The main contribution to the irreducible background arises from WZ production in the 2ℓss and 3ℓ categories, and ZZ production in the remaining five categories. The production of pairs of bosons (γ, W, Z, or H) other than WZ, ZZ and HH, and production of bosons with top quarks, including $W\gamma$, $Z\gamma$, WH, ZH, tH, $t\bar{t}H$, tW, $t\bar{t}W$, tZ, $t\bar{t}Z$, $t\gamma$, and $t\bar{t}\gamma$, constitute subdominant additional backgrounds. The tZ and $t\bar{t}Z$ backgrounds also include contributions from off-shell $t\bar{t}\gamma^*$ and $t\gamma^*$ production. Background processes which include at least one top quark are suppressed by the b jet veto described in section 5, but are still sizable compared to the expected HH signal. All irreducible backgrounds are modeled using the MC simulation.

The modeling of the dominant irreducible WZ and ZZ backgrounds is validated using the "3ℓ WZ" and "4ℓ ZZ" CRs introduced in section 5. Distributions in kinematic observables from these CRs (shown in figure 5) are included in the ML fit that is used to extract the HH signal, described in section 9. This provides in-situ constraints on the WZ and ZZ backgrounds and on systematic uncertainties related to lepton identification and trigger efficiency. The transverse mass, $m_T = \sqrt{2\,p_T^\ell\,p_T^{miss}\,(1 - \cos\Delta\phi)}$, in the 3ℓ WZ CR is computed using the ℓ that is not identified as originating from the Z boson decay. The
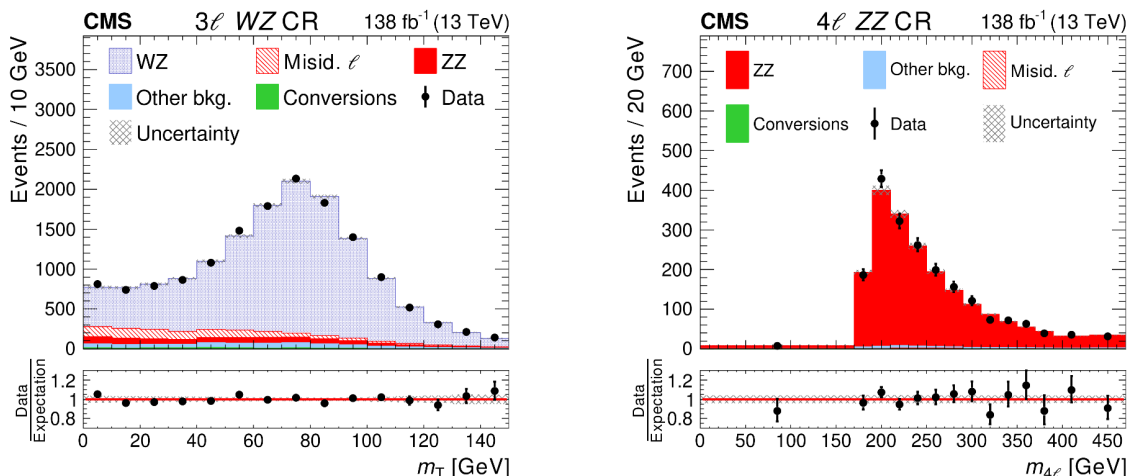
Figure 5. Distributions in m_T in the 3ℓ WZ CR (left) and in $m_{4\ell}$ in the 4ℓ ZZ CR (right). The normalization and shape of the distributions expected for WZ, ZZ, and other background processes are shown for the values of nuisance parameters obtained from the ML fit described in section 9. The gray shaded area indicates the sum of statistical and systematic uncertainties on the background prediction obtained from the ML fit.

symbol $\Delta\phi$ refers to the angle in the transverse plane between the ℓ momentum and the $\vec{p}_T^{\text{miss}}$. The observable $m_{4\ell}$ refers to the mass of the 4ℓ system in the 4ℓ ZZ CR.

The modeling of the reducible ℓ/τ_h misidentification background is validated in two further CRs, the "2ℓss CR" and the "$2\ell + 2\tau_h$ CR". They are based on the signal regions (SRs) of the 2ℓss and $2\ell + 2\tau_h$ categories. In the 2ℓss CR, no b jet veto is applied, and at least one small-radius jet passing the medium b jet identification is required. The $2\ell + 2\tau_h$ CR differs from the SR of the $2\ell + 2\tau_h$ category in that the sum of ℓ plus τ_h charges is required to be non-zero, and no Z boson veto is applied. The 2ℓss CR is dominated by events with misidentified ℓ, while the $2\ell + 2\tau_h$ CR is dominated by events with misidentified τ_h. Distributions in the transverse mass m_T in the 2ℓss CR and in the mass of the HH candidate in the $2\ell + 2\tau_h$ CR, reconstructed by the algorithm described in ref. [117], are shown in figure 6. The transverse mass in the 2ℓss CR is computed using the leading ℓ. The data agree well with the background prediction in both CRs.

Simulated events are only considered as irreducible background if every selected e, μ, and τ_h candidate matches a prompt MC generator-level counterpart. Events with at least one selected electron from a photon conversion, and the remaining ℓ and τ_h candidates matched to prompt leptons in MC simulation, are classified as conversion background. Electrons that are misidentified as τ_h, and τ_h that are misidentified as e are also modeled using the MC simulation. All other simulated events are discarded, as the ℓ/τ_h misidentification and charge misidentification backgrounds are estimated from data, as described below.

7.1 Lepton and τ_h misidentification background

The background from events with misidentified ℓ and τ_h candidates is estimated using the "fake factor" or "FF" method from ref. [115]. An estimate of this background's contribution
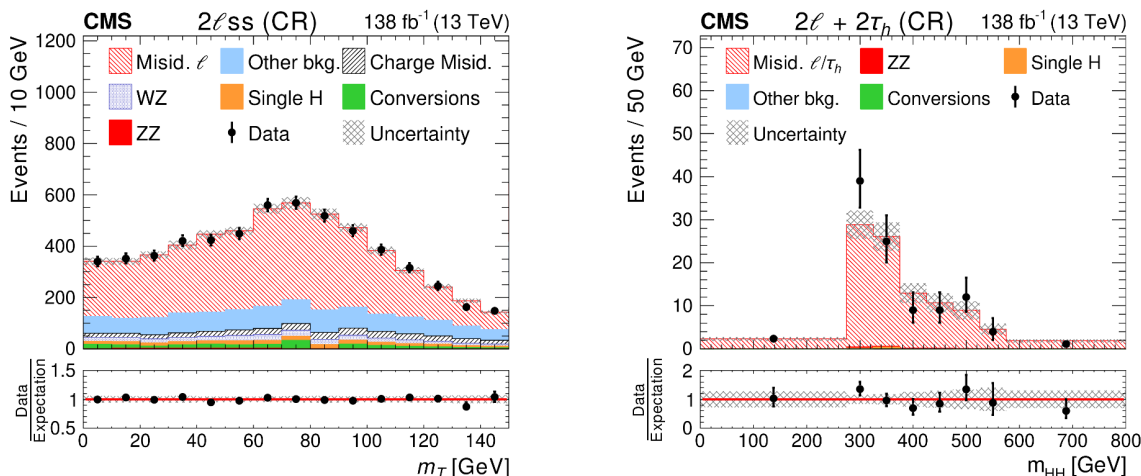
Figure 6. Distributions in m_T in the 2ℓss CR (left) and in the mass of the HH candidate in the 2ℓ+2τ_h CR (right). The normalization and shape of the distributions expected for the misidentified ℓ/τ_h background and other background processes are shown for the values of nuisance parameters obtained from an ML fit in which the HH signal is constrained to be zero. The gray shaded area indicates the sum of statistical and systematic uncertainties on the background prediction obtained from this ML fit.

to the SR of each search category is obtained by selecting a sample of events that satisfy all selection criteria of the SR for the respective search category, except that the e, μ, and τ_h are required to pass the medium selections instead of the tight ones. The sample of events thus obtained is referred to as the application region (AR) of the FF method. Events in which every ℓ and τ_h satisfies the tight selections are excluded from the AR.

The prediction for misidentification backgrounds in the SR is obtained by applying suitably chosen weights w to the events selected in the AR, where w is given by the expression

$$w = (-1)^{n+1} \prod_{i=1}^{n} \frac{f_i(p_T, \eta)}{1 - f_i(p_T, \eta)}. \tag{7.1}$$

The product extends over all e, μ, and τ_h that pass the medium, but fail the tight selection criteria, and n refers to the total number of such ℓ and τ_h. The symbol $f_i(p_T, \eta)$ corresponds to the probability for a single e, μ, or τ_h that passes the medium selection to also pass the tight selection. These probabilities are measured separately for e, μ, and τ_h candidates, parametrized as a function of p_T and η, and vary between 5 and 30%. The contributions of irreducible backgrounds to the AR are subtracted based on the MC expectation of such processes. The alternating sign in eq. (7.1) is necessary to avoid double-counting arising from events with more than one misidentified ℓ or τ_h [115].

The probabilities $f_i(p_T, \eta)$ for electrons and muons are measured in multijet events, as described in ref. [103]. The $f_i(p_T, \eta)$ for τ_h are measured using $Z \rightarrow \mu\mu$+jets events, where the misidentified τ_h candidates arise from quark or gluon jets. These events are selected by requiring a muon pair passing the tight selection, with opposite charge and invariant mass

$60 < m_{\mu\mu} < 120\,\text{GeV}$, plus at least one τ_h candidate that passes the medium τ_h selection. The leading and subleading muons must have $p_\text{T} > 25$ and $15\,\text{GeV}$, respectively. Events must also pass the b jet veto described in section 5 to remove $t\bar{t}$ background.

7.2 Charge misidentification background

The electron charge misidentification background in the 2ℓss category is estimated using the method described in ref. [103]. A sample of dielectron events passing all selection criteria of the SR of the 2ℓss category, except that both electrons are required to have opposite-instead of same-sign charge, is selected and assigned appropriately chosen weights. The weights are computed by summing the probabilities for the charge of either electron to be mismeasured. The probability for the mismeasurement of the electron charge is determined using $Z \to ee$ events, and ranges from under 0.1% in the barrel up to 0.4% in the endcap. The probability for mismeasuring the charge of muons is negligible [103].

8 Systematic uncertainties

Multiple sources of systematic uncertainty affect the predicted event yields, the distributions in the output of the BDT classifiers, or both. These uncertainties may be theoretical, affecting the predicted cross section or decay kinematics of the collision process, or experimental, accounting for differences in object reconstruction and calibration between data and the MC simulation, or for uncertainties on the estimates of the ℓ/τ_h misidentification and electron charge misidentification background obtained from data. The systematic uncertainties may be correlated or uncorrelated across the three data-taking years, and among the various signal and background processes considered in the analysis.

The SM prediction for the ggHH production cross section at $\sqrt{s} = 13\,\text{TeV}$ has a relative uncertainty of $+6.7\%/-23.2\%$ [122], while the qqHH cross section uncertainty is $\pm 2.1\%$ [19]. The predicted H boson decay branching fractions to WW^*, $\tau\tau$, and ZZ^* have relative uncertainties of 1.54%, 1.65%, and 1.54%, respectively [123]. Correlations between these uncertainties have a negligible effect. Alternate HH predictions are generated with the renormalization and factorization scales varied up and down by a factor of 2. Variations that increase the factorization scale and decrease the renormalization scale (and vice versa) are excluded, following the recommendation of ref. [123]. All theoretical uncertainties in the HH signal model are correlated across all three data-taking years and among the seven search categories. The uncertainties in the H boson decay branching fractions and the effect of renormalization and factorization scale uncertainties in the signal acceptance impact the measurement of cross sections for both nonresonant and resonant HH production. Conversely, the uncertainties in the SM prediction for the ggHH and qqHH cross sections only affect the measurement of the HH production rate as a ratio to the SM prediction.

Theoretical uncertainties also affect the irreducible background prediction. The relative uncertainties in the cross sections of the dominant WZ and ZZ backgrounds are 2.1 and 6.3%, respectively [124–126]. The uncertainties in the cross sections for the subdominant single H boson backgrounds range from 2 to 9% for ggHH, qqHH, WH, and ZH. The cross sections for the production of W, Z, or H bosons with one or two top quarks are known with uncertainties of 8–15%. The event yields of extremely rare backgrounds not

mentioned above (e.g., triple boson or four top quark production) are given a conservative uncertainty of 50%, since the analysis has little sensitivity to these processes. Following ref. [103], background contributions arising from photon conversions are assigned a 30% yield uncertainty. The theoretical uncertainties affecting background cross sections are partially correlated among different processes. Here, contributions arising from uncertainties in the proton PDFs are correlated among processes with a similar initial state. Processes involving single H boson production are an exception. These uncertainties are uncorrelated from other background processes but correlated among each other depending on the initial state. Uncertainties arising from the choice of the renormalization and factorization scales are correlated for processes with similar production modes, for example among all processes involving diboson production (WW, WZ, ZZ, Wγ, and Zγ). Uncertainties in α_s are correlated among all background processes. The theoretical cross section uncertainties for signal processes are uncorrelated with those of background processes, but otherwise follow the same uncertainty scheme for proton PDF, scale, and α_s contributions. All theoretical cross section uncertainties are treated as correlated across the different data-taking years and among all seven search categories.

The rate of the misidentified ℓ/τ_h background is assigned a 30% uncertainty in all search categories, to account for variations in the misidentification rates between the ARs of the FF method and the multijet (Z $\to \mu\mu$+jets) event samples used to measure the $f_i(p_T, \eta)$ for e and μ (τ_h). In the $3\ell + 1\tau_h$ and $1\ell + 3\tau_h$ categories, an additional uncertainty of 30% (uncorrelated with the other 30% uncertainty) is assigned to the rate of the misidentified ℓ/τ_h background, to account for the extra uncertainty arising from the modified τ_h selection criteria that suppress the misidentification of electrons as τ_h. The effect of statistical uncertainties in the probabilities $f_i(p_T, \eta)$ for electrons and muons is evaluated by varying these probabilities in bins of p_T and η and determining the resulting change in the shape of the BDT classifier output distribution obtained for the misidentified ℓ/τ_h background. For τ_h, the effect of statistical uncertainties in $f_i(p_T, \eta)$ is evaluated by fitting the probabilities in bins of η with functions that are linear in p_T, varying the slope of these functions up and down within the uncertainties obtained from the fit, and determining the resulting change in the shape of the BDT classifier output distribution.

An additional uncertainty in the BDT output shape in each category is evaluated for events with a nonprompt or misidentified ℓ or τ_h as follows: Simulated events passing all signal selection criteria are compared to those with at least one ℓ or τ_h candidate failing the tight identification criteria, scaled according to the FF method described in section 7, but with the probabilities $f_i(p_T, \eta)$ taken from the MC simulation instead of from the data. The ratio of these two shapes is fitted with a linear function, which is convoluted with the misidentified ℓ/τ_h background prediction from the data to serve as an uncertainty in the BDT output shape for these events in the SR. The systematic uncertainties associated with the misidentified ℓ/τ_h background prediction and the uncertainty associated with the electron charge misidentification rate are treated as uncorrelated among the different data-taking years.

The rate of the electron charge misidentification background in the 2ℓss category is assigned a 30% uncertainty. It covers the uncertainty on the electron charge misidentification

rates measured in Z → ee events, including the effect of background contamination in these samples, and accounts for differences observed in the following "closure" test: Simulated events are required to pass all signal selection criteria of the 2ℓss category, except that the two leptons are required to have opposite-sign electric charges. The selected events are scaled according to the electron charge misidentification probability in simulated events, determined by applying the procedure detailed in section 7.2 to MC simulation. The resulting background estimate is compared to the one obtained by applying the nominal signal selection criteria of the 2ℓss category to simulated events.

Uncertainties in the modeling of the trigger and object reconstruction efficiency affect all signal and background processes that are estimated using MC simulation. Trigger efficiencies for events with at least two ℓ are compared between data and MC simulation in control regions enriched in the $t\bar{t}$, WZ, and ZZ background processes, as a function of lepton flavor, p_T, and η. This results in a small p_T-dependent uncertainty correlated between the 2ℓss and $2\ell + 2\tau_h$ categories, and a 1% normalization uncertainty, which is correlated among the 3ℓ, $3\ell + 1\tau_h$, and 4ℓ categories. The data-to-simulation agreement in trigger efficiency for the $4\tau_h$ and $1\ell + 3\tau_h$ categories is computed using an independent set of data, as a function of the p_T and η of the ℓ and all τ_h, and the reconstructed decay modes of all τ_h. The trigger uncertainties for these two categories are treated as uncorrelated. All systematic uncertainties related to trigger modeling are correlated across different physics processes, but uncorrelated among the three data-taking years.

The uncertainties in the reconstruction and identification efficiencies for e, μ, and τ_h candidates have been measured in Z boson enriched regions in data for each level of identification criteria (tight, medium, and loose), and are applied to each event as a function of p_T and η for leptons and of p_T and the reconstructed hadronic decay mode for τ_h. The reconstructed τ_h energy has an uncertainty of around 1%, depending on the data-taking year and reconstructed τ_h decay mode. These uncertainties affect the predicted rate and BDT output shape for signal and background, and are correlated among the different physics processes, but uncorrelated across different data-taking years.

The jet energy scale and resolution are determined using dijet control regions [111, 127]. The jet energy scale is evaluated using 11 separate components, accounting for partial correlations between the data recorded in different years. The jet energy resolution uncertainty is uncorrelated among the three data-taking years. Jet energy uncertainties are also propagated to the p_T^{miss} calculation. An additional uncertainty in $\vec{p}_T^{\text{miss}}$ comes from uncertainty in the energy of "unclustered" PF hadrons (PF hadrons not clustered into either small- or large-radius jets), which is uncorrelated across different years. The probability for true b jets to fail the multivariate b jet identification criteria, or for jets from gluons or light flavored quarks to be misidentified as b jets, is compared in data and MC simulation in event regions that are enriched in light-flavor quark or gluon, or heavy-flavor jets. The resulting uncertainty in the data-to-simulation agreement affects the yields and BDT output shapes of multiple physics processes. The statistical component of this uncertainty is treated as uncorrelated across different data-taking years, while other experimental sources are correlated.

The integrated luminosities for data collected in 2016, 2017, and 2018 have 1.2–2.5% individual uncertainties [59–61], while the overall uncertainty for the 2016–2018 period is

1.6%. The uncertainty in the measured cross section for inelastic pp collisions, amounting to 5% [128], is taken into account by varying the number of pileup interactions in MC simulation, which impacts the jet reconstruction and the isolation of ℓ and τ_{h}.

The sources of systematic uncertainty which create the largest uncertainties in the measured ratio of the HH production cross section to its SM prediction are the theoretical uncertainties in the HH production cross section and decay branching fractions (25%), the uncertainties in the rate and shape of backgrounds from misidentified ℓ or τ_{h} (22%), and in the rates of backgrounds modeled using MC simulation (13%). These uncertainties in the signal measurement are determined by removing uncertainties that correspond to a given systematic source from an ML fit to pseudodata, as described in section 9, and subtracting the obtained uncertainty in the signal measurement in quadrature from the total uncertainty. The impacts of systematic uncertainties are small compared to the effect of the statistical uncertainty in the data (79%), and are comparable to the statistical uncertainties in the distributions in the BDT classifier output for background processes (33%). The latter includes the effect of statistical uncertainties in the MC simulation and in the ℓ/τ_{h} misidentification and electron charge misidentification backgrounds obtained from data. All other sources of uncertainty have an impact of 5% or less.

9 Results

The data selected in the seven search categories are tested against multiple HH production hypotheses: the SM prediction; variations of the SM coupling strength modifiers κ_λ, κ_{t}, κ_{V}, and κ_{2V}; the effective couplings c_{g}, c_{2g}, and c_2 in the EFT approach; and resonant production of H boson pairs originating from the decay of heavy particles with spins of 0 or 2 and masses m_{X} ranging from 250 to 1000 GeV. In each case, the data observed in the seven search categories is fit simultaneously to a model composed of the background prediction (with uncertainties) and the HH signal hypothesis under consideration. The distributions in m_{T} in the 3ℓ WZ CR and in $m_{4\ell}$ in the 4ℓ ZZ CR shown in figure 5 are included in these fits, in order to obtain in-situ constraints on the systematic uncertainties described in section 8. This in turn reduces the uncertainties in the signal and background predictions.

The SM "signal strength" parameter μ is defined as the ratio of the measured HH production cross section to its predicted value in the SM. This parameter modifies the expected signal yield by the same proportion in each category. By contrast, variations in the κ modifiers may affect the signal yields in each category differently, and also change the BDT classifier output shape for HH events. The twenty benchmark scenarios spanning combinations of κ_λ, κ_{t}, c_{g}, c_{2g}, and c_2 values in the coupling parameter space each correspond to different kinematic distributions, so the HH production cross section for each point is measured separately. Similarly, signal efficiency and BDT classifier output shapes vary dramatically for different resonant masses, and thus a separate measurement is performed for each mass and spin hypothesis. The SM signal strength measurement is performed using the output of the BDT classifier that has been trained for SM nonresonant HH production, while the κ_λ measurement uses the BDT trained for benchmark scenario

JHEP04 BM7. In the scenario JHEP04 BM7, the m_{HH} value tends to be close to the lower limit of $250\,\mathrm{GeV}$, which matches the event kinematics for nonresonant HH production in the κ_λ range of the expected limit. When setting limits on the twenty different benchmark scenarios, the binary BDT inputs correspond to the given scenario, or in case of the benchmarks from ref. [96] the kinematically closest scenario. In case of resonant HH production, the BDT input for the resonance mass is set to the m_{X} value for which the limit is computed.

The SM signal strength is measured using a profile likelihood test statistic [129], with systematic uncertainties treated as nuisance parameters θ in a frequentist approach [130]. The effect of variations in θ on the shape of the BDT classifier output distribution for the HH signal and for background processes is incorporated into the ML fit using the technique described in ref. [131]. Statistical uncertainties in these distributions are also taken into account using the approach detailed in ref. [131]. The likelihood ratio q_μ for a fixed "test" signal strength value μ is

$$q_\mu = -2\Delta \ln \mathcal{L} = -2 \ln \frac{\mathcal{L}(\mathrm{data}|\mu, \hat{\theta}_\mu)}{\mathcal{L}(\mathrm{data}|\hat{\mu}, \hat{\theta})},$$

where $\hat{\mu}$ and $\hat{\theta}$ are the signal strength and nuisance parameter values that give the maximum value of the likelihood function $\mathcal{L}$ for the given set of data (requiring $\hat{\mu} \geq 0$), and $\hat{\theta}_\mu$ is the set of θ values which maximize $\mathcal{L}$ for the fixed μ. The 95% confidence level (CL) upper limit for μ is obtained using the CL_{s} criterion [132, 133], with q_μ set to 0 when $\mu < \hat{\mu}$. The probabilities to observe a given value of the likelihood ratio q_μ under the signal-plus-background and background-only hypotheses are computed using the asymptotic approximation from ref. [129]. The limits on μ obtained using the asymptotic approximation, match the limits obtained with toy MC experiments [130] within 10%. The SM coupling strength modifiers and the cross sections for the various HH production hypotheses are measured by scanning the likelihood ratio q_μ as a function of μ. Theoretical and experimental uncertainties affecting the signal and background yields or the shape of the BDT classifier output distributions may be correlated or uncorrelated across different years, search categories, and BDT output bins, as described in section 8.

For the case of nonresonant HH production with event kinematics as predicted by the SM, the best-fit value of the HH production rate, obtained from the simultaneous fit of all seven search categories, amounts to $\hat{\mu} = 2 \pm 8\,(\mathrm{stat.}) \pm 6\,(\mathrm{syst.})$ times the SM expectation. The measured value of the signal strength refers to the sum of ggHH and qqHH production and is compatible with both the SM and background-only hypotheses, within statistical and systematic uncertainties. Distributions in the output of the BDT classifier for SM nonresonant HH production in the seven search categories are shown in figures 7 and 8, and the corresponding expected event yields are given in table 7. The data excess in the rightmost bin of the BDT classifier output distribution for the 3ℓ category is not statistically significant: 11 events are observed in this bin, while $5.2 \pm 0.7\,(\mathrm{stat.}) \pm 0.2\,(\mathrm{syst.})$ are expected from background processes, amounting to a local significance of about 1.7 standard deviations. The observed (expected) 95% CL upper limit on the cross section for
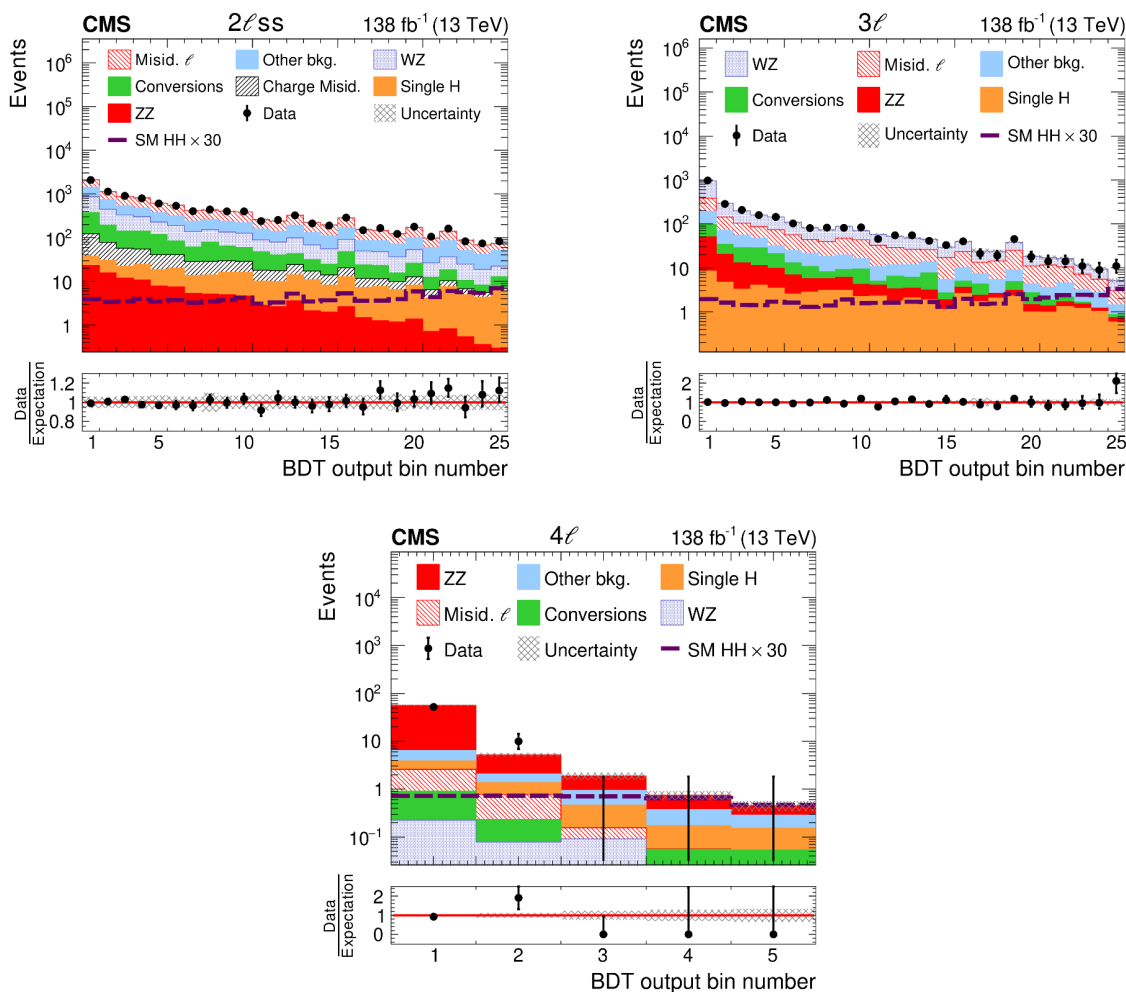
Figure 7. Distribution in the output of the BDT trained for nonresonant HH production and evaluated for the benchmark scenario JHEP04 BM7 for the 2ℓss (upper left), 3ℓ (upper right), and 4ℓ (lower) categories. The SM HH signal is shown for a cross section amounting to 30 times the value predicted in the SM. The normalization and shape of the distributions expected for the background processes are shown for the values of nuisance parameters obtained from the ML fit of the signal+background hypothesis to the data. The gray shaded area indicates the sum of statistical and systematic uncertainties on the background prediction obtained from the ML fit. No data events are observed in the three rightmost bins of the BDT output distribution in the 4ℓ category.

nonresonant HH production is 651 (592) fb. Taking into account the theoretical uncertainties in the SM HH production cross section, this corresponds to an observed (expected) limit on the nonresonant HH production rate of 21.3 (19.4) times the SM expectation. These limits are shown in figure 9 for individual categories and for the combination of all seven search categories, which is referred to as the "HH → multilepton" result. The 3ℓ and $1\ell + 3\tau_{\mathrm{h}}$ categories are the most sensitive to SM HH production, followed closely by the other categories.

Process	$2\ell\mathrm{ss}$	3ℓ	4ℓ
SM HH $\to$ WW*WW* ($\times 30$)	73 ± 6	33 ± 3	2.2 ± 0.2
SM HH $\to$ WW$^*\tau\tau$ ($\times 30$)	31 ± 3	12 ± 1	0.9 ± 0.1
SM HH $\to \tau\tau\tau\tau$ ($\times 30$)	3 ± 0	1 ± 0	0.1 ± 0.0
WZ	2003 ± 58	1321 ± 27	0.4 ± 0.1
ZZ	121 ± 2	109 ± 2	54.7 ± 1.8
Misidentified ℓ	3939 ± 267	670 ± 55	2.3 ± 1.0
Conversion electrons	1009 ± 170	146 ± 24	0.9 ± 0.4
Electron charge misid.	366 ± 52	—	—
Single Higgs boson	216 ± 4	62 ± 1	2.4 ± 0.3
Other backgrounds	2690 ± 224	293 ± 20	4.1 ± 0.4
Total expected background	$10\,346 \pm 396$	2601 ± 68	64.8 ± 2.1
Data	$10\,344$	2621	62

Process	$3\ell + 1\tau_\mathrm{h}$	$2\ell + 2\tau_\mathrm{h}$	$1\ell + 3\tau_\mathrm{h}$	$4\tau_\mathrm{h}$
SM HH $\to$ WW*WW* ($\times 30$)	0.9 ± 0.1	0.2 ± 0.0	0.2 ± 0.0	0.3 ± 0.0
SM HH $\to$ WW$^*\tau\tau$ ($\times 30$)	4.1 ± 0.3	3.9 ± 0.4	0.6 ± 0.1	0.1 ± 0.0
SM HH $\to \tau\tau\tau\tau$ ($\times 30$)	0.9 ± 0.1	2.3 ± 0.3	2.6 ± 0.4	1.3 ± 0.2
WZ	0.2 ± 0.0	<0.1	<0.1	<0.1
ZZ	24.3 ± 0.8	18.5 ± 1.0	1.9 ± 0.2	0.7 ± 0.1
Misidentified ℓ and τ_h	25.1 ± 4.4	33.5 ± 4.6	2.1 ± 1.7	1.5 ± 0.9
Conversion electrons	0.1 ± 0.0	0.1 ± 0.1	<0.1	<0.1
Single Higgs boson	3.8 ± 0.2	2.9 ± 0.5	0.8 ± 0.4	0.4 ± 0.1
Other backgrounds	2.7 ± 0.3	2.1 ± 0.4	0.1 ± 0.0	<0.1
Total expected background	56.2 ± 4.5	57.0 ± 4.8	4.9 ± 1.7	2.6 ± 0.9
Data	55	55	6	1

Process	3ℓ WZ CR	4ℓ ZZ CR
WZ	$12\,546 \pm 148$	<1
ZZ	799 ± 24	2032 ± 60
Misidentified ℓ	908 ± 122	13 ± 4
Conversion electrons	134 ± 22	3 ± 0
Other backgrounds	620 ± 54	59 ± 6
Total expected background	$15\,006 \pm 202$	2108 ± 60
Data	$14\,994$	2096

Table 7. The number of expected and observed events in each of the seven search categories, and in two CRs, which validate the modeling of the WZ and ZZ backgrounds. The ℓ/τ_h misidentification and electron charge misidentification backgrounds are determined from data, as described in section 7, while the HH signal and all other backgrounds are modeled using MC simulation. The symbol "—" indicates that the background is not relevant for the category. The HH signal represents the sum of the ggHH and qqHH production processes and is normalized to 30 times the event yield expected in the SM, corresponding to a cross section of about 1 pb. The expected event yields are computed for the values of nuisance parameters obtained from the ML fit described in section 9. Quoted uncertainties represent the sum of statistical and systematic components. Uncertainties that are smaller than half the value of the least significant digit have been rounded to zero.
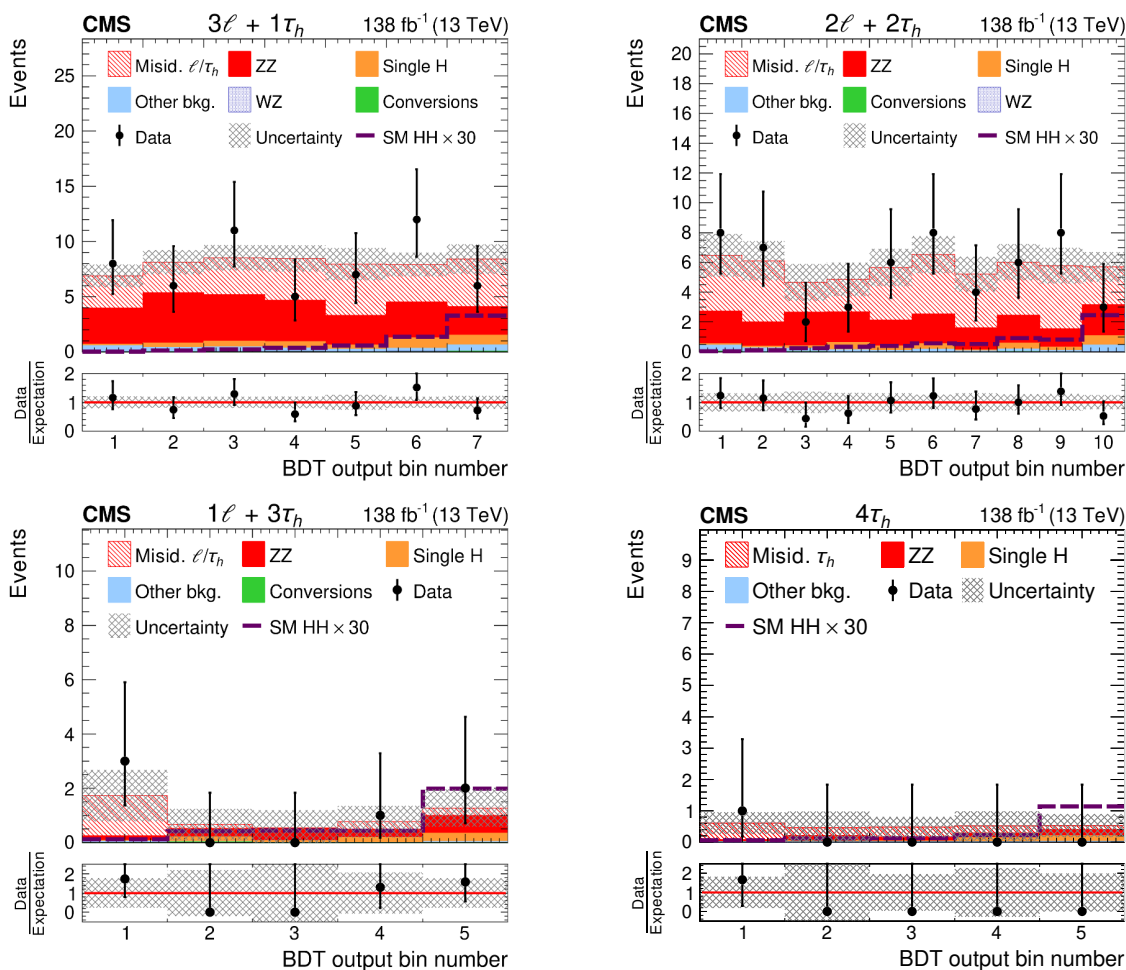
Figure 8. Distribution in the output of the BDT trained for nonresonant HH production and evaluated for the benchmark scenario JHEP04 BM7 for the $3\ell + 1\tau_h$ (upper left), $2\ell + 2\tau_h$ (upper right), $1\ell + 3\tau_h$ (lower left), and $4\tau_h$ (lower right) categories. The SM HH signal is shown for a cross section amounting to 30 times the value predicted in the SM. The normalization and shape of the distributions expected for the background processes are shown for the values of nuisance parameters obtained from the ML fit of the signal+background hypothesis to the data. The gray shaded area indicates the sum of statistical and systematic uncertainties on the background prediction obtained from the ML fit.

The observed (expected) 95% CL interval for the H boson trilinear self-coupling strength modifier is measured to be $-6.9 < \kappa_\lambda < 11.1$ ($-6.9 < \kappa_\lambda < 11.7$). The upper limit on κ_λ is one of the strongest constraints on this fundamental SM parameter to date, with only HH searches in the bb$\gamma\gamma$ [42, 43] and bbbb [45] decay modes providing tighter bounds. The observed and expected upper limits on the HH production cross section as a function of κ_λ, obtained from the simultaneous fit of all seven search categories, are shown in figure 10, along with the limits obtained for each category individually.

The observed and expected limits on the ggHH production cross section for the twenty benchmark scenarios are shown in figure 11 and summarized in table 8. Signal contribu-
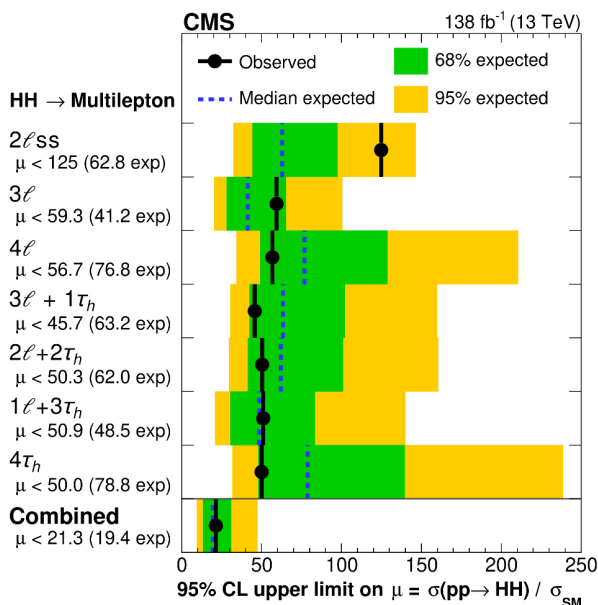
Figure 9. Observed and expected 95% CL upper limits on the SM HH production cross section, obtained for both individual search categories and from a simultaneous fit of all seven categories combined.
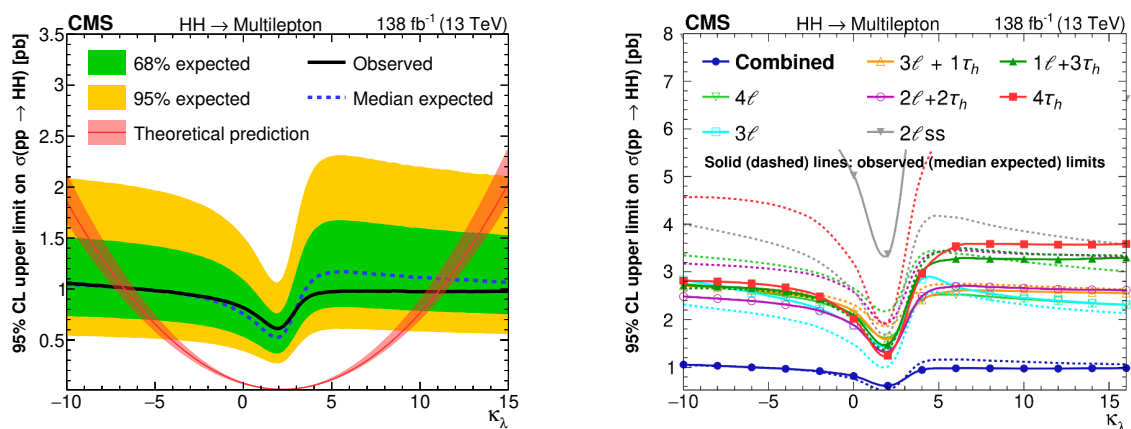
Figure 10. Observed and expected 95% CL upper limits on the HH production cross section as a function of the H boson self-coupling strength modifier κ_λ. All H boson couplings other than λ are assumed to have the values predicted in the SM. The left plot shows the result obtained by combining all seven search categories, while the right plot shows the limits obtained for each category separately. The red curve in the left plot represents the SM prediction for the HH production cross section as a function of κ_λ, and the red shaded band the theoretical uncertainty in this prediction.
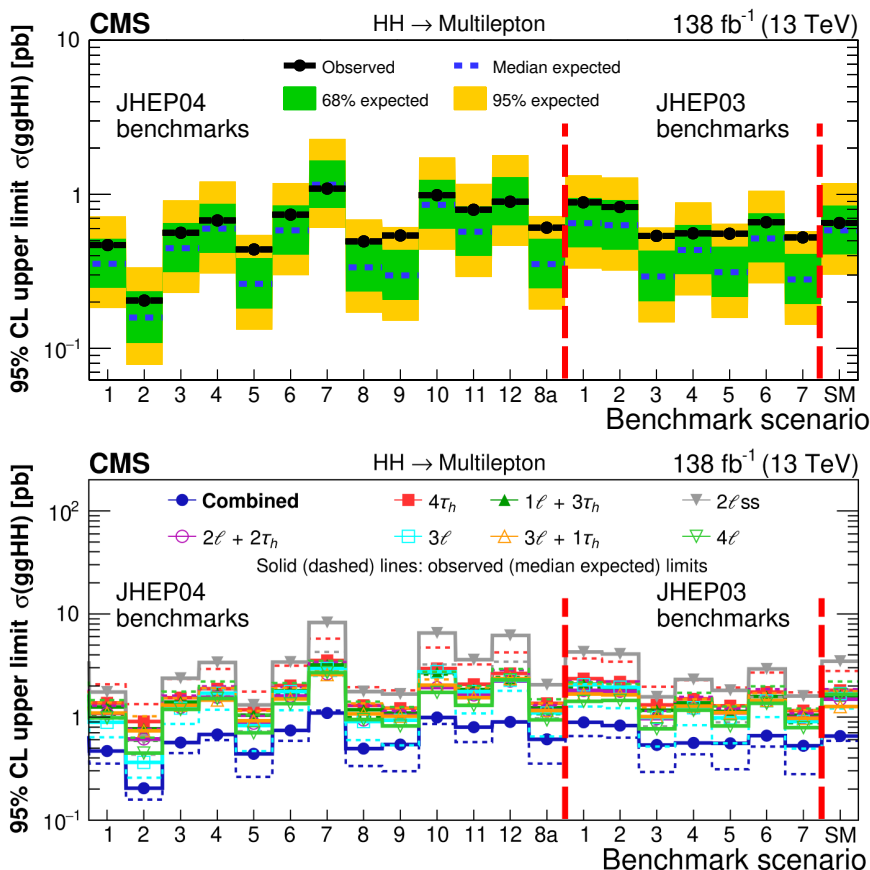
Figure 11. Observed and expected 95% CL upper limits on the HH production cross section for the twelve benchmark scenarios from ref. [24], the additional benchmark scenario 8a from ref. [97], the seven benchmark scenarios from ref. [96], and for the SM. The upper plot shows the result obtained by combining all seven search categories, while the lower plot shows the limits obtained for each category separately, and the combined limit.

tions from the qqHH process, at the rate expected in the SM, are about two orders of magnitude lower than the limits that we set on the rate of the ggHH signal in these measurements and are therefore neglected. The observed (expected) limits on nonresonant HH production in the different benchmark scenarios range from 0.21 to 1.09 (0.16 to 1.16) pb, depending on the scenario. These limits are a factor of 2–3 higher than those obtained by the CMS measurement in the bb$\gamma\gamma$ final state [42]. The variation in expected limits reflects differences in the m_{HH} distribution among the benchmark scenarios, which in turn affect the p_{T} and angles between the particles produced in the H boson decays. As a consequence, the signal acceptance can change, along with the separation of the HH signal from backgrounds through the BDT classifiers described in section 6. The most and least stringent limits on the cross section are expected for the benchmark scenarios JHEP04 BM2 and BM7, respectively. The former has a pronounced tail of the m_{HH} distribution extending to high values, while the latter is characterized by low m_{HH} values, as seen in figure 5 of ref. [24].

| JHEP04 | Observed (expected) |
benchmark	limit [fb]
BM1	469 (354)
BM2	205 (159)
BM3	563 (447)
BM4	677 (600)
BM5	439 (263)
BM6	739 (584)
BM7	1090 (1156)
BM8	495 (336)
BM9	541 (298)
BM10	988 (855)
BM11	795 (572)
BM12	897 (898)
BM8a	608 (353)
JHEP03	Observed (expected)
benchmark	limit [fb]
BM1	888 (650)
BM2	828 (632)
BM3	538 (293)
BM4	559 (436)
BM5	556 (313)
BM6	660 (518)
BM7	525 (280)

Table 8. Observed (expected) 95% CL upper limits on the ggHH production cross section for the twelve benchmark scenarios from ref. [24], the additional benchmark scenario 8a from ref. [97] and the seven benchmark scenarios from ref. [96]. The corresponding observed (expected) upper limit for the SM is 652 (583) fb. The limits correspond to the combination of all seven search categories.

Figure 12 shows the observed and expected upper limits on the HH production cross section as a function of the coupling c_2, and the region excluded in the κ_t–c_2 plane. The effects of variations in κ_λ and κ_t on the rate of the SM single H boson background [21] and on the H boson decay branching fractions [20] are taken into account when computing these limits and those shown in figure 10. The magnitude of these effects is typically 5 to 10% within the scanned range of κ_λ and κ_t. Assuming κ_t and κ_λ are both equal to 1, the coupling c_2 is observed (expected) to be constrained to the interval $-1.05 < c_2 < 1.48$ ($-0.96 < c_2 < 1.37$) at 95% CL.

Similar to the right part of figure 12, Figure 13 shows the observed and expected regions excluded in the κ_t–κ_λ and κ_λ–c_2 planes.

Figure 14 shows the observed and expected limits on the resonant HH production cross section as a function of m_X for a spin-0 or spin-2 particle X decaying to HH. The mass points probed are listed in the fourth paragraph of section 3. The limits are expected to become more stringent as m_X increases, as the acceptance for the HH signal increases and the signal can be more easily distinguished from backgrounds. The observed (expected) 95% CL upper limits on the resonant HH production cross section range from 0.18 to 0.90 (0.08 to 1.06) pb, depending on the mass and spin. Tabulated results are provided
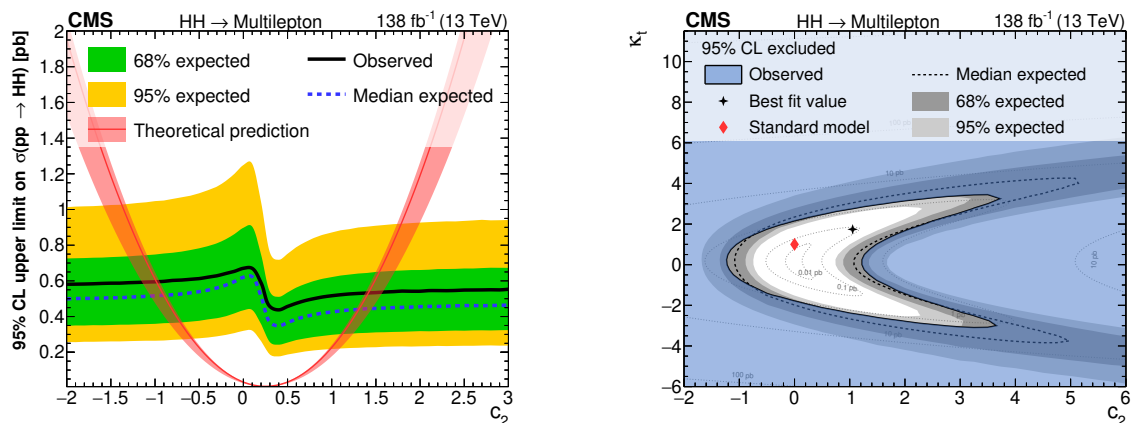
Figure 12. Observed and expected limits on the HH production cross section as a function of the effective coupling c_2 (left), and the region excluded in the κ_t–c_2 plane (right). All limits are computed at 95% CL. H boson couplings other than the ones shown in the plots (c_2 in the left plot and c_2 and κ_t in the right plot) are assumed to have the values predicted by the SM.
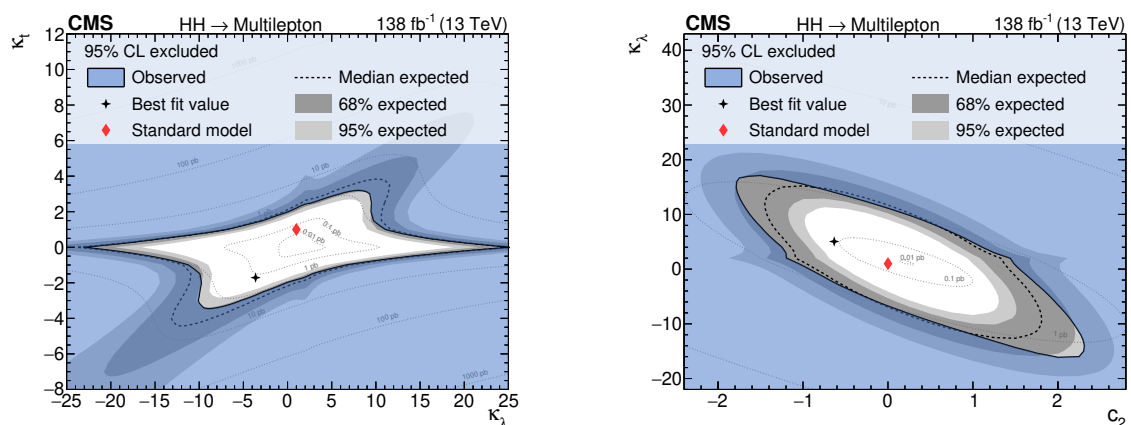
Figure 13. Observed and expected regions excluded in the κ_t–κ_λ (left) and κ_λ–c_2 (right) planes. H boson couplings other than the ones shown in the plots (κ_λ and κ_t in the left plot, and c_2 and κ_λ in the right plot) are assumed to have the values predicted by the SM.

in the HEPData record for this analysis [134]. Only the ATLAS search in the bb$\gamma\gamma$ final state achieves more stringent limits at low masses (close to 250 GeV) [43], while the low-mass limits from ATLAS in the bb$\tau\tau$ decay mode are roughly the same [35]. Both these analyses, along with the ATLAS search for bbbb decays [33], set much more stringent limits at higher masses.

For $m_X \gtrsim 600$ GeV, the observed limit is less stringent than the expected limit, due to a small excess of events in the data that is concentrated near $m_X = 750$ GeV in the 2ℓss and 3ℓ categories. The distributions in the output of the BDT classifier targeting resonances with spin 2 and mass 750 GeV in the 2ℓss and 3ℓ categories are shown in figure 15. A small excess of events can be seen in the rightmost bin of both distributions. In the 2ℓss (3ℓ) category, 42 (17) events are observed in this bin in the data, while $27.3 \pm 2.8\,(\text{stat.}) \pm 0.7\,(\text{syst.})$ $(8.0 \pm 0.8\,(\text{stat.}) \pm 0.5\,(\text{syst.}))$ are expected from background processes, amounting to a
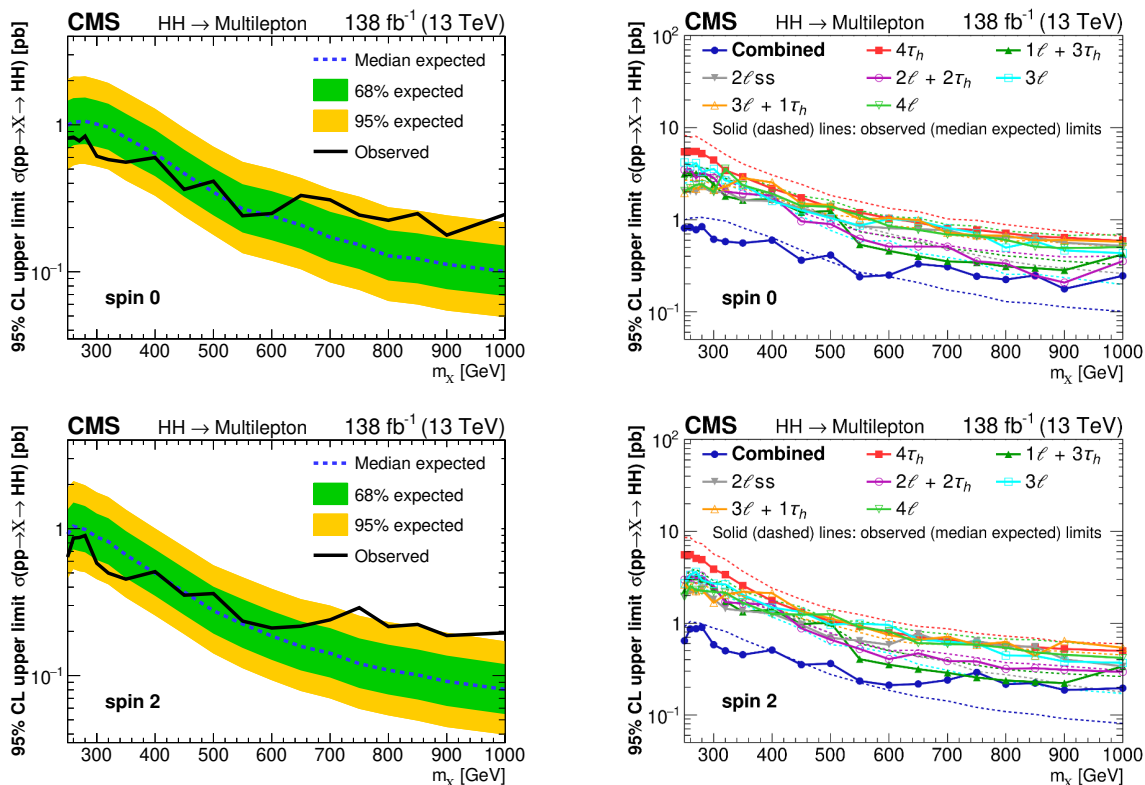
Figure 14. Observed and expected 95% CL upper limits on the production of new particles X of spin 0 (upper) and spin 2 (lower) and mass m_X in the range 250–1000 GeV, which decay to H boson pairs. The plot on the left shows the result obtained by combining all seven search categories, while the plot on the right shows the limits obtained for each category separately, and the combined limit.

local significance of about 2.1 (2.1) standard deviations. The excess affects the observed limits in a broad mass range from 600 to 1000 GeV. No measurement is made for masses above 1000 GeV, as limits on HH decays producing at least one bottom quark pair are much more stringent in this phase space [33, 34]. The presence of multiple neutrinos in HH signal events in these categories, coming from W boson or τ lepton decays, limits the experimental resolution on m_X and causes the BDT classifier output distributions to be highly correlated for resonances of similar mass. No significant excess is observed in any of the other five search categories. The significance for the combination of all seven search categories at 750 GeV amounts to 1.9 standard deviations, without accounting for the "look elsewhere effect" [135].

10 Summary

The results of a search for nonresonant and resonant Higgs boson pair (HH) production in final states with multiple reconstructed leptons, including electrons and muons (ℓ) and hadronically decaying tau leptons (τ_h), has been presented. The search targets the HH decay modes WW^*WW^*, $WW^*\tau\tau$, and $\tau\tau\tau\tau$, using proton-proton collision data recorded by the CMS experiment at a center-of-mass energy of 13 TeV and corresponding to an
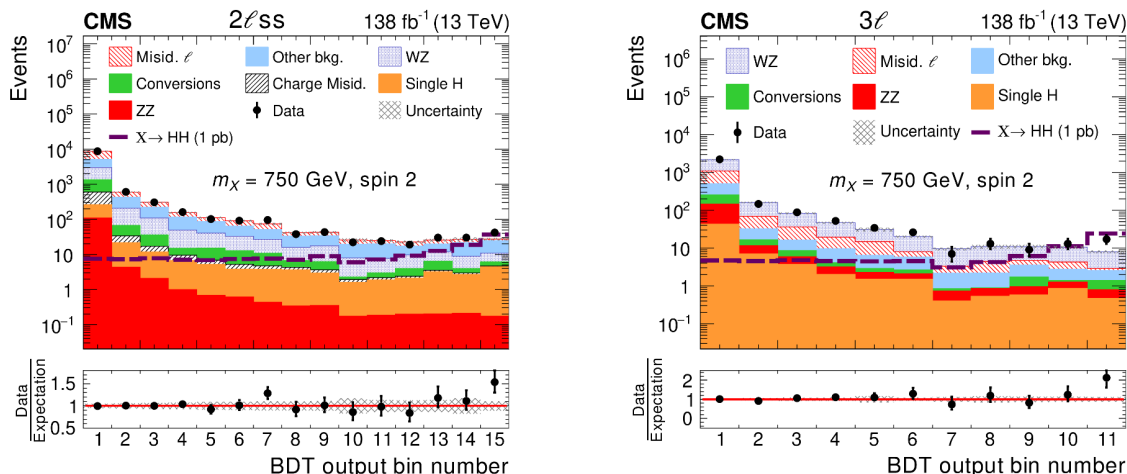
Figure 15. Distribution in BDT classifier output for resonances of spin 2 and mass 750 GeV in the 2ℓss (left) and 3ℓ (right) categories. The resonant HH signal is shown for a cross section amounting to 1 pb. The distributions expected for the background processes are shown for the values of nuisance parameters obtained from the ML fit of the signal+background hypothesis to the data.

integrated luminosity of 138 fb^{-1}. Seven search categories, distinguished by ℓ and τ_h multiplicity, are included in the analysis: 2ℓss, 3ℓ, 4ℓ, 3ℓ + 1τ_h, 2ℓ + 2τ_h, 1ℓ + 3τ_h, and 4τ_h, where "ss" indicates an $\ell\ell$ pair with the same charge. No evidence for a signal is found in the data. Upper limits on the cross sections for both nonresonant and resonant HH production are set. The observed (expected) limits on the nonresonant HH production cross section in twenty EFT benchmark scenarios range from 0.21 to 1.09 (0.16 to 1.16) pb at 95% confidence level (CL), depending on the scenario. For nonresonant HH production with event kinematics as predicted by the standard model (SM), the observed (expected) 95% CL upper limit on the HH production rate is 21.3 (19.4) times the rate expected in the SM. The results of the search for nonresonant HH production are used to exclude regions in the plane of the H boson coupling to the top quark, y_t, and of the trilinear Higgs boson self-coupling, λ. Assuming y_t has the value expected in the SM, the observed (expected) 95% CL interval for λ is between -6.9 and 11.1 (-6.9 and 11.7) times the value expected in the SM. The resonant production of H boson pairs, resulting from decays of new heavy particles X with mass m_X, is probed within the mass range 250–1000 GeV. The corresponding observed (expected) 95% CL upper limits on the cross section for resonant HH production range from 0.18 to 0.90 (0.08 to 1.06) pb, depending on the mass and spin of the resonance.

Acknowledgments

We congratulate our colleagues in the CERN accelerator departments for the excellent performance of the LHC and thank the technical and administrative staffs at CERN and at other CMS institutes for their contributions to the success of the CMS effort. In addition, we gratefully acknowledge the computing centers and personnel of the Worldwide

References

[1] ATLAS collaboration, *Observation of a new particle in the search for the Standard Model Higgs boson with the ATLAS detector at the LHC*, *Phys. Lett. B* **716** (2012) 1 [`arXiv:1207.7214`] [InSPIRE].

[2] CMS collaboration, *Observation of a new boson at a mass of* 125 *GeV with the CMS experiment at the LHC*, *Phys. Lett. B* **716** (2012) 30 [`arXiv:1207.7235`] [InSPIRE].

[3] CMS collaboration, *Observation of a new boson with mass near* 125 *GeV in pp collisions at* $\sqrt{s} = 7$ *and* 8 *TeV*, *JHEP* **06** (2013) 081 [`arXiv:1303.4571`] [InSPIRE].

[4] CMS collaboration, *Combined measurements of Higgs boson couplings in proton–proton collisions at* $\sqrt{s} = 13$ *TeV*, *Eur. Phys. J. C* **79** (2019) 421 [`arXiv:1809.10733`] [InSPIRE].

[5] ATLAS collaboration, *Combined measurements of Higgs boson production and decay using up to* 80 fb^{-1} *of proton-proton collision data at* $\sqrt{s} = 13$ *TeV collected with the ATLAS experiment*, *Phys. Rev. D* **101** (2020) 012002 [`arXiv:1909.02845`] [InSPIRE].

[6] CMS collaboration, *Measurement of the Higgs boson width and evidence of its off-shell contributions to ZZ production*, *Nature Phys.* **18** (2022) 1329 [`arXiv:2202.06923`] [InSPIRE].

[7] F. Englert and R. Brout, *Broken symmetry and the mass of gauge vector mesons*, *Phys. Rev. Lett.* **13** (1964) 321 [InSPIRE].

[8] P.W. Higgs, *Broken symmetries, massless particles and gauge fields*, *Phys. Lett.* **12** (1964) 132 [InSPIRE].

[9] P.W. Higgs, *Broken symmetries and the masses of gauge bosons*, *Phys. Rev. Lett.* **13** (1964) 508 [InSPIRE].

[10] G.S. Guralnik, C.R. Hagen and T.W.B. Kibble, *Global conservation laws and massless particles*, *Phys. Rev. Lett.* **13** (1964) 585 [InSPIRE].

[11] P.W. Higgs, *Spontaneous symmetry breakdown without massless bosons*, *Phys. Rev.* **145** (1966) 1156 [InSPIRE].

[12] T.W.B. Kibble, *Symmetry breaking in non-Abelian gauge theories*, *Phys. Rev.* **155** (1967) 1554 [InSPIRE].

[13] S.L. Glashow, *Partial symmetries of weak interactions*, *Nucl. Phys.* **22** (1961) 579 [InSPIRE].

[14] S. Weinberg, *A model of leptons*, *Phys. Rev. Lett.* **19** (1967) 1264 [InSPIRE].

[15] A. Salam, *Weak and electromagnetic interactions*, *Conf. Proc. C* **680519** (1968) 367 [InSPIRE].

[16] D. de Florian, I. Fabre and J. Mazzitelli, *Triple Higgs production at hadron colliders at NNLO in QCD*, *JHEP* **03** (2020) 155 [`arXiv:1912.02760`] [InSPIRE].

[17] O. Aberle et al., *High-Luminosity Large Hadron Collider (HL-LHC): Technical Design Report V. 0.1*, CERN-2017-007-M (2017) [DOI:10.23731/CYRM-2017-004] [INSPIRE].

[18] M. Grazzini et al., *Higgs boson pair production at NNLO with top quark mass effects*, *JHEP* **05** (2018) 059 [arXiv:1803.02463] [INSPIRE].

[19] F.A. Dreyer and A. Karlberg, *Vector-boson fusion Higgs pair production at N^3LO*, *Phys. Rev. D* **98** (2018) 114016 [arXiv:1811.07906] [INSPIRE].

[20] G. Degrassi, P.P. Giardino, F. Maltoni and D. Pagani, *Probing the Higgs self coupling via single Higgs production at the LHC*, *JHEP* **12** (2016) 080 [arXiv:1607.04251] [INSPIRE].

[21] F. Maltoni, D. Pagani, A. Shivaji and X. Zhao, *Trilinear Higgs coupling determination via single-Higgs differential measurements at the LHC*, *Eur. Phys. J. C* **77** (2017) 887 [arXiv:1709.08649] [INSPIRE].

[22] W. Buchmuller and D. Wyler, *Effective Lagrangian analysis of new interactions and flavor conservation*, *Nucl. Phys. B* **268** (1986) 621 [INSPIRE].

[23] B. Grzadkowski, M. Iskrzynski, M. Misiak and J. Rosiek, *Dimension-six terms in the Standard Model Lagrangian*, *JHEP* **10** (2010) 085 [arXiv:1008.4884] [INSPIRE].

[24] A. Carvalho et al., *Higgs pair production: choosing benchmarks with cluster analysis*, *JHEP* **04** (2016) 126 [arXiv:1507.02245] [INSPIRE].

[25] N. Craig, J. Galloway and S. Thomas, *Searching for signs of the second Higgs doublet*, arXiv:1305.2424 [INSPIRE].

[26] D.T. Nhung, M. Mühlleitner, J. Streicher and K. Walz, *Higher order corrections to the trilinear Higgs self-couplings in the real NMSSM*, *JHEP* **11** (2013) 181 [arXiv:1306.3926] [INSPIRE].

[27] R. Grober and M. Mühlleitner, *Composite Higgs boson pair production at the LHC*, *JHEP* **06** (2011) 020 [arXiv:1012.1562] [INSPIRE].

[28] R. Contino et al., *Strong double Higgs production at the LHC*, *JHEP* **05** (2010) 089 [arXiv:1002.1011] [INSPIRE].

[29] C. Englert, T. Plehn, D. Zerwas and P.M. Zerwas, *Exploring the Higgs portal*, *Phys. Lett. B* **703** (2011) 298 [arXiv:1106.3097] [INSPIRE].

[30] J.M. No and M. Ramsey-Musolf, *Probing the Higgs portal at the LHC through resonant di-Higgs production*, *Phys. Rev. D* **89** (2014) 095031 [arXiv:1310.6035] [INSPIRE].

[31] L. Randall and R. Sundrum, *A large mass hierarchy from a small extra dimension*, *Phys. Rev. Lett.* **83** (1999) 3370 [hep-ph/9905221] [INSPIRE].

[32] K.-M. Cheung, *Phenomenology of radion in Randall-Sundrum scenario*, *Phys. Rev. D* **63** (2001) 056007 [hep-ph/0009232] [INSPIRE].

[33] ATLAS collaboration, *Search for resonant pair production of Higgs bosons in the $b\bar{b}b\bar{b}$ final state using pp collisions at $\sqrt{s} = 13$ TeV with the ATLAS detector*, *Phys. Rev. D* **105** (2022) 092002 [arXiv:2202.07288] [INSPIRE].

[34] CMS collaboration, *Search for heavy resonances decaying to a pair of Lorentz-boosted Higgs bosons in final states with leptons and a bottom quark pair at $\sqrt{s} = 13$ TeV*, *JHEP* **05** (2022) 005 [arXiv:2112.03161] [INSPIRE].

[35] ATLAS collaboration, *Search for resonant and non-resonant Higgs boson pair production in the $b\bar{b}\tau^+\tau^-$ decay channel using 13 TeV pp collision data from the ATLAS detector*, arXiv:2209.10910 [InSPIRE].

[36] U. Baur, T. Plehn and D.L. Rainwater, *Measuring the Higgs boson self coupling at the LHC and finite top mass matrix elements*, *Phys. Rev. Lett.* **89** (2002) 151801 [hep-ph/0206024] [InSPIRE].

[37] U. Baur, T. Plehn and D.L. Rainwater, *Determining the Higgs boson selfcoupling at hadron colliders*, *Phys. Rev. D* **67** (2003) 033003 [hep-ph/0211224] [InSPIRE].

[38] Q. Li, Z. Li, Q.-S. Yan and X. Zhao, *Probe Higgs boson pair production via the $3\ell\,2j+\not{E}$ mode*, *Phys. Rev. D* **92** (2015) 014015 [arXiv:1503.07611] [InSPIRE].

[39] A. Adhikary et al., *Revisiting the non-resonant Higgs pair production at the HL-LHC*, *JHEP* **07** (2018) 116 [arXiv:1712.05346] [InSPIRE].

[40] J. Ren et al., *LHC search of new Higgs boson via resonant di-Higgs production with decays into 4W*, *JHEP* **06** (2018) 090 [arXiv:1706.05980] [InSPIRE].

[41] ATLAS collaboration, *Search for Higgs boson pair production in the $WW^{(*)}WW^{(*)}$ decay channel using ATLAS data recorded at $\sqrt{s} = 13$ TeV*, *JHEP* **05** (2019) 124 [arXiv:1811.11028] [InSPIRE].

[42] CMS collaboration, *Search for nonresonant Higgs boson pair production in final states with two bottom quarks and two photons in proton-proton collisions at $\sqrt{s} = 13$ TeV*, *JHEP* **03** (2021) 257 [arXiv:2011.12373] [InSPIRE].

[43] ATLAS collaboration, *Search for Higgs boson pair production in the two bottom quarks plus two photons final state in pp collisions at $\sqrt{s} = 13$ TeV with the ATLAS detector*, *Phys. Rev. D* **106** (2022) 052001 [arXiv:2112.11876] [InSPIRE].

[44] ATLAS collaboration, *Search for the $HH \to b\bar{b}b\bar{b}$ process via vector-boson fusion production using proton-proton collisions at $\sqrt{s} = 13$ TeV with the ATLAS detector*, *JHEP* **07** (2020) 108 [*Erratum ibid.* **01** (2021) 145] [arXiv:2001.05178] [InSPIRE].

[45] CMS collaboration, *Search for Higgs boson pair production in the four b quark final state in proton-proton collisions at $\sqrt{s} = 13$ TeV*, *Phys. Rev. Lett.* **129** (2022) 081802 [arXiv:2202.09617] [InSPIRE].

[46] CMS collaboration, *Search for nonresonant pair production of highly energetic Higgs bosons decaying to bottom quarks*, arXiv:2205.06667 [InSPIRE].

[47] CMS collaboration, *Search for resonant pair production of Higgs bosons decaying to bottom quark-antiquark pairs in proton-proton collisions at 13 TeV*, *JHEP* **08** (2018) 152 [arXiv:1806.03548] [InSPIRE].

[48] CMS collaboration, *Search for nonresonant Higgs boson pair production in final state with two bottom quarks and two tau leptons in proton-proton collisions at $\sqrt{s} = 13$ TeV*, *Phys. Lett. B* **842** (2023) 137531 [arXiv:2206.09401] [InSPIRE].

[49] ATLAS collaboration, *Reconstruction and identification of boosted di-τ systems in a search for Higgs boson pairs using 13 TeV proton-proton collision data in ATLAS*, *JHEP* **11** (2020) 163 [arXiv:2007.14811] [InSPIRE].

[50] CMS collaboration, *Search for resonant and nonresonant Higgs boson pair production in the $b\bar{b}\ell\nu\ell\nu$ final state in proton-proton collisions at $\sqrt{s} = 13$ TeV*, *JHEP* **01** (2018) 054 [arXiv:1708.04188] [InSPIRE].

[51] ATLAS collaboration, *Search for non-resonant Higgs boson pair production in the $bb\ell\nu\ell\nu$ final state with the ATLAS detector in pp collisions at $\sqrt{s} = 13$ TeV*, *Phys. Lett. B* **801** (2020) 135145 [arXiv:1908.06765] [INSPIRE].

[52] ATLAS collaboration, *Search for Higgs boson pair production in the $b\bar{b}WW^*$ decay mode at $\sqrt{s} = 13$ TeV with the ATLAS detector*, *JHEP* **04** (2019) 092 [arXiv:1811.04671] [INSPIRE].

[53] ATLAS collaboration, *Search for Higgs boson pair production in the $\gamma\gamma WW^*$ channel using pp collision data recorded at $\sqrt{s} = 13$ TeV with the ATLAS detector*, *Eur. Phys. J. C* **78** (2018) 1007 [arXiv:1807.08567] [INSPIRE].

[54] CMS collaboration, *Combination of searches for Higgs boson pair production in proton-proton collisions at $\sqrt{s} = 13$ TeV*, *Phys. Rev. Lett.* **122** (2019) 121803 [arXiv:1811.09689] [INSPIRE].

[55] ATLAS collaboration, *Combination of searches for Higgs boson pairs in pp collisions at $\sqrt{s} = 13$ TeV with the ATLAS detector*, *Phys. Lett. B* **800** (2020) 135103 [arXiv:1906.02025] [INSPIRE].

[56] CMS collaboration, *Performance of the CMS Level-1 trigger in proton-proton collisions at $\sqrt{s} = 13$ TeV*, 2020 *JINST* **15** P10017 [arXiv:2006.10165] [INSPIRE].

[57] CMS collaboration, *The CMS trigger system*, 2017 *JINST* **12** P01020 [arXiv:1609.02366] [INSPIRE].

[58] CMS collaboration, *The CMS Experiment at the CERN LHC*, 2008 *JINST* **3** S08004 [INSPIRE].

[59] CMS collaboration, *Precision luminosity measurement in proton-proton collisions at $\sqrt{s} = 13$ TeV in 2015 and 2016 at CMS*, *Eur. Phys. J. C* **81** (2021) 800 [arXiv:2104.01927] [INSPIRE].

[60] CMS collaboration, *CMS luminosity measurement for the 2017 data-taking period at $\sqrt{s} = 13$ TeV*, CMS-PAS-LUM-17-004, CERN, Geneva (2018).

[61] CMS collaboration, *CMS luminosity measurement for the 2018 data-taking period at $\sqrt{s} = 13$ TeV*, CMS-PAS-LUM-18-002, CERN, Geneva (2019).

[62] J. Alwall et al., *The automated computation of tree-level and next-to-leading order differential cross sections, and their matching to parton shower simulations*, *JHEP* **07** (2014) 079 [arXiv:1405.0301] [INSPIRE].

[63] A. Kalogeropoulos and J. Alwall, *The SysCalc code: a tool to derive theoretical systematic uncertainties*, arXiv:1801.08401 [INSPIRE].

[64] P. Nason, *A New method for combining NLO QCD with shower Monte Carlo algorithms*, *JHEP* **11** (2004) 040 [hep-ph/0409146] [INSPIRE].

[65] S. Frixione, P. Nason and C. Oleari, *Matching NLO QCD computations with Parton Shower simulations: the POWHEG method*, *JHEP* **11** (2007) 070 [arXiv:0709.2092] [INSPIRE].

[66] S. Alioli, P. Nason, C. Oleari and E. Re, *A general framework for implementing NLO calculations in shower Monte Carlo programs: the POWHEG BOX*, *JHEP* **06** (2010) 043 [arXiv:1002.2581] [INSPIRE].

[67] J.M. Campbell and R.K. Ellis, *An Update on vector boson pair production at hadron colliders*, *Phys. Rev. D* **60** (1999) 113006 [hep-ph/9905386] [INSPIRE].

[68] J.M. Campbell, R.K. Ellis and C. Williams, *Vector boson pair production at the LHC*, *JHEP* **07** (2011) 018 [arXiv:1105.0020] [InSPIRE].

[69] J.M. Campbell, R.K. Ellis and W.T. Giele, *A multi-threaded version of MCFM*, *Eur. Phys. J. C* **75** (2015) 246 [arXiv:1503.06182] [InSPIRE].

[70] T. Sjöstrand et al., *An introduction to PYTHIA 8.2*, *Comput. Phys. Commun.* **191** (2015) 159 [arXiv:1410.3012] [InSPIRE].

[71] B. Hespel, D. Lopez-Val and E. Vryonidou, *Higgs pair production via gluon fusion in the Two-Higgs-Doublet Model*, *JHEP* **09** (2014) 124 [arXiv:1407.0281] [InSPIRE].

[72] A. Carvalho, *Gravity particles from warped extra dimensions, predictions for LHC*, arXiv:1404.0102 [InSPIRE].

[73] G. Heinrich et al., *NLO predictions for Higgs boson pair production with full top quark mass dependence matched to parton showers*, *JHEP* **08** (2017) 088 [arXiv:1703.09252] [InSPIRE].

[74] G. Heinrich et al., *Probing the trilinear Higgs boson coupling in di-Higgs production at NLO QCD including parton shower effects*, *JHEP* **06** (2019) 066 [arXiv:1903.08137] [InSPIRE].

[75] G. Heinrich, S.P. Jones, M. Kerner and L. Scyboz, *A non-linear EFT description of $gg \to HH$ at NLO interfaced to POWHEG*, *JHEP* **10** (2020) 021 [arXiv:2006.16877] [InSPIRE].

[76] E. Bagnaschi, G. Degrassi, P. Slavich and A. Vicini, *Higgs production via gluon fusion in the POWHEG approach in the SM and in the MSSM*, *JHEP* **02** (2012) 088 [arXiv:1111.2854] [InSPIRE].

[77] P. Nason and C. Oleari, *NLO Higgs boson production via vector-boson fusion matched with shower in POWHEG*, *JHEP* **02** (2010) 037 [arXiv:0911.5299] [InSPIRE].

[78] G. Luisoni, P. Nason, C. Oleari and F. Tramontano, *$HW^{\pm}/HZ + 0$ and 1 jet at NLO with the POWHEG BOX interfaced to GoSam and their merging within MiNLO*, *JHEP* **10** (2013) 083 [arXiv:1306.2542] [InSPIRE].

[79] T. Melia, P. Nason, R. Rontsch and G. Zanderighi, *W^+W^-, WZ and ZZ production in the POWHEG BOX*, *JHEP* **11** (2011) 078 [arXiv:1107.5051] [InSPIRE].

[80] P. Nason and G. Zanderighi, *W^+W^-, WZ and ZZ production in the POWHEG-BOX-V2*, *Eur. Phys. J. C* **74** (2014) 2702 [arXiv:1311.1365] [InSPIRE].

[81] J.M. Campbell, R.K. Ellis and C. Williams, *Bounding the Higgs width at the LHC using full analytic results for $gg \to e^- e^+ \mu^- \mu^+$*, *JHEP* **04** (2014) 060 [arXiv:1311.3589] [InSPIRE].

[82] R. Frederix, E. Re and P. Torrielli, *Single-top t-channel hadroproduction in the four-flavour scheme with POWHEG and aMC@NLO*, *JHEP* **09** (2012) 130 [arXiv:1207.5391] [InSPIRE].

[83] E. Re, *Single-top Wt-channel production matched with parton showers using the POWHEG method*, *Eur. Phys. J. C* **71** (2011) 1547 [arXiv:1009.2450] [InSPIRE].

[84] S. Frixione, P. Nason and G. Ridolfi, *A positive-weight next-to-leading-order Monte Carlo for heavy flavour hadroproduction*, *JHEP* **09** (2007) 126 [arXiv:0707.3088] [InSPIRE].

[85] NNPDF collaboration, *Parton distributions for the LHC Run II*, *JHEP* **04** (2015) 040 [arXiv:1410.8849] [InSPIRE].

[86] NNPDF collaboration, *Parton distributions from high-precision collider data*, *Eur. Phys. J.*
C **77** (2017) 663 [`arXiv:1706.00428`] [INSPIRE].

[87] J. Butterworth et al., *PDF4LHC recommendations for LHC Run II*, *J. Phys. G* **43** (2016)
023001 [`arXiv:1510.03865`] [INSPIRE].

[88] J. Rojo et al., *The PDF4LHC report on PDFs and LHC data: Results from Run I and*
preparation for Run II, *J. Phys. G* **42** (2015) 103103 [`arXiv:1507.00556`] [INSPIRE].

[89] A. Accardi et al., *A critical appraisal and evaluation of modern PDFs*, *Eur. Phys. J. C* **76**
(2016) 471 [`arXiv:1603.08906`] [INSPIRE].

[90] CMS collaboration, *Event generator tunes obtained from underlying event and multiparton*
scattering measurements, *Eur. Phys. J. C* **76** (2016) 155 [`arXiv:1512.00815`] [INSPIRE].

[91] CMS collaboration, *Extraction and validation of a new set of CMS PYTHIA8 tunes from*
underlying-event measurements, *Eur. Phys. J. C* **80** (2020) 4 [`arXiv:1903.12179`]
[INSPIRE].

[92] P. Skands, S. Carrazza and J. Rojo, *Tuning PYTHIA 8.1: the Monash 2013 tune*, *Eur.*
Phys. J. C **74** (2014) 3024 [`arXiv:1404.5630`] [INSPIRE].

[93] J. Alwall et al., *Comparative study of various algorithms for the merging of parton showers*
and matrix elements in hadronic collisions, *Eur. Phys. J. C* **53** (2008) 473
[`arXiv:0706.2569`] [INSPIRE].

[94] R. Frederix and S. Frixione, *Merging meets matching in MC@NLO*, *JHEP* **12** (2012) 061
[`arXiv:1209.6215`] [INSPIRE].

[95] GEANT4 collaboration, *GEANT4 — a simulation toolkit*, *Nucl. Instrum. Meth. A* **506**
(2003) 250 [INSPIRE].

[96] M. Capozi and G. Heinrich, *Exploring anomalous couplings in Higgs boson pair production*
through shape analysis, *JHEP* **03** (2020) 091 [`arXiv:1908.08923`] [INSPIRE].

[97] G. Buchalla et al., *Higgs boson pair production in non-linear Effective Field Theory with*
full m_t-dependence at NLO QCD, *JHEP* **09** (2018) 057 [`arXiv:1806.05162`] [INSPIRE].

[98] A. Carvalho et al., *On the reinterpretation of non-resonant searches for Higgs boson pairs*,
JHEP **02** (2021) 049 [`arXiv:1710.08261`] [INSPIRE].

[99] CMS collaboration, *Particle-flow reconstruction and global event description with the CMS*
detector, 2017 *JINST* **12** P10003 [`arXiv:1706.04965`] [INSPIRE].

[100] M. Cacciari, G.P. Salam and G. Soyez, *The anti-k_t jet clustering algorithm*, *JHEP* **04**
(2008) 063 [`arXiv:0802.1189`] [INSPIRE].

[101] M. Cacciari, G.P. Salam and G. Soyez, *FastJet user manual*, *Eur. Phys. J. C* **72** (2012)
1896 [`arXiv:1111.6097`] [INSPIRE].

[102] CMS collaboration, *Electron and photon reconstruction and identification with the CMS*
experiment at the CERN LHC, 2021 *JINST* **16** P05014 [`arXiv:2012.06888`] [INSPIRE].

[103] CMS collaboration, *Measurement of the Higgs boson production rate in association with top*
quarks in final states with electrons, muons, and hadronically decaying tau leptons at
$\sqrt{s} = 13$ *TeV*, *Eur. Phys. J. C* **81** (2021) 378 [`arXiv:2011.03652`] [INSPIRE].

[104] CMS collaboration, *Performance of electron reconstruction and selection with the CMS*
detector in proton-proton collisions at $\sqrt{s} = 8$ TeV, 2015 *JINST* **10** P06005
[`arXiv:1502.02701`] [INSPIRE].

[105] CMS collaboration, *Performance of the CMS muon detector and muon reconstruction with proton-proton collisions at $\sqrt{s} = 13$ TeV*, 2018 *JINST* **13** P06015 [arXiv:1804.04528] [INSPIRE].

[106] CMS collaboration, *Performance of reconstruction and identification of τ leptons decaying to hadrons and ν_τ in pp collisions at $\sqrt{s} = 13$ TeV*, 2018 *JINST* **13** P10005 [arXiv:1809.02816] [INSPIRE].

[107] CMS collaboration, *Identification of hadronic tau lepton decays using a deep neural network*, 2022 *JINST* **17** P07023 [arXiv:2201.08458] [INSPIRE].

[108] Y. LeCun, *Generalization and network design strategies*, in *Connectionism in perspective*, R. Pfeife et al. eds., Zurich, Switzerland (1989).

[109] CMS collaboration, *Pileup mitigation at CMS in 13 TeV data*, 2020 *JINST* **15** P09018 [arXiv:2003.00503] [INSPIRE].

[110] D. Bertolini, P. Harris, M. Low and N. Tran, *Pileup per particle identification*, *JHEP* **10** (2014) 059 [arXiv:1407.6013] [INSPIRE].

[111] CMS collaboration, *Jet energy scale and resolution in the CMS experiment in pp collisions at 8 TeV*, 2017 *JINST* **12** P02014 [arXiv:1607.03663] [INSPIRE].

[112] CMS collaboration, *Search for resonances decaying to a pair of Higgs bosons in the $b\bar{b}q\bar{q}'\ell\nu$ final state in proton-proton collisions at $\sqrt{s} = 13$ TeV*, *JHEP* **10** (2019) 125 [arXiv:1904.04193] [INSPIRE].

[113] E. Bols et al., *Jet flavour classification using DeepJet*, 2020 *JINST* **15** P12012 [arXiv:2008.10519] [INSPIRE].

[114] CMS collaboration, *Performance of missing transverse momentum reconstruction in proton-proton collisions at $\sqrt{s} = 13$ TeV using the CMS detector*, 2019 *JINST* **14** P07004 [arXiv:1903.06078] [INSPIRE].

[115] CMS collaboration, *Evidence for associated production of a Higgs boson with a top quark pair in final states with electrons, muons, and hadronically decaying τ leptons at $\sqrt{s} = 13$ TeV*, *JHEP* **08** (2018) 066 [arXiv:1803.05485] [INSPIRE].

[116] L. Breiman, J. Friedman, R.A. Olshen and C.J. Stone, *Classification and regression trees*, Chapman and Hall/CRC (1984) [INSPIRE].

[117] K. Ehatäht, L. Marzola and C. Veelken, *Reconstruction of the mass of Higgs boson pairs in events with Higgs boson pairs decaying into four τ leptons*, arXiv:1809.06140 [INSPIRE].

[118] T. Chen and C. Guestrin, *XGBoost: a scalable tree boosting system*, arXiv:1603.02754 [DOI:10.1145/2939672.2939785] [INSPIRE].

[119] F. Pedregosa et al., *Scikit-learn: machine learning in Python*, *J. Machine Learning Res.* **12** (2011) 2825 [arXiv:1201.0490] [INSPIRE].

[120] L. Tani, D. Rand, C. Veelken and M. Kadastik, *Evolutionary algorithms for hyperparameter optimization in machine learning for application in high energy physics*, *Eur. Phys. J. C* **81** (2021) 170 [arXiv:2011.04434] [INSPIRE].

[121] CMS collaboration, *Search for electroweak production of charginos and neutralinos in multilepton final states in proton-proton collisions at $\sqrt{s} = 13$ TeV*, *JHEP* **03** (2018) 166 [arXiv:1709.05406] [INSPIRE].

[122] J. Baglio et al., *gg → HH: combined uncertainties*, *Phys. Rev. D* **103** (2021) 056002 [arXiv:2008.11626] [INSPIRE].

[123] LHC HIGGS CROSS SECTION WORKING GROUP collaboration, *Handbook of LHC Higgs Cross Sections: 4. Deciphering the nature of the Higgs sector*, arXiv:1610.07922 [DOI:10.23731/CYRM-2017-002] [INSPIRE].

[124] M. Grazzini, S. Kallweit, D. Rathlev and M. Wiesemann, $W^\pm Z$ *production at hadron colliders in NNLO QCD*, *Phys. Lett. B* **761** (2016) 179 [arXiv:1604.08576] [INSPIRE].

[125] F. Cascioli et al., *ZZ production at hadron colliders in NNLO QCD*, *Phys. Lett. B* **735** (2014) 311 [arXiv:1405.2219] [INSPIRE].

[126] F. Caola, K. Melnikov, R. Röntsch and L. Tancredi, *QCD corrections to ZZ production in gluon fusion at the LHC*, *Phys. Rev. D* **92** (2015) 094028 [arXiv:1509.06734] [INSPIRE].

[127] CMS collaboration, *Jet algorithms performance in 13 TeV data*, CMS-PAS-JME-16-003, CERN, Geneva (2017).

[128] CMS collaboration, *Measurement of the inelastic proton-proton cross section at $\sqrt{s} = 13$ TeV*, *JHEP* **07** (2018) 161 [arXiv:1802.02613] [INSPIRE].

[129] G. Cowan, K. Cranmer, E. Gross and O. Vitells, *Asymptotic formulae for likelihood-based tests of new physics*, *Eur. Phys. J. C* **71** (2011) 1554 [*Erratum ibid.* **73** (2013) 2501] [arXiv:1007.1727] [INSPIRE].

[130] ATLAS, CMS collaboration and L.H.C.H.C. Group, *Procedure for the LHC Higgs boson search combination in summer 2011*, ATL-PHYS-PUB-2011-011 (2011).

[131] J.S. Conway, *Incorporating Nuisance Parameters in Likelihoods for Multisource Spectra*, in the proceedings of the *PHYSTAT 2011*, (2011), p. 115–120 [DOI:10.5170/CERN-2011-006.115] [arXiv:1103.0354] [INSPIRE].

[132] T. Junk, *Confidence level computation for combining searches with small statistics*, *Nucl. Instrum. Meth. A* **434** (1999) 435 [hep-ex/9902006] [INSPIRE].

[133] A.L. Read, *Presentation of search results: The CL_s technique*, *J. Phys. G* **28** (2002) 2693 [INSPIRE].

[134] CMS collaboration, *Search for Higgs boson pairs decaying to WWWW, WWττ, and ττττ in proton-proton collisions at $\sqrt{s} = 13$ TeV*, https://www.hepdata.net/record/ins2098277 [DOI:10.17182/HEPDATA.130795].

[135] E. Gross and O. Vitells, *Trial factors for the look elsewhere effect in high energy physics*, *Eur. Phys. J. C* **70** (2010) 525 [arXiv:1005.1891] [INSPIRE].

The CMS collaboration

Yerevan Physics Institute, Yerevan, Armenia

A. Tumasyan [1]

Institut für Hochenergiephysik, Vienna, Austria

W. Adam, J.W. Andrejkovic, T. Bergauer, S. Chatterjee, K. Damanakis, M. Dragicevic, A. Escalante Del Valle, M. Jeitler [2], N. Krammer, L. Lechner, D. Liko, I. Mikulec, P. Paulitsch, F.M. Pitters, J. Schieck [2], R. Schöfbeck, D. Schwarz, S. Templ, W. Waltenberger, C.-E. Wulz [2]

Universiteit Antwerpen, Antwerpen, Belgium

M.R. Darwish [3], E.A. De Wolf, T. Janssen, T. Kello [4], A. Lelek, H. Rejeb Sfar, P. Van Mechelen, N. Van Remortel

Vrije Universiteit Brussel, Brussel, Belgium

E.S. Bols, J. D'Hondt, A. De Moor, M. Delcourt, H. El Faham, S. Lowette, S. Moortgat, A. Morton, D. Müller, A.R. Sahasransu, S. Tavernier, W. Van Doninck, D. Vannerom

Université Libre de Bruxelles, Bruxelles, Belgium

D. Beghin, B. Clerbaux, G. De Lentdecker, L. Favart, J. Jaramillo, K. Lee, M. Mahdavikhorrami, I. Makarenko, A. Malara, S. Paredes, L. Pétré, A. Popov, N. Postiau, E. Starling, L. Thomas, M. Vanden Bemden, C. Vander Velde, P. Vanlaer

Ghent University, Ghent, Belgium

D. Dobur, J. Knolle, L. Lambrecht, G. Mestdach, M. Niedziela, C. Rendón, C. Roskas, A. Samalan, K. Skovpen, M. Tytgat, N. Van Den Bossche, B. Vermassen, L. Wezenbeek

Université Catholique de Louvain, Louvain-la-Neuve, Belgium

A. Benecke, A. Bethani, G. Bruno, F. Bury, C. Caputo, P. David, C. Delaere, I.S. Donertas, A. Giammanco, K. Jaffel, Sa. Jain, V. Lemaitre, K. Mondal, J. Prisciandaro, A. Taliercio, T.T. Tran, P. Vischia, S. Wertz

Centro Brasileiro de Pesquisas Fisicas, Rio de Janeiro, Brazil

G.A. Alves, E. Coelho, C. Hensel, A. Moraes, P. Rebello Teles

Universidade do Estado do Rio de Janeiro, Rio de Janeiro, Brazil

W.L. Aldá Júnior, M. Alves Gallo Pereira, M. Barroso Ferreira Filho, H. Brandao Malbouisson, W. Carvalho, J. Chinellato [5], E.M. Da Costa, G.G. Da Silveira [6], D. De Jesus Damiao, V. Dos Santos Sousa, S. Fonseca De Souza, J. Martins [7], C. Mora Herrera, K. Mota Amarilo, L. Mundim, H. Nogima, A. Santoro, S.M. Silva Do Amaral, A. Sznajder, M. Thiel, F. Torres Da Silva De Araujo [8], A. Vilela Pereira

Universidade Estadual Paulista, Universidade Federal do ABC, São Paulo, Brazil

C.A. Bernardes [6], L. Calligaris, T.R. Fernandez Perez Tomei, E.M. Gregores, P.G. Mercadante, S.F. Novaes, Sandra S. Padula

Institute for Nuclear Research and Nuclear Energy, Bulgarian Academy of Sciences, Sofia, Bulgaria

A. Aleksandrov, G. Antchev, R. Hadjiiska, P. Iaydjiev, M. Misheva, M. Rodozov, M. Shopova, G. Sultanov

University of Sofia, Sofia, Bulgaria

A. Dimitrov, T. Ivanov, L. Litov, B. Pavlov, P. Petkov, A. Petrov

Beihang University, Beijing, China

T. Cheng, T. Javaid [9], M. Mittal, L. Yuan

Department of Physics, Tsinghua University, Beijing, China

M. Ahmad, G. Bauer[10], Z. Hu, K. Yi[10,11]

Institute of High Energy Physics, Beijing, China

G.M. Chen [9], H.S. Chen [9], M. Chen [9], F. Iemmi, C.H. Jiang, A. Kapoor, H. Liao, Z.-A. Liu[12], V. Milosevic, F. Monti, R. Sharma, J. Tao, J. Thomas-Wilsker, J. Wang, H. Zhang, J. Zhao

State Key Laboratory of Nuclear Physics and Technology, Peking University, Beijing, China

A. Agapitos, Y. An, Y. Ban, C. Chen, A. Levin, Q. Li, X. Lyu, Y. Mao, S.J. Qian, X. Sun, D. Wang, J. Xiao, H. Yang

Sun Yat-Sen University, Guangzhou, China

M. Lu, Z. You

Institute of Modern Physics and Key Laboratory of Nuclear Physics and Ion-beam Application (MOE) — Fudan University, Shanghai, China

X. Gao [4], D. Leggat, H. Okawa, Y. Zhang

Zhejiang University, Hangzhou, Zhejiang, China

Z. Lin, M. Xiao

Universidad de Los Andes, Bogota, Colombia

C. Avila, A. Cabrera, C. Florez, J. Fraga

Universidad de Antioquia, Medellin, Colombia

J. Mejia Guisao, F. Ramirez, J.D. Ruiz Alvarez

University of Split, Faculty of Electrical Engineering, Mechanical Engineering and Naval Architecture, Split, Croatia

D. Giljanovic, N. Godinovic, D. Lelas, I. Puljak

University of Split, Faculty of Science, Split, Croatia

Z. Antunovic, M. Kovac [iD], T. Sculac [iD]

Institute Rudjer Boskovic, Zagreb, Croatia

V. Brigljevic [iD], B.K. Chitroda [iD], D. Ferencek [iD], D. Majumder [iD], M. Roguljic [iD], A. Starodumov [iD][13], T. Susa [iD]

University of Cyprus, Nicosia, Cyprus

A. Attikis [iD], K. Christoforou [iD], G. Kole [iD], M. Kolosova [iD], S. Konstantinou [iD], J. Mousa [iD], C. Nicolaou, F. Ptochos [iD], P.A. Razis [iD], H. Rykaczewski, H. Saka [iD]

Charles University, Prague, Czech Republic

M. Finger [iD][13], M. Finger Jr. [iD][13], A. Kveton [iD]

Escuela Politecnica Nacional, Quito, Ecuador

E. Ayala [iD]

Universidad San Francisco de Quito, Quito, Ecuador

E. Carrera Jarrin [iD]

Academy of Scientific Research and Technology of the Arab Republic of Egypt, Egyptian Network of High Energy Physics, Cairo, Egypt

H. Abdalla [iD][14], Y. Assran[15,16]

Center for High Energy Physics (CHEP-FU), Fayoum University, El-Fayoum, Egypt

M.A. Mahmoud [iD], Y. Mohammed [iD]

National Institute of Chemical Physics and Biophysics, Tallinn, Estonia

S. Bhowmik [iD], R.K. Dewanjee [iD], K. Ehataht [iD], M. Kadastik, S. Nandan [iD], C. Nielsen [iD], J. Pata [iD], M. Raidal [iD], L. Tani [iD], C. Veelken [iD]

Department of Physics, University of Helsinki, Helsinki, Finland

P. Eerola [iD], H. Kirschenmann [iD], K. Osterberg [iD], M. Voutilainen [iD]

Helsinki Institute of Physics, Helsinki, Finland

S. Bharthuar [iD], E. Brücken [iD], F. Garcia [iD], J. Havukainen [iD], M.S. Kim [iD], R. Kinnunen, T. Lampén [iD], K. Lassila-Perini [iD], S. Lehti [iD], T. Lindén [iD], M. Lotti, L. Martikainen [iD], M. Myllymäki [iD], J. Ott [iD], M.m. Rantanen [iD], H. Siikonen [iD], E. Tuominen [iD], J. Tuominiemi [iD]

Lappeenranta-Lahti University of Technology, Lappeenranta, Finland

P. Luukka [iD], H. Petrow [iD], T. Tuuva

IRFU, CEA, Université Paris-Saclay, Gif-sur-Yvette, France

C. Amendola [iD], M. Besancon [iD], F. Couderc [iD], M. Dejardin [iD], D. Denegri, J.L. Faure, F. Ferri [iD], S. Ganjour [iD], P. Gras [iD], G. Hamel de Monchenault [iD], P. Jarry [iD], V. Lohezic, J. Malcles [iD], J. Rander, A. Rosowsky [iD], M.Ö. Sahin [iD], A. Savoy-Navarro [iD][17], P. Simkina [iD], M. Titov [iD]

Laboratoire Leprince-Ringuet, CNRS/IN2P3, Ecole Polytechnique, Institut Polytechnique de Paris, Palaiseau, France

S. Ahuja, C. Baldenegro Barrera, F. Beaudette, M. Bonanomi, A. Buchot Perraguin, P. Busson, A. Cappati, C. Charlot, O. Davignon, B. Diab, G. Falmagne, B.A. Fontana Santos Alves, S. Ghosh, R. Granier de Cassagnac, A. Hakimi, B. Harikrishnan, J. Motta, M. Nguyen, C. Ochando, L. Portales, J. Rembser, R. Salerno, U. Sarkar, J.B. Sauvan, Y. Sirois, A. Tarabini, E. Vernazza, A. Zabi, A. Zghiche

Université de Strasbourg, CNRS, IPHC UMR 7178, Strasbourg, France

J.-L. Agram[18], J. Andrea, D. Apparu, D. Bloch, G. Bourgatte, J.-M. Brom, E.C. Chabert, C. Collard, D. Darej, U. Goerlach, C. Grimault, A.-C. Le Bihan, E. Nibigira, P. Van Hove

Institut de Physique des 2 Infinis de Lyon (IP2I), Villeurbanne, France

S. Beauceron, C. Bernet, G. Boudoul, C. Camen, A. Carle, N. Chanon, D. Contardo, P. Depasse, H. El Mamouni, J. Fay, S. Gascon, M. Gouzevitch, G. Grenier, B. Ille, I.B. Laktineh, M. Lethuillier, L. Mirabito, S. Perries, K. Shchablo, V. Sordini, L. Torterotot, M. Vander Donckt, S. Viret

Georgian Technical University, Tbilisi, Georgia

I. Bagaturia[19], I. Lomidze, Z. Tsamalaidze[13]

RWTH Aachen University, I. Physikalisches Institut, Aachen, Germany

V. Botta, L. Feld, K. Klein, M. Lipinski, D. Meuser, A. Pauls, N. Röwert, M. Teroerde

RWTH Aachen University, III. Physikalisches Institut A, Aachen, Germany

A. Dodonova, N. Eich, D. Eliseev, M. Erdmann, P. Fackeldey, B. Fischer, T. Hebbeker, K. Hoepfner, F. Ivone, M.y. Lee, L. Mastrolorenzo, M. Merschmeyer, A. Meyer, S. Mondal, S. Mukherjee, D. Noll, A. Novak, A. Pozdnyakov, Y. Rath, H. Reithler, A. Schmidt, S.C. Schuler, A. Sharma, L. Vigilante, S. Wiedenbeck, S. Zaleski

RWTH Aachen University, III. Physikalisches Institut B, Aachen, Germany

C. Dziwok, G. Flügge, W. Haj Ahmad[20], O. Hlushchenko, T. Kress, A. Nowack, O. Pooth, A. Stahl[21], T. Ziemons, A. Zotz

Deutsches Elektronen-Synchrotron, Hamburg, Germany

H. Aarup Petersen, M. Aldaya Martin, P. Asmuss, S. Baxter, M. Bayatmakou, O. Behnke, A. Bermúdez Martínez, S. Bhattacharya, A.A. Bin Anuar, F. Blekman[22], K. Borras[23], D. Brunner, A. Campbell, A. Cardini, C. Cheng, F. Colombina, S. Consuegra Rodríguez, G. Correia Silva, M. De Silva, L. Didukh, G. Eckerlin, D. Eckstein, L.I. Estevez Banos, O. Filatov, E. Gallo[22], A. Geiser, A. Giraldi, G. Greau, A. Grohsjean, V. Guglielmi, M. Guthoff, A. Jafari[24], N.Z. Jomhari, B. Kaech, A. Kasem[23], M. Kasemann, H. Kaveh, C. Kleinwort, R. Kogler,

D. Krücker ⓘ, W. Lange, K. Lipka ⓘ, W. Lohmann [25], R. Mankel ⓘ, I.-A. Melzer-Pellmann ⓘ,
M. Mendizabal Morentin ⓘ, J. Metwally, A.B. Meyer ⓘ, G. Milella ⓘ, M. Mormile ⓘ,
A. Mussgiller ⓘ, A. Nürnberg ⓘ, Y. Otarid, D. Pérez Adán ⓘ, A. Raspereza ⓘ,
B. Ribeiro Lopes ⓘ, J. Rübenach, A. Saggio ⓘ, A. Saibel ⓘ, M. Savitskyi ⓘ, M. Scham ⓘ [26,23],
V. Scheurer, S. Schnake ⓘ [23], P. Schütze ⓘ, C. Schwanenberger ⓘ [22], M. Shchedrolosiev ⓘ,
R.E. Sosa Ricardo ⓘ, D. Stafford, N. Tonon ⓘ [†], M. Van De Klundert ⓘ, F. Vazzoler ⓘ,
R. Walsh ⓘ, D. Walter ⓘ, Q. Wang ⓘ, Y. Wen ⓘ, K. Wichmann, L. Wiens ⓘ [23], C. Wissing ⓘ,
S. Wuchterl ⓘ, A. Zimermmane Castro Santos ⓘ

University of Hamburg, Hamburg, Germany

R. Aggleton, S. Albrecht ⓘ, S. Bein ⓘ, L. Benato ⓘ, P. Connor ⓘ, K. De Leo ⓘ, M. Eich,
K. El Morabit ⓘ, F. Feindt, A. Fröhlich, C. Garbers ⓘ, E. Garutti ⓘ, M. Hajheidari, J. Haller ⓘ,
A. Hinzmann ⓘ, G. Kasieczka ⓘ, R. Klanner ⓘ, W. Korcari ⓘ, T. Kramer ⓘ, V. Kutzner ⓘ,
J. Lange ⓘ, T. Lange ⓘ, A. Lobanov ⓘ, C. Matthies, A. Mehta ⓘ, L. Moureaux ⓘ,
M. Mrowietz, A. Nigamova ⓘ, K.J. Pena Rodriguez ⓘ, M. Rieger ⓘ, O. Rieger, P. Schleper ⓘ,
M. Schröder ⓘ, J. Schwandt ⓘ, H. Stadie ⓘ, G. Steinbrück ⓘ, A. Tews, M. Wolf ⓘ

Karlsruher Institut fuer Technologie, Karlsruhe, Germany

J. Bechtel ⓘ, S. Brommer ⓘ, M. Burkart, E. Butz ⓘ, R. Caspart ⓘ, T. Chwalek ⓘ,
A. Dierlamm ⓘ, A. Droll, N. Faltermann ⓘ, M. Giffels ⓘ, J.O. Gosewisch, A. Gottmann,
F. Hartmann ⓘ [21], C. Heidecker, M. Horzela ⓘ, U. Husemann ⓘ, P. Keicher, R. Koppenhöfer ⓘ,
S. Maier ⓘ, S. Mitra ⓘ, Th. Müller ⓘ, M. Neukum, G. Quast ⓘ, K. Rabbertz ⓘ, J. Rauser,
D. Savoiu ⓘ, M. Schnepf, D. Seith, I. Shvetsov ⓘ, H.J. Simonis ⓘ, R. Ulrich ⓘ,
J. van der Linden ⓘ, R.F. Von Cube ⓘ, M. Wassmer ⓘ, M. Weber ⓘ, S. Wieland ⓘ, R. Wolf ⓘ,
S. Wozniewski ⓘ, S. Wunsch

Institute of Nuclear and Particle Physics (INPP), NCSR Demokritos, Aghia Paraskevi, Greece

G. Anagnostou, P. Assiouras ⓘ, G. Daskalakis ⓘ, A. Kyriakis, A. Stakia ⓘ

National and Kapodistrian University of Athens, Athens, Greece

M. Diamantopoulou, D. Karasavvas, P. Kontaxakis ⓘ, A. Manousakis-Katsikakis ⓘ,
A. Panagiotou, I. Papavergou ⓘ, N. Saoulidou ⓘ, K. Theofilatos ⓘ, E. Tziaferi ⓘ, K. Vellidis ⓘ,
E. Vourliotis ⓘ

National Technical University of Athens, Athens, Greece

G. Bakas ⓘ, K. Kousouris ⓘ, I. Papakrivopoulos ⓘ, G. Tsipolitis, A. Zacharopoulou

University of Ioánnina, Ioánnina, Greece

K. Adamidis, I. Bestintzanos, I. Evangelou ⓘ, C. Foudas, P. Gianneios ⓘ, P. Katsoulis,
P. Kokkas ⓘ, N. Manthos ⓘ, I. Papadopoulos ⓘ, J. Strologas ⓘ

MTA-ELTE Lendület CMS Particle and Nuclear Physics Group, Eötvös Loránd University, Budapest, Hungary

M. Csanád ⓘ, K. Farkas ⓘ, M.M.A. Gadallah ⓘ [27], S. Lökös ⓘ [28], P. Major ⓘ, K. Mandal ⓘ,
G. Pásztor ⓘ, A.J. Rádl ⓘ, O. Surányi ⓘ, G.I. Veres ⓘ

Wigner Research Centre for Physics, Budapest, Hungary

M. Bartók [29], G. Bencze, C. Hajdu, D. Horvath [30,31], F. Sikler, V. Veszpremi

Institute of Nuclear Research ATOMKI, Debrecen, Hungary

N. Beni, S. Czellar, D. Fasanella, J. Karancsi [29], J. Molnar, Z. Szillasi, D. Teyssier

Institute of Physics, University of Debrecen, Debrecen, Hungary

P. Raics, B. Ujvari [32], G. Zilizi

Karoly Robert Campus, MATE Institute of Technology, Gyongyos, Hungary

T. Csorgo [33], F. Nemes [33], T. Novak

Panjab University, Chandigarh, India

J. Babbar, S. Bansal, S.B. Beri, V. Bhatnagar, G. Chaudhary, S. Chauhan, N. Dhingra [34], R. Gupta, A. Kaur, H. Kaur, M. Kaur, P. Kumari, M. Meena, K. Sandeep, J.B. Singh [35], A. K. Virdi

University of Delhi, Delhi, India

A. Ahmed, A. Bhardwaj, B.C. Choudhary, M. Gola, S. Keshri, A. Kumar, M. Naimuddin, P. Priyanka, K. Ranjan, S. Saumya, A. Shah

Saha Institute of Nuclear Physics, HBNI, Kolkata, India

R. Bhattacharya, S. Bhattacharya, D. Bhowmik, S. Dutta, S. Dutta, B. Gomber [36], M. Maity [37], P. Palit, P.K. Rout, G. Saha, B. Sahu, S. Sarkar

Indian Institute of Technology Madras, Madras, India

P.K. Behera, S.C. Behera, P. Kalbhor, J.R. Komaragiri [38], D. Kumar [38], A. Muhammad, L. Panwar [38], R. Pradhan, P.R. Pujahari, A. Sharma, A.K. Sikdar, P.C. Tiwari [38]

Bhabha Atomic Research Centre, Mumbai, India

K. Naskar [39]

Tata Institute of Fundamental Research-A, Mumbai, India

T. Aziz, S. Dugad, M. Kumar, G.B. Mohanty, P. Suryadevara

Tata Institute of Fundamental Research-B, Mumbai, India

S. Banerjee, R. Chudasama, M. Guchait, S. Karmakar, S. Kumar, G. Majumder, K. Mazumdar, S. Mukherjee

National Institute of Science Education and Research, An OCC of Homi Bhabha National Institute, Bhubaneswar, Odisha, India

S. Bahinipati [40], C. Kar, P. Mal, T. Mishra, V.K. Muraleedharan Nair Bindhu [41], A. Nayak [41], P. Saha, N. Sur, S.K. Swain, D. Vats [41]

Indian Institute of Science Education and Research (IISER), Pune, India

A. Alpana, S. Dube, B. Kansal, A. Laha, S. Pandey, A. Rastogi, S. Sharma

Isfahan University of Technology, Isfahan, Iran

H. Bakhshiansohi [42], E. Khazaie, M. Zeinali [43]

Institute for Research in Fundamental Sciences (IPM), Tehran, Iran

S. Chenarani [44], S.M. Etesami, M. Khakzad, M. Mohammadi Najafabadi

University College Dublin, Dublin, Ireland

M. Grunewald

INFN Sezione di Bari[a], Università di Bari[b], Politecnico di Bari[c], Bari, Italy

M. Abbrescia [a,b], R. Aly [a,c,45], C. Aruta [a,b], A. Colaleo [a], D. Creanza [a,c],
N. De Filippis [a,c], M. De Palma [a,b], A. Di Florio [a,b], W. Elmetenawee [a,b], F. Errico [a,b],
L. Fiore [a], G. Iaselli [a,c], M. Ince [a,b], S. Lezki [a,b], G. Maggi [a,c], M. Maggi [a],
I. Margjeka [a,b], V. Mastrapasqua [a,b], S. My [a,b], S. Nuzzo [a,b], A. Pellecchia [a,b],
A. Pompili [a,b], G. Pugliese [a,c], R. Radogna [a], D. Ramos [a], A. Ranieri [a], G. Selvaggi [a,b],
L. Silvestris [a], F.M. Simone [a,b], Ü. Sözbilir [a], R. Venditti [a], P. Verwilligen [a]

INFN Sezione di Bologna[a], Università di Bologna[b], Bologna, Italy

G. Abbiendi [a], C. Battilana [a,b], D. Bonacorsi [a,b], L. Borgonovi [a], L. Brigliadori[a],
R. Campanini [a,b], P. Capiluppi [a,b], A. Castro [a,b], F.R. Cavallo [a], M. Cuffiani [a,b],
G.M. Dallavalle [a], T. Diotalevi [a,b], F. Fabbri [a], A. Fanfani [a,b], P. Giacomelli [a],
L. Giommi [a,b], C. Grandi [a], L. Guiducci [a,b], S. Lo Meo [a,46], L. Lunerti [a,b],
S. Marcellini [a], G. Masetti [a], F.L. Navarria [a,b], A. Perrotta [a], F. Primavera [a,b],
A.M. Rossi [a,b], T. Rovelli [a,b], G.P. Siroli [a,b]

INFN Sezione di Catania[a], Università di Catania[b], Catania, Italy

S. Costa [a,b,47], A. Di Mattia [a], R. Potenza[a,b], A. Tricomi [a,b,47], C. Tuve [a,b]

INFN Sezione di Firenze[a], Università di Firenze[b], Firenze, Italy

G. Barbagli [a], B. Camaiani [a,b], A. Cassese [a], R. Ceccarelli [a,b], V. Ciulli [a,b], C. Civinini [a],
R. D'Alessandro [a,b], E. Focardi [a,b], G. Latino [a,b], P. Lenzi [a,b], M. Lizzo [a,b],
M. Meschini [a], S. Paoletti [a], R. Seidita [a,b], G. Sguazzoni [a], L. Viliani [a]

INFN Laboratori Nazionali di Frascati, Frascati, Italy

L. Benussi, S. Bianco, D. Piccolo

INFN Sezione di Genova[a], Università di Genova[b], Genova, Italy

M. Bozzo [a,b], F. Ferro [a], R. Mulargia [a], E. Robutti [a], S. Tosi [a,b]

INFN Sezione di Milano-Bicocca[a], Università di Milano-Bicocca[b], Milano, Italy

A. Benaglia [a], G. Boldrini [a], F. Brivio [a,b], F. Cetorelli [a,b], F. De Guio [a,b],
M.E. Dinardo [a,b], P. Dini [a], S. Gennai [a], A. Ghezzi [a,b], P. Govoni [a,b], L. Guzzi [a,b],
M.T. Lucchini [a,b], M. Malberti [a], S. Malvezzi [a], A. Massironi [a], D. Menasce [a],

L. Moroni [a], M. Paganoni [a,b], D. Pedrini [a], B.S. Pinolini [a], S. Ragazzi [a,b], N. Redaelli [a], T. Tabarelli de Fatis [a,b], D. Zuolo [a,b]

INFN Sezione di Napoli[a], Università di Napoli 'Federico II'[b], Napoli, Italy; Università della Basilicata[c], Potenza, Italy; Università G. Marconi[d], Roma, Italy

S. Buontempo [a], F. Carnevali[a,b], N. Cavallo [a,c], A. De Iorio [a,b], F. Fabozzi [a,c], A.O.M. Iorio [a,b], L. Lista [a,b,48], S. Meola [a,d,21], P. Paolucci [a,21], B. Rossi [a], C. Sciacca [a,b]

INFN Sezione di Padova[a], Università di Padova[b], Padova, Italy; Università di Trento[c], Trento, Italy

P. Azzi [a], N. Bacchetta [a], D. Bisello [a,b], P. Bortignon [a], A. Bragagnolo [a,b], R. Carlin [a,b], P. Checchia [a], T. Dorigo [a], F. Gasparini [a,b], U. Gasparini [a,b], G. Grosso[a], L. Layer[a,49], E. Lusiani [a], M. Margoni [a,b], F. Marini [a], A.T. Meneguzzo [a,b], J. Pazzini [a,b], P. Ronchese [a,b], R. Rossin [a,b], F. Simonetto [a,b], G. Strong [a], M. Tosi [a,b], H. Yarar[a,b], M. Zanetti [a,b], P. Zotto [a,b], A. Zucchetta [a,b], G. Zumerle [a,b]

INFN Sezione di Pavia[a], Università di Pavia[b], Pavia, Italy

C. Aimè [a,b], A. Braghieri [a], S. Calzaferri [a,b], D. Fiorina [a,b], P. Montagna [a,b], V. Re [a], C. Riccardi [a,b], P. Salvini [a], I. Vai [a], P. Vitulo [a,b]

INFN Sezione di Perugia[a], Università di Perugia[b], Perugia, Italy

P. Asenov [a,50], G.M. Bilei [a], D. Ciangottini [a,b], L. Fanò [a,b], M. Magherini [a,b], G. Mantovani[a,b], V. Mariani [a,b], M. Menichelli [a], F. Moscatelli [a,50], A. Piccinelli [a,b], M. Presilla [a,b], A. Rossi [a,b], A. Santocchia [a,b], D. Spiga [a], T. Tedeschi [a,b]

INFN Sezione di Pisa[a], Università di Pisa[b], Scuola Normale Superiore di Pisa[c], Pisa, Italy; Università di Siena[d], Siena, Italy

P. Azzurri [a], G. Bagliesi [a], V. Bertacchi [a,c], L. Bianchini [a,b], T. Boccali [a], E. Bossini [a,b], D. Bruschini [a,c], R. Castaldi [a], M.A. Ciocci [a,b], V. D'Amante [a,d], R. Dell'Orso [a], M.R. Di Domenico [a,d], S. Donato [a], A. Giassi [a], F. Ligabue [a,c], E. Manca [a,c], G. Mandorli [a,c], D. Matos Figueiredo [a], A. Messineo [a,b], M. Musich [a,b], F. Palla [a], S. Parolia [a,b], G. Ramirez-Sanchez [a,c], A. Rizzi [a,b], G. Rolandi [a,c], S. Roy Chowdhury [a,c], A. Scribano [a], N. Shafiei [a,b], P. Spagnolo [a], R. Tenchini [a], G. Tonelli [a,b], N. Turini [a,d], A. Venturi [a], P.G. Verdini [a]

INFN Sezione di Roma[a], Sapienza Università di Roma[b], Roma, Italy

P. Barria [a], M. Campana [a,b], F. Cavallari [a], D. Del Re [a,b], E. Di Marco [a], M. Diemoz [a], E. Longo [a,b], P. Meridiani [a], G. Organtini [a,b], F. Pandolfi [a], R. Paramatti [a,b], C. Quaranta [a,b], S. Rahatlou [a,b], C. Rovelli [a], F. Santanastasio [a,b], L. Soffi [a], R. Tramontano [a,b]

INFN Sezione di Torino[a], Università di Torino[b], Torino, Italy; Università del Piemonte Orientale[c], Novara, Italy

N. Amapane [a,b], R. Arcidiacono [a,c], S. Argiro [a,b], M. Arneodo [a,c], N. Bartosik [a], R. Bellan [a,b], A. Bellora [a,b], J. Berenguer Antequera [a,b], C. Biino [a], N. Cartiglia [a],

M. Costa^{a,b}, R. Covarelli^{a,b}, N. Demaria^{a}, M. Grippo^{a,b}, B. Kiani^{a,b}, F. Legger^{a}, C. Mariotti^{a}, S. Maselli^{a}, A. Mecca^{a,b}, E. Migliore^{a,b}, E. Monteil^{a,b}, M. Monteno^{a}, M.M. Obertino^{a,b}, G. Ortona^{a}, L. Pacher^{a,b}, N. Pastrone^{a}, M. Pelliccioni^{a}, M. Ruspa^{a,c}, K. Shchelina^{a}, F. Siviero^{a,b}, V. Sola^{a}, A. Solano^{a,b}, D. Soldi^{a,b}, A. Staiano^{a}, M. Tornago^{a,b}, D. Trocino^{a}, G. Umoret^{a,b}, A. Vagnerini^{a,b}

INFN Sezione di Trieste^{a}, Università di Trieste^{b}, Trieste, Italy

S. Belforte^{a}, V. Candelise^{a,b}, M. Casarsa^{a}, F. Cossutti^{a}, A. Da Rold^{a,b}, G. Della Ricca^{a,b}, G. Sorrentino^{a,b}

Kyungpook National University, Daegu, Korea

S. Dogra, C. Huh, B. Kim, D.H. Kim, G.N. Kim, J. Kim, J. Lee, S.W. Lee, C.S. Moon, Y.D. Oh, S.I. Pak, S. Sekmen, Y.C. Yang

Chonnam National University, Institute for Universe and Elementary Particles, Kwangju, Korea

H. Kim, D.H. Moon

Hanyang University, Seoul, Korea

E. Asilar, J. Choi, T.J. Kim, J. Park

Korea University, Seoul, Korea

S. Cho, S. Choi, B. Hong, K. Lee, K.S. Lee, J. Lim, J. Park, S.K. Park, J. Yoo

Kyung Hee University, Department of Physics, Seoul, Korea

J. Goh

Sejong University, Seoul, Korea

H. S. Kim, Y. Kim

Seoul National University, Seoul, Korea

J. Almond, J.H. Bhyun, J. Choi, S. Jeon, J. Kim, J. Kim, J.S. Kim, S. Ko, H. Kwon, H. Lee, S. Lee, B.H. Oh, M. Oh, S.B. Oh, H. Seo, U.K. Yang, I. Yoon

University of Seoul, Seoul, Korea

W. Jang, D.Y. Kang, Y. Kang, D. Kim, S. Kim, B. Ko, J.S.H. Lee, Y. Lee, J.A. Merlin, I.C. Park, Y. Roh, M.S. Ryu, D. Song, Watson, I.J., S. Yang

Yonsei University, Department of Physics, Seoul, Korea

S. Ha, H.D. Yoo

Sungkyunkwan University, Suwon, Korea

M. Choi, H. Lee, Y. Lee, I. Yu

College of Engineering and Technology, American University of the Middle East (AUM), Dasman, Kuwait

T. Beyrouthy, Y. Maghrbi

Riga Technical University, Riga, Latvia

K. Dreimanis, V. Veckalns

Vilnius University, Vilnius, Lithuania

M. Ambrozas, A. Carvalho Antunes De Oliveira, A. Juodagalvis, A. Rinkevicius, G. Tamulaitis

National Centre for Particle Physics, Universiti Malaya, Kuala Lumpur, Malaysia

N. Bin Norjoharuddeen, S.Y. Hoh[51], I. Yusuff[51], Z. Zolkapli

Universidad de Sonora (UNISON), Hermosillo, Mexico

J.F. Benitez, A. Castaneda Hernandez, H.A. Encinas Acosta, L.G. Gallegos Maríñez, M. León Coello, J.A. Murillo Quijada, A. Sehrawat, L. Valencia Palomo

Centro de Investigacion y de Estudios Avanzados del IPN, Mexico City, Mexico

G. Ayala, H. Castilla-Valdez, E. De La Cruz-Burelo, I. Heredia-De La Cruz[52], R. Lopez-Fernandez, C.A. Mondragon Herrera, D.A. Perez Navarro, A. Sánchez Hernández

Universidad Iberoamericana, Mexico City, Mexico

C. Oropeza Barrera, F. Vazquez Valencia

Benemerita Universidad Autonoma de Puebla, Puebla, Mexico

I. Pedraza, H.A. Salazar Ibarguen, C. Uribe Estrada

University of Montenegro, Podgorica, Montenegro

I. Bubanja, J. Mijuskovic[53], N. Raicevic

National Centre for Physics, Quaid-I-Azam University, Islamabad, Pakistan

A. Ahmad, M.I. Asghar, A. Awais, M.I.M. Awan, H.R. Hoorani, W.A. Khan, M. Shoaib, M. Waqas

AGH University of Science and Technology Faculty of Computer Science, Electronics and Telecommunications, Krakow, Poland

V. Avati, L. Grzanka, M. Malawski

National Centre for Nuclear Research, Swierk, Poland

H. Bialkowska, M. Bluj, B. Boimska, M. Górski, M. Kazana, M. Szleper, P. Zalewski

Institute of Experimental Physics, Faculty of Physics, University of Warsaw, Warsaw, Poland

K. Bunkowski, K. Doroba, A. Kalinowski, M. Konecki, J. Krolikowski

Laboratório de Instrumentação e Física Experimental de Partículas, Lisboa, Portugal

M. Araujo ⓘ, P. Bargassa ⓘ, D. Bastos ⓘ, A. Boletti ⓘ, P. Faccioli ⓘ, M. Gallinaro ⓘ, J. Hollar ⓘ, N. Leonardo ⓘ, T. Niknejad ⓘ, M. Pisano ⓘ, J. Seixas ⓘ, O. Toldaiev ⓘ, J. Varela ⓘ

VINCA Institute of Nuclear Sciences, University of Belgrade, Belgrade, Serbia

P. Adzic ⓘ[54], M. Dordevic ⓘ, P. Milenovic ⓘ, J. Milosevic ⓘ

Centro de Investigaciones Energéticas Medioambientales y Tecnológicas (CIEMAT), Madrid, Spain

M. Aguilar-Benitez, J. Alcaraz Maestre ⓘ, A. Álvarez Fernández ⓘ, M. Barrio Luna, Cristina F. Bedoya ⓘ, C.A. Carrillo Montoya ⓘ, M. Cepeda ⓘ, M. Cerrada ⓘ, N. Colino ⓘ, B. De La Cruz ⓘ, A. Delgado Peris ⓘ, J.P. Fernández Ramos ⓘ, J. Flix ⓘ, M.C. Fouz ⓘ, O. Gonzalez Lopez ⓘ, S. Goy Lopez ⓘ, J.M. Hernandez ⓘ, M.I. Josa ⓘ, J. León Holgado ⓘ, D. Moran ⓘ, C. Perez Dengra ⓘ, A. Pérez-Calero Yzquierdo ⓘ, J. Puerta Pelayo ⓘ, I. Redondo ⓘ, D.D. Redondo Ferrero ⓘ, L. Romero, S. Sánchez Navas ⓘ, J. Sastre ⓘ, L. Urda Gómez ⓘ, J. Vazquez Escobar ⓘ, C. Willmott

Universidad Autónoma de Madrid, Madrid, Spain

J.F. de Trocóniz ⓘ

Universidad de Oviedo, Instituto Universitario de Ciencias y Tecnologías Espaciales de Asturias (ICTEA), Oviedo, Spain

B. Alvarez Gonzalez ⓘ, J. Cuevas ⓘ, J. Fernandez Menendez ⓘ, S. Folgueras ⓘ, I. Gonzalez Caballero ⓘ, J.R. González Fernández ⓘ, E. Palencia Cortezon ⓘ, C. Ramón Álvarez ⓘ, V. Rodríguez Bouza ⓘ, A. Soto Rodríguez ⓘ, A. Trapote ⓘ, N. Trevisani ⓘ, C. Vico Villalba ⓘ

Instituto de Física de Cantabria (IFCA), CSIC-Universidad de Cantabria, Santander, Spain

J.A. Brochero Cifuentes ⓘ, I.J. Cabrillo ⓘ, A. Calderon ⓘ, J. Duarte Campderros ⓘ, M. Fernandez ⓘ, C. Fernandez Madrazo ⓘ, P.J. Fernández Manteca ⓘ, A. García Alonso, G. Gomez ⓘ, C. Lasaosa García ⓘ, C. Martinez Rivero ⓘ, P. Martinez Ruiz del Arbol ⓘ, F. Matorras ⓘ, P. Matorras Cuevas ⓘ, J. Piedra Gomez ⓘ, C. Prieels, A. Ruiz-Jimeno ⓘ, L. Scodellaro ⓘ, I. Vila ⓘ, J.M. Vizan Garcia ⓘ

University of Colombo, Colombo, Sri Lanka

M.K. Jayananda ⓘ, B. Kailasapathy ⓘ[55], D.U.J. Sonnadara ⓘ, D.D.C. Wickramarathna ⓘ

University of Ruhuna, Department of Physics, Matara, Sri Lanka

W.G.D. Dharmaratna ⓘ, K. Liyanage ⓘ, N. Perera ⓘ, N. Wickramage ⓘ

CERN, European Organization for Nuclear Research, Geneva, Switzerland

T.K. Aarrestad, D. Abbaneo, J. Alimena, E. Auffray, G. Auzinger, J. Baechler, P. Baillon[†], D. Barney, J. Bendavid, M. Bianco, B. Bilin, A. Bocci, E. Brondolin, C. Caillol, T. Camporesi, G. Cerminara, N. Chernyavskaya, S.S. Chhibra, S. Choudhury, M. Cipriani, L. Cristella, D. d'Enterria, A. Dabrowski, A. David, A. De Roeck, M.M. Defranchis, M. Deile, M. Dobson, M. Dünser, A. Elliott-Peisert, F. Fallavollita[56], A. Florent, L. Forthomme, W. Funk, S. Ghosh, S. Giani, D. Gigi, K. Gill, F. Glege, L. Gouskos, E. Govorkova, M. Haranko, J. Hegeman, V. Innocente, T. James, P. Janot, J. Kaspar, J. Kieseler, M. Komm, N. Kratochwil, S. Laurila, P. Lecoq, A. Lintuluoto, C. Lourenço, B. Maier, L. Malgeri, M. Mannelli, A.C. Marini, F. Meijers, S. Mersi, E. Meschi, F. Moortgat, M. Mulders, S. Orfanelli, L. Orsini, F. Pantaleo, E. Perez, M. Peruzzi, A. Petrilli, G. Petrucciani, A. Pfeiffer, M. Pierini, D. Piparo, M. Pitt, H. Qu, T. Quast, D. Rabady, A. Racz, G. Reales Gutiérrez, M. Rovere, H. Sakulin, S. Scarfi, M. Selvaggi, A. Sharma, P. Silva, W. Snoeys, P. Sphicas[57], A.G. Stahl Leiton, S. Summers, K. Tatar, V.R. Tavolaro, D. Treille, P. Tropea, A. Tsirou, J. Wanczyk[58], K.A. Wozniak, W.D. Zeuner

Paul Scherrer Institut, Villigen, Switzerland

L. Caminada[59], A. Ebrahimi, W. Erdmann, R. Horisberger, Q. Ingram, H.C. Kaestli, D. Kotlinski, C. Lange, M. Missiroli[59], L. Noehte[59], T. Rohe

ETH Zurich — Institute for Particle Physics and Astrophysics (IPA), Zurich, Switzerland

K. Androsov[58], M. Backhaus, P. Berger, A. Calandri, A. De Cosa, G. Dissertori, M. Dittmar, M. Donegà, C. Dorfer, F. Eble, K. Gedia, F. Glessgen, T.A. Gómez Espinosa, C. Grab, D. Hits, W. Lustermann, A.-M. Lyon, R.A. Manzoni, L. Marchese, C. Martin Perez, A. Mascellani[58], M.T. Meinhard, F. Nessi-Tedaldi, J. Niedziela, F. Pauss, V. Perovic, S. Pigazzini, M.G. Ratti, M. Reichmann, C. Reissel, T. Reitenspiess, B. Ristic, D. Ruini, D.A. Sanz Becerra, J. Steggemann[58], D. Valsecchi[21], R. Wallny

Universität Zürich, Zurich, Switzerland

C. Amsler[60], P. Bärtschi, C. Botta, D. Brzhechko, M.F. Canelli, K. Cormier, A. De Wit, R. Del Burgo, J.K. Heikkilä, M. Huwiler, W. Jin, A. Jofrehei, B. Kilminster, S. Leontsinis, S.P. Liechti, A. Macchiolo, P. Meiring, V.M. Mikuni, U. Molinatti, I. Neutelings, A. Reimers, P. Robmann, S. Sanchez Cruz, K. Schweiger, M. Senger, Y. Takahashi

National Central University, Chung-Li, Taiwan

C. Adloff[61], C.M. Kuo, W. Lin, S.S. Yu

National Taiwan University (NTU), Taipei, Taiwan

L. Ceard, Y. Chao, K.F. Chen, P.H. Chen, P.s. Chen, H. Cheng, W.-S. Hou, Y.y. Li, R.-S. Lu, E. Paganis, A. Psallidas, A. Steen, H.y. Wu, E. Yazgan, P.r. Yu

Chulalongkorn University, Faculty of Science, Department of Physics, Bangkok, Thailand

C. Asawatangtrakuldee ©, N. Srimanobhas ©

Çukurova University, Physics Department, Science and Art Faculty, Adana, Turkey

D. Agyel ©, F. Boran ©, Z.S. Demiroglu ©, F. Dolek ©, I. Dumanoglu ©[62], E. Eskut ©, Y. Guler ©[63], E. Gurpinar Guler ©[63], C. Isik ©, O. Kara, A. Kayis Topaksu ©, U. Kiminsu ©, G. Onengut ©, K. Ozdemir ©[64], A. Polatoz ©, A.E. Simsek ©, B. Tali ©[65], U.G. Tok ©, S. Turkcapar ©, E. Uslan ©, I.S. Zorbakir ©

Middle East Technical University, Physics Department, Ankara, Turkey

G. Karapinar, K. Ocalan ©[66], M. Yalvac ©[67]

Bogazici University, Istanbul, Turkey

B. Akgun ©, I.O. Atakisi ©, E. Gülmez ©, M. Kaya ©[68], O. Kaya ©[69], Ö. Özçelik ©, S. Tekten ©[70]

Istanbul Technical University, Istanbul, Turkey

A. Cakir ©, K. Cankocak ©[62], Y. Komurcu ©, S. Sen ©[71]

Istanbul University, Istanbul, Turkey

O. Aydilek ©, S. Cerci ©[65], B. Hacisahinoglu ©, I. Hos ©[72], B. Isildak ©[73], B. Kaynak ©, S. Ozkorucuklu ©, C. Simsek ©, D. Sunar Cerci ©[65]

Institute for Scintillation Materials of National Academy of Science of Ukraine, Kharkiv, Ukraine

B. Grynyov ©

National Science Centre, Kharkiv Institute of Physics and Technology, Kharkiv, Ukraine

L. Levchuk ©

University of Bristol, Bristol, United Kingdom

D. Anthony ©, E. Bhal ©, J.J. Brooke ©, A. Bundock ©, E. Clement ©, D. Cussans ©, H. Flacher ©, M. Glowacki, J. Goldstein ©, G.P. Heath, H.F. Heath ©, L. Kreczko ©, B. Krikler ©, S. Paramesvaran ©, S. Seif El Nasr-Storey, V.J. Smith ©, N. Stylianou ©[74], K. Walkingshaw Pass, R. White ©

Rutherford Appleton Laboratory, Didcot, United Kingdom

A.H. Ball, K.W. Bell ©, A. Belyaev ©[75], C. Brew ©, R.M. Brown ©, D.J.A. Cockerill ©, C. Cooke ©, K.V. Ellis, K. Harder ©, S. Harper ©, M.-L. Holmberg ©[76], J. Linacre ©, K. Manolopoulos, D.M. Newbold ©, E. Olaiya, D. Petyt ©, T. Reis ©, T. Schuh, C.H. Shepherd-Themistocleous ©, I.R. Tomalin, T. Williams ©

Imperial College, London, United Kingdom

R. Bainbridge ⓘ, P. Bloch ⓘ, S. Bonomally, J. Borg ⓘ, S. Breeze, O. Buchmuller, V. Cepaitis ⓘ, G.S. Chahal ⓘ[77], D. Colling ⓘ, P. Dauncey ⓘ, G. Davies ⓘ, M. Della Negra ⓘ, S. Fayer, G. Fedi ⓘ, G. Hall ⓘ, M.H. Hassanshahi ⓘ, G. Iles ⓘ, J. Langford ⓘ, L. Lyons ⓘ, A.-M. Magnan ⓘ, S. Malik, D.G. Monk ⓘ, J. Nash ⓘ[78], M. Pesaresi, B.C. Radburn-Smith ⓘ, D.M. Raymond, A. Richards, A. Rose ⓘ, E. Scott ⓘ, C. Seez ⓘ, A. Shtipliyski, R. Shukla ⓘ, A. Tapper ⓘ, K. Uchida ⓘ, T. Virdee ⓘ[21], M. Vojinovic ⓘ, N. Wardle ⓘ, D. Winterbottom

Brunel University, Uxbridge, United Kingdom

K. Coldham, J.E. Cole ⓘ, A. Khan, P. Kyberd ⓘ, I.D. Reid ⓘ, L. Teodorescu, S. Zahid ⓘ

Baylor University, Waco, Texas, USA

S. Abdullin ⓘ, A. Brinkerhoff ⓘ, B. Caraway ⓘ, J. Dittmann ⓘ, K. Hatakeyama ⓘ, A.R. Kanuganti ⓘ, B. McMaster ⓘ, M. Saunders ⓘ, S. Sawant ⓘ, C. Sutantawibul ⓘ, J. Wilson ⓘ

Catholic University of America, Washington, DC, USA

R. Bartek ⓘ, A. Dominguez ⓘ, R. Uniyal ⓘ, A.M. Vargas Hernandez ⓘ

The University of Alabama, Tuscaloosa, Alabama, USA

A. Buccilli ⓘ, S.I. Cooper ⓘ, D. Di Croce ⓘ, S.V. Gleyzer ⓘ, C. Henderson ⓘ, C.U. Perez ⓘ, P. Rumerio ⓘ[79], C. West ⓘ

Boston University, Boston, Massachusetts, USA

A. Akpinar ⓘ, A. Albert ⓘ, D. Arcaro ⓘ, C. Cosby ⓘ, Z. Demiragli ⓘ, C. Erice ⓘ, E. Fontanesi ⓘ, D. Gastler ⓘ, S. May ⓘ, J. Rohlf ⓘ, K. Salyer ⓘ, D. Sperka ⓘ, D. Spitzbart ⓘ, I. Suarez ⓘ, A. Tsatsos ⓘ, S. Yuan ⓘ

Brown University, Providence, Rhode Island, USA

G. Benelli ⓘ, B. Burkle ⓘ, X. Coubez[23], D. Cutts ⓘ, M. Hadley ⓘ, U. Heintz ⓘ, J.M. Hogan ⓘ[80], T. Kwon ⓘ, G. Landsberg ⓘ, K.T. Lau ⓘ, D. Li ⓘ, M. Lukasik, J. Luo ⓘ, M. Narain ⓘ, N. Pervan ⓘ, S. Sagir ⓘ[81], F. Simpson ⓘ, E. Usai ⓘ, W.Y. Wong, X. Yan ⓘ, D. Yu, W. Zhang

University of California, Davis, Davis, California, USA

J. Bonilla ⓘ, C. Brainerd ⓘ, R. Breedon ⓘ, M. Calderon De La Barca Sanchez ⓘ, M. Chertok ⓘ, J. Conway ⓘ, P.T. Cox ⓘ, R. Erbacher ⓘ, G. Haza ⓘ, F. Jensen ⓘ, O. Kukral ⓘ, G. Mocellin ⓘ, M. Mulhearn ⓘ, D. Pellett ⓘ, B. Regnery ⓘ, D. Taylor ⓘ, Y. Yao ⓘ, F. Zhang ⓘ

University of California, Los Angeles, California, USA

M. Bachtis ⓘ, R. Cousins ⓘ, A. Datta ⓘ, D. Hamilton ⓘ, J. Hauser ⓘ, M. Ignatenko ⓘ, M.A. Iqbal ⓘ, T. Lam ⓘ, W.A. Nash ⓘ, S. Regnard ⓘ, D. Saltzberg ⓘ, B. Stone ⓘ, V. Valuev ⓘ

University of California, Riverside, Riverside, California, USA

Y. Chen, R. Clare ⓘ, J.W. Gary ⓘ, M. Gordon, G. Hanson ⓘ, G. Karapostoli ⓘ, O.R. Long ⓘ, N. Manganelli ⓘ, W. Si ⓘ, S. Wimpenny ⓘ, Y. Zhang

University of California, San Diego, La Jolla, California, USA

J.G. Branson, P. Chang ⓘ, S. Cittolin, S. Cooperstein ⓘ, D. Diaz ⓘ, J. Duarte ⓘ, R. Gerosa ⓘ,
L. Giannini ⓘ, J. Guiang, R. Kansal ⓘ, V. Krutelyov ⓘ, R. Lee ⓘ, J. Letts ⓘ,
M. Masciovecchio ⓘ, F. Mokhtar ⓘ, M. Pieri ⓘ, B.V. Sathia Narayanan ⓘ, V. Sharma ⓘ,
M. Tadel ⓘ, F. Würthwein ⓘ, Y. Xiang ⓘ, A. Yagil ⓘ

**University of California, Santa Barbara — Department of Physics, Santa
Barbara, California, USA**

N. Amin, C. Campagnari ⓘ, M. Citron ⓘ, G. Collura ⓘ, A. Dorsett ⓘ, V. Dutta ⓘ, J. Incandela ⓘ,
M. Kilpatrick ⓘ, J. Kim ⓘ, B. Marsh, P. Masterson ⓘ, H. Mei ⓘ, M. Oshiro ⓘ, M. Quinnan ⓘ,
J. Richman ⓘ, U. Sarica ⓘ, F. Setti ⓘ, J. Sheplock ⓘ, P. Siddireddy, D. Stuart, S. Wang ⓘ

California Institute of Technology, Pasadena, California, USA

A. Bornheim ⓘ, O. Cerri, I. Dutta ⓘ, J.M. Lawhorn ⓘ, N. Lu ⓘ, J. Mao ⓘ, H.B. Newman ⓘ,
T. Q. Nguyen ⓘ, M. Spiropulu ⓘ, J.R. Vlimant ⓘ, C. Wang ⓘ, S. Xie ⓘ, Z. Zhang ⓘ, R.Y. Zhu ⓘ

Carnegie Mellon University, Pittsburgh, Pennsylvania, USA

J. Alison ⓘ, S. An ⓘ, M.B. Andrews ⓘ, P. Bryant ⓘ, T. Ferguson ⓘ, A. Harilal ⓘ, C. Liu ⓘ,
T. Mudholkar ⓘ, S. Murthy ⓘ, M. Paulini ⓘ, A. Roberts ⓘ, A. Sanchez ⓘ, W. Terrill ⓘ

University of Colorado Boulder, Boulder, Colorado, USA

J.P. Cumalat ⓘ, W.T. Ford ⓘ, A. Hassani ⓘ, G. Karathanasis ⓘ, E. MacDonald, R. Patel,
A. Perloff ⓘ, C. Savard ⓘ, N. Schonbeck ⓘ, K. Stenson ⓘ, K.A. Ulmer ⓘ, S.R. Wagner ⓘ,
N. Zipper ⓘ

Cornell University, Ithaca, New York, USA

J. Alexander ⓘ, S. Bright-Thonney ⓘ, X. Chen ⓘ, Y. Cheng ⓘ, D.J. Cranshaw ⓘ, J. Fan ⓘ,
X. Fan ⓘ, D. Gadkari ⓘ, S. Hogan ⓘ, J. Monroy ⓘ, J.R. Patterson ⓘ, D. Quach ⓘ, J. Reichert ⓘ,
M. Reid ⓘ, A. Ryd ⓘ, J. Thom ⓘ, P. Wittich ⓘ, R. Zou ⓘ

Fermi National Accelerator Laboratory, Batavia, Illinois, USA

M. Albrow ⓘ, M. Alyari ⓘ, G. Apollinari ⓘ, A. Apresyan ⓘ, L.A.T. Bauerdick ⓘ, D. Berry ⓘ,
J. Berryhill ⓘ, P.C. Bhat ⓘ, K. Burkett ⓘ, J.N. Butler ⓘ, A. Canepa ⓘ, G.B. Cerati ⓘ,
H.W.K. Cheung ⓘ, F. Chlebana ⓘ, K.F. Di Petrillo ⓘ, J. Dickinson ⓘ, V.D. Elvira ⓘ, Y. Feng ⓘ,
J. Freeman ⓘ, A. Gandrakota ⓘ, Z. Gecse ⓘ, L. Gray ⓘ, D. Green, S. Grünendahl ⓘ,
O. Gutsche ⓘ, R.M. Harris ⓘ, R. Heller ⓘ, T.C. Herwig ⓘ, J. Hirschauer ⓘ, L. Horyn ⓘ,
B. Jayatilaka ⓘ, S. Jindariani ⓘ, M. Johnson ⓘ, U. Joshi ⓘ, T. Klijnsma ⓘ, B. Klima ⓘ,
K.H.M. Kwok ⓘ, S. Lammel ⓘ, D. Lincoln ⓘ, R. Lipton ⓘ, T. Liu ⓘ, C. Madrid ⓘ,
K. Maeshima ⓘ, C. Mantilla ⓘ, D. Mason ⓘ, P. McBride ⓘ, P. Merkel ⓘ, S. Mrenna ⓘ, S. Nahn ⓘ,
J. Ngadiuba ⓘ, V. Papadimitriou ⓘ, K. Pedro ⓘ, C. Pena ⓘ[82], F. Ravera ⓘ, A. Reinsvold Hall ⓘ[83],
L. Ristori ⓘ, E. Sexton-Kennedy ⓘ, N. Smith ⓘ, A. Soha ⓘ, L. Spiegel ⓘ, J. Strait ⓘ, L. Taylor ⓘ,
S. Tkaczyk ⓘ, N.V. Tran ⓘ, L. Uplegger ⓘ, E.W. Vaandering ⓘ, H.A. Weber ⓘ, I. Zoi ⓘ

University of Florida, Gainesville, Florida, USA

P. Avery ⓘ, D. Bourilkov ⓘ, L. Cadamuro ⓘ, V. Cherepanov ⓘ, R.D. Field, D. Guerrero ⓘ,
M. Kim, E. Koenig ⓘ, J. Konigsberg ⓘ, A. Korytov ⓘ, K.H. Lo, K. Matchev ⓘ, N. Menendez ⓘ,
G. Mitselmakher ⓘ, A. Muthirakalayil Madhu ⓘ, N. Rawal ⓘ, D. Rosenzweig ⓘ, S. Rosenzweig ⓘ,
K. Shi ⓘ, J. Wang ⓘ, Z. Wu ⓘ

Florida State University, Tallahassee, Florida, USA

T. Adams ⓘ, A. Askew ⓘ, R. Habibullah ⓘ, V. Hagopian ⓘ, R. Khurana, T. Kolberg ⓘ,
G. Martinez, H. Prosper ⓘ, C. Schiber, O. Viazlo ⓘ, R. Yohay ⓘ, J. Zhang

Florida Institute of Technology, Melbourne, Florida, USA

M.M. Baarmand ⓘ, S. Butalla ⓘ, T. Elkafrawy ⓘ[84], M. Hohlmann ⓘ, R. Kumar Verma ⓘ,
D. Noonan ⓘ, M. Rahmani, F. Yumiceva ⓘ

University of Illinois at Chicago (UIC), Chicago, Illinois, USA

M.R. Adams ⓘ, H. Becerril Gonzalez ⓘ, R. Cavanaugh ⓘ, S. Dittmer ⓘ, O. Evdokimov ⓘ,
C.E. Gerber ⓘ, D.J. Hofman ⓘ, D. S. Lemos ⓘ, A.H. Merrit ⓘ, C. Mills ⓘ, G. Oh ⓘ, T. Roy ⓘ,
S. Rudrabhatla ⓘ, M.B. Tonjes ⓘ, N. Varelas ⓘ, J. Viinikainen ⓘ, X. Wang ⓘ, Z. Ye ⓘ

The University of Iowa, Iowa City, Iowa, USA

M. Alhusseini ⓘ, K. Dilsiz ⓘ[85], L. Emediato ⓘ, R.P. Gandrajula ⓘ, O.K. Köseyan ⓘ, J.-P. Merlo,
A. Mestvirishvili ⓘ[86], J. Nachtman ⓘ, H. Ogul ⓘ[87], Y. Onel ⓘ, A. Penzo ⓘ, C. Snyder,
E. Tiras ⓘ[88]

Johns Hopkins University, Baltimore, Maryland, USA

O. Amram ⓘ, B. Blumenfeld ⓘ, L. Corcodilos ⓘ, J. Davis ⓘ, A.V. Gritsan ⓘ, S. Kyriacou ⓘ,
P. Maksimovic ⓘ, J. Roskes ⓘ, M. Swartz ⓘ, T.Á. Vámi ⓘ

The University of Kansas, Lawrence, Kansas, USA

A. Abreu ⓘ, J. Anguiano ⓘ, P. Baringer ⓘ, A. Bean ⓘ, Z. Flowers ⓘ, T. Isidori ⓘ, S. Khalil ⓘ,
J. King ⓘ, G. Krintiras ⓘ, M. Lazarovits ⓘ, C. Le Mahieu ⓘ, C. Lindsey, J. Marquez ⓘ,
N. Minafra ⓘ, M. Murray ⓘ, M. Nickel ⓘ, C. Rogan ⓘ, C. Royon ⓘ, R. Salvatico, S. Sanders ⓘ,
E. Schmitz ⓘ, C. Smith ⓘ, Q. Wang ⓘ, Z. Warner, J. Williams ⓘ, G. Wilson ⓘ

Kansas State University, Manhattan, Kansas, USA

S. Duric, A. Ivanov ⓘ, K. Kaadze ⓘ, D. Kim, Y. Maravin ⓘ, T. Mitchell, A. Modak, D. Roy ⓘ

Lawrence Livermore National Laboratory, Livermore, California, USA

F. Rebassoo ⓘ, D. Wright ⓘ

University of Maryland, College Park, Maryland, USA

E. Adams ⓘ, A. Baden ⓘ, O. Baron, A. Belloni ⓘ, S.C. Eno ⓘ, N.J. Hadley ⓘ, S. Jabeen ⓘ,
R.G. Kellogg ⓘ, T. Koeth ⓘ, Y. Lai ⓘ, S. Lascio ⓘ, A.C. Mignerey ⓘ, S. Nabili ⓘ, C. Palmer ⓘ,
C. Papageorgakis ⓘ, M. Seidel ⓘ, L. Wang ⓘ, K. Wong ⓘ

Massachusetts Institute of Technology, Cambridge, Massachusetts, USA

D. Abercrombie, G. Andreassi, R. Bi, W. Busza ⬤, I.A. Cali ⬤, Y. Chen ⬤, M. D'Alfonso ⬤,
G. Gomez-Ceballos ⬤, M. Goncharov, P. Harris, M. Hu ⬤, M. Klute ⬤, D. Kovalskyi ⬤,
J. Krupa ⬤, Y.-J. Lee ⬤, C. Mironov ⬤, C. Paus ⬤, D. Rankin ⬤, C. Roland ⬤, G. Roland ⬤,
Z. Shi ⬤, G.S.F. Stephans ⬤, J. Wang, B. Wyslouch ⬤

University of Minnesota, Minneapolis, Minnesota, USA

R.M. Chatterjee, A. Evans ⬤, J. Hiltbrand ⬤, Sh. Jain ⬤, B.M. Joshi ⬤, M. Krohn ⬤,
Y. Kubota ⬤, J. Mans ⬤, M. Revering ⬤, R. Rusack ⬤, R. Saradhy ⬤, N. Schroeder ⬤,
N. Strobbe ⬤, M.A. Wadud ⬤

University of Mississippi, Oxford, Mississippi, USA

L.M. Cremaldi ⬤

University of Nebraska-Lincoln, Lincoln, Nebraska, USA

K. Bloom ⬤, M. Bryson, S. Chauhan ⬤, D.R. Claes ⬤, C. Fangmeier ⬤, L. Finco ⬤, F. Golf ⬤,
C. Joo ⬤, I. Kravchenko ⬤, I. Reed ⬤, J.E. Siado ⬤, G.R. Snow[†], W. Tabb ⬤, A. Wightman ⬤,
F. Yan ⬤, A.G. Zecchinelli ⬤

State University of New York at Buffalo, Buffalo, New York, USA

G. Agarwal ⬤, H. Bandyopadhyay ⬤, L. Hay ⬤, I. Iashvili ⬤, A. Kharchilava ⬤, C. McLean ⬤,
D. Nguyen ⬤, J. Pekkanen ⬤, S. Rappoccio ⬤, A. Williams ⬤

Northeastern University, Boston, Massachusetts, USA

G. Alverson ⬤, E. Barberis ⬤, Y. Haddad ⬤, Y. Han ⬤, A. Hortiangtham ⬤, A. Krishna ⬤,
J. Li ⬤, J. Lidrych ⬤, G. Madigan ⬤, B. Marzocchi ⬤, D.M. Morse ⬤, V. Nguyen ⬤,
T. Orimoto ⬤, A. Parker ⬤, L. Skinnari ⬤, A. Tishelman-Charny ⬤, T. Wamorkar ⬤, B. Wang ⬤,
A. Wisecarver ⬤, D. Wood ⬤

Northwestern University, Evanston, Illinois, USA

S. Bhattacharya ⬤, J. Bueghly, Z. Chen ⬤, A. Gilbert ⬤, T. Gunter ⬤, K.A. Hahn ⬤, Y. Liu ⬤,
N. Odell ⬤, M.H. Schmitt ⬤, M. Velasco

University of Notre Dame, Notre Dame, Indiana, USA

R. Band ⬤, R. Bucci, M. Cremonesi, A. Das ⬤, R. Goldouzian ⬤, M. Hildreth ⬤,
K. Hurtado Anampa ⬤, C. Jessop ⬤, K. Lannon ⬤, J. Lawrence ⬤, N. Loukas ⬤, L. Lutton ⬤,
J. Mariano, N. Marinelli, I. Mcalister, T. McCauley ⬤, C. Mcgrady ⬤, K. Mohrman ⬤,
C. Moore ⬤, Y. Musienko ⬤[13], R. Ruchti ⬤, A. Townsend ⬤, M. Wayne, H. Yockey,
M. Zarucki ⬤, L. Zygala ⬤

The Ohio State University, Columbus, Ohio, USA

B. Bylsma, L.S. Durkin ⬤, B. Francis ⬤, C. Hill ⬤, A. Lesauvage ⬤, M. Nunez Ornelas ⬤, K. Wei,
B.L. Winer ⬤, B.R. Yates ⬤

Princeton University, Princeton, New Jersey, USA

F.M. Addesa ©, B. Bonham ©, G. Dezoort ©, P. Elmer ©, A. Frankenthal ©, B. Greenberg ©,
N. Haubrich ©, S. Higginbotham ©, A. Kalogeropoulos ©, G. Kopp ©, S. Kwan ©, D. Lange ©,
D. Marlow ©, K. Mei ©, I. Ojalvo ©, J. Olsen ©, D. Stickland ©, C. Tully ©

University of Puerto Rico, Mayaguez, Puerto Rico, USA

S. Malik ©, S. Norberg

Purdue University, West Lafayette, Indiana, USA

A.S. Bakshi ©, V.E. Barnes ©, R. Chawla ©, S. Das ©, L. Gutay, M. Jones ©, A.W. Jung ©,
D. Kondratyev ©, A.M. Koshy, M. Liu ©, G. Negro ©, N. Neumeister ©, G. Paspalaki ©,
S. Piperov ©, A. Purohit ©, J.F. Schulte ©, M. Stojanovic ©, J. Thieman ©, F. Wang ©,
R. Xiao ©, W. Xie ©

Purdue University Northwest, Hammond, Indiana, USA

J. Dolen ©, N. Parashar ©

Rice University, Houston, Texas, USA

D. Acosta ©, A. Baty ©, T. Carnahan ©, M. Decaro, S. Dildick ©, K.M. Ecklund ©, S. Freed,
P. Gardner, F.J.M. Geurts ©, A. Kumar ©, W. Li ©, B.P. Padley ©, R. Redjimi, J. Rotter ©,
W. Shi ©, S. Yang ©, E. Yigitbasi ©, L. Zhang[89], Y. Zhang ©, X. Zuo ©

**University of Rochester, Rochester, New York, USA**

A. Bodek ©, P. de Barbaro ©, R. Demina ©, J.L. Dulemba ©, C. Fallon, T. Ferbel ©, M. Galanti,
A. Garcia-Bellido ©, O. Hindrichs ©, A. Khukhunaishvili, E. Ranken ©, R. Taus ©,
G.P. Van Onsem ©

The Rockefeller University, New York, New York, USA

K. Goulianos ©

Rutgers, The State University of New Jersey, Piscataway, New Jersey, USA

B. Chiarito, J.P. Chou ©, Y. Gershtein ©, E. Halkiadakis ©, A. Hart ©, M. Heindl ©,
O. Karacheban ©[25], I. Laflotte ©, A. Lath ©, R. Montalvo, K. Nash, M. Osherson ©, S. Salur ©,
S. Schnetzer, S. Somalwar ©, R. Stone ©, S.A. Thayil ©, S. Thomas, H. Wang ©

University of Tennessee, Knoxville, Tennessee, USA

H. Acharya, A.G. Delannoy ©, S. Fiorendi ©, T. Holmes ©, S. Spanier ©

Texas A&M University, College Station, Texas, USA

O. Bouhali ©[90], M. Dalchenko ©, A. Delgado ©, R. Eusebi ©, J. Gilmore ©, T. Huang ©,
T. Kamon ©[91], H. Kim ©, S. Luo ©, S. Malhotra, R. Mueller ©, D. Overton ©, D. Rathjens ©,
A. Safonov ©

Texas Tech University, Lubbock, Texas, USA

N. Akchurin ©, J. Damgov ©, V. Hegde ©, K. Lamichhane ©, S.W. Lee ©, T. Mengke,
S. Muthumuni ©, T. Peltola ©, I. Volobouev ©, Z. Wang, A. Whitbeck ©

Vanderbilt University, Nashville, Tennessee, USA

E. Appelt ⓘ, S. Greene, A. Gurrola ⓘ, W. Johns ⓘ, A. Melo ⓘ, F. Romeo ⓘ, P. Sheldon ⓘ,
S. Tuo ⓘ, J. Velkovska ⓘ

University of Virginia, Charlottesville, Virginia, USA

B. Cardwell ⓘ, B. Cox ⓘ, G. Cummings ⓘ, J. Hakala ⓘ, R. Hirosky ⓘ, M. Joyce ⓘ,
A. Ledovskoy ⓘ, A. Li ⓘ, C. Neu ⓘ, C.E. Perez Lara ⓘ, B. Tannenwald ⓘ

Wayne State University, Detroit, Michigan, USA

P.E. Karchin ⓘ, N. Poudyal ⓘ

University of Wisconsin — Madison, Madison, Wisconsin, USA

S. Banerjee ⓘ, K. Black ⓘ, T. Bose ⓘ, S. Dasu ⓘ, I. De Bruyn ⓘ, P. Everaerts ⓘ, C. Galloni,
H. He ⓘ, M. Herndon ⓘ, A. Herve ⓘ, C.K. Koraka ⓘ, A. Lanaro, A. Loeliger ⓘ, R. Loveless ⓘ,
J. Madhusudanan Sreekala ⓘ, A. Mallampalli ⓘ, A. Mohammadi ⓘ, D. Pinna, A. Savin,
V. Shang ⓘ, V. Sharma ⓘ, W.H. Smith ⓘ, D. Teague, S. Trembath-Reichert, W. Vetens ⓘ

Authors affiliated with an institute or an international laboratory covered by a cooperation agreement with CERN

S. Afanasiev ⓘ, V. Andreev ⓘ, Yu. Andreev ⓘ, T. Aushev ⓘ, M. Azarkin ⓘ, A. Babaev ⓘ,
A. Belyaev ⓘ, V. Blinov[92], E. Boos ⓘ, V. Borshch ⓘ, D. Budkouski ⓘ, V. Bunichev ⓘ,
M. Chadeeva ⓘ[92], V. Chekhovsky, A. Dermenev ⓘ, T. Dimova ⓘ[92], I. Dremin ⓘ, M. Dubinin ⓘ[82],
L. Dudko ⓘ, V. Epshteyn ⓘ, A. Ershov ⓘ, G. Gavrilov ⓘ, V. Gavrilov ⓘ, S. Gninenko ⓘ,
V. Golovtcov ⓘ, N. Golubev ⓘ, I. Golutvin ⓘ, I. Gorbunov ⓘ, V. Ivanchenko ⓘ, Y. Ivanov ⓘ,
V. Kachanov ⓘ, L. Kardapoltsev ⓘ[92], V. Karjavine ⓘ, A. Karneyeu ⓘ, V. Kim ⓘ[92],
M. Kirakosyan, D. Kirpichnikov ⓘ, M. Kirsanov ⓘ, V. Klyukhin ⓘ, O. Kodolova ⓘ[93],
D. Konstantinov ⓘ, V. Korenkov ⓘ, A. Kozyrev ⓘ[92], N. Krasnikov ⓘ, E. Kuznetsova ⓘ[94],
A. Lanev ⓘ, P. Levchenko ⓘ, A. Litomin, N. Lychkovskaya ⓘ, V. Makarenko ⓘ, A. Malakhov ⓘ,
V. Matveev ⓘ[92], V. Murzin, A. Nikitenko ⓘ[95], S. Obraztsov ⓘ, V. Okhotnikov, A. Oskin,
I. Ovtin ⓘ[92], V. Palichik ⓘ, P. Parygin ⓘ, V. Perelygin ⓘ, M. Perfilov, S. Petrushanko ⓘ,
G. Pivovarov ⓘ, V. Popov, E. Popova ⓘ, O. Radchenko ⓘ[92], V. Rusinov, M. Savina ⓘ,
V. Savrin ⓘ, D. Selivanova ⓘ, V. Shalaev ⓘ, S. Shmatov ⓘ, S. Shulha ⓘ, Y. Skovpen ⓘ[92],
S. Slabospitskii ⓘ, V. Smirnov, D. Sosnov ⓘ, A. Stepennov, V. Sulimov ⓘ, E. Tcherniaev ⓘ,
A. Terkulov ⓘ, O. Teryaev ⓘ, I. Tlisova ⓘ, M. Toms ⓘ, A. Toropin ⓘ, L. Uvarov ⓘ, A. Uzunian ⓘ,
E. Vlasov ⓘ, A. Vorobyev, N. Voytishin ⓘ, B.S. Yuldashev[96], A. Zarubin ⓘ, I. Zhizhin ⓘ,
A. Zhokin ⓘ

† *Deceased*
1 *Also at Yerevan State University, Yerevan, Armenia*
2 *Also at TU Wien, Vienna, Austria*
3 *Also at Institute of Basic and Applied Sciences, Faculty of Engineering, Arab Academy for Science, Technology and Maritime Transport, Alexandria, Egypt*
4 *Also at Université Libre de Bruxelles, Bruxelles, Belgium*
5 *Also at Universidade Estadual de Campinas, Campinas, Brazil*
6 *Also at Federal University of Rio Grande do Sul, Porto Alegre, Brazil*
7 *Also at UFMS, Nova Andradina, Brazil*

[8] Also at The University of the State of Amazonas, Manaus, Brazil

[9] Also at University of Chinese Academy of Sciences, Beijing, China

[10] Also at Nanjing Normal University Department of Physics, Nanjing, China

[11] Now at The University of Iowa, Iowa City, Iowa, USA

[12] Also at University of Chinese Academy of Sciences, Beijing, China

[13] Also at an institute or an international laboratory covered by a cooperation agreement with CERN

[14] Also at Cairo University, Cairo, Egypt

[15] Also at Suez University, Suez, Egypt

[16] Now at British University in Egypt, Cairo, Egypt

[17] Also at Purdue University, West Lafayette, Indiana, USA

[18] Also at Université de Haute Alsace, Mulhouse, France

[19] Also at Ilia State University, Tbilisi, Georgia

[20] Also at Erzincan Binali Yildirim University, Erzincan, Turkey

[21] Also at CERN, European Organization for Nuclear Research, Geneva, Switzerland

[22] Also at University of Hamburg, Hamburg, Germany

[23] Also at RWTH Aachen University, III. Physikalisches Institut A, Aachen, Germany

[24] Also at Isfahan University of Technology, Isfahan, Iran

[25] Also at Brandenburg University of Technology, Cottbus, Germany

[26] Also at Forschungszentrum Jülich, Juelich, Germany

[27] Also at Physics Department, Faculty of Science, Assiut University, Assiut, Egypt

[28] Also at Karoly Robert Campus, MATE Institute of Technology, Gyongyos, Hungary

[29] Also at Institute of Physics, University of Debrecen, Debrecen, Hungary

[30] Also at Institute of Nuclear Research ATOMKI, Debrecen, Hungary

[31] Now at Universitatea Babes-Bolyai — Facultatea de Fizica, Cluj-Napoca, Romania

[32] Also at Faculty of Informatics, University of Debrecen, Debrecen, Hungary

[33] Also at Wigner Research Centre for Physics, Budapest, Hungary

[34] Also at Punjab Agricultural University, Ludhiana, India

[35] Also at UPES — University of Petroleum and Energy Studies, Dehradun, India

[36] Also at University of Hyderabad, Hyderabad, India

[37] Also at University of Visva-Bharati, Santiniketan, India

[38] Also at Indian Institute of Science (IISc), Bangalore, India

[39] Also at Indian Institute of Technology (IIT), Mumbai, India

[40] Also at IIT Bhubaneswar, Bhubaneswar, India

[41] Also at Institute of Physics, Bhubaneswar, India

[42] Also at Deutsches Elektronen-Synchrotron, Hamburg, Germany

[43] Also at Sharif University of Technology, Tehran, Iran

[44] Also at Department of Physics, University of Science and Technology of Mazandaran, Behshahr, Iran

[45] Also at Helwan University, Cairo, Egypt

[46] Also at Italian National Agency for New Technologies, Energy and Sustainable Economic Development, Bologna, Italy

[47] Also at Centro Siciliano di Fisica Nucleare e di Struttura Della Materia, Catania, Italy

[48] Also at Scuola Superiore Meridionale, Università di Napoli 'Federico II', Napoli, Italy

[49] Also at Università di Napoli 'Federico II', Napoli, Italy

[50] Also at Consiglio Nazionale delle Ricerche — Istituto Officina dei Materiali, Perugia, Italy

[51] Also at Department of Applied Physics, Faculty of Science and Technology, Universiti Kebangsaan Malaysia, Bangi, Malaysia

[52] Also at Consejo Nacional de Ciencia y Tecnología, Mexico City, Mexico

[53] Also at IRFU, CEA, Université Paris-Saclay, Gif-sur-Yvette, France

[54] Also at Faculty of Physics, University of Belgrade, Belgrade, Serbia

[55] Also at Trincomalee Campus, Eastern University, Sri Lanka, Nilaveli, Sri Lanka

[56] Also at INFN Sezione di Pavia, Università di Pavia, Pavia, Italy

[57] Also at National and Kapodistrian University of Athens, Athens, Greece

[58] Also at Ecole Polytechnique Fédérale Lausanne, Lausanne, Switzerland

[59] Also at Universität Zürich, Zurich, Switzerland

[60] Also at Stefan Meyer Institute for Subatomic Physics, Vienna, Austria

[61] Also at Laboratoire d'Annecy-le-Vieux de Physique des Particules, IN2P3-CNRS, Annecy-le-Vieux, France

[62] Also at Near East University, Research Center of Experimental Health Science, Mersin, Turkey

[63] Also at Konya Technical University, Konya, Turkey

[64] Also at Izmir Bakircay University, Izmir, Turkey

[65] Also at Adiyaman University, Adiyaman, Turkey

[66] Also at Necmettin Erbakan University, Konya, Turkey

[67] Also at Bozok Universitetesi Rektörlügü, Yozgat, Turkey

[68] Also at Marmara University, Istanbul, Turkey

[69] Also at Milli Savunma University, Istanbul, Turkey

[70] Also at Kafkas University, Kars, Turkey

[71] Also at Hacettepe University, Ankara, Turkey

[72] Also at Istanbul University — Cerrahpasa, Faculty of Engineering, Istanbul, Turkey

[73] Also at Yildiz Technical University, Istanbul, Turkey

[74] Also at Vrije Universiteit Brussel, Brussel, Belgium

[75] Also at School of Physics and Astronomy, University of Southampton, Southampton, United Kingdom

[76] Also at University of Bristol, Bristol, United Kingdom

[77] Also at IPPP Durham University, Durham, United Kingdom

[78] Also at Monash University, Faculty of Science, Clayton, Australia

[79] Also at Università di Torino, Torino, Italy

[80] Also at Bethel University, St. Paul, Minnesota, USA

[81] Also at Karamanoğlu Mehmetbey University, Karaman, Turkey

[82] Also at California Institute of Technology, Pasadena, California, USA

[83] Also at United States Naval Academy, Annapolis, Maryland, USA

[84] Also at Ain Shams University, Cairo, Egypt

[85] Also at Bingol University, Bingol, Turkey

[86] Also at Georgian Technical University, Tbilisi, Georgia

[87] Also at Sinop University, Sinop, Turkey

[88] Also at Erciyes University, Kayseri, Turkey

[89] Also at Institute of Modern Physics and Key Laboratory of Nuclear Physics and Ion-beam Application (MOE) — Fudan University, Shanghai, China

[90] Also at Texas A&M University at Qatar, Doha, Qatar

[91] Also at Kyungpook National University, Daegu, Korea

[92] Also at another institute or international laboratory covered by a cooperation agreement with CERN

[93] Also at Yerevan Physics Institute, Yerevan, Armenia

[94] Now at University of Florida, Gainesville, Florida, USA

[95] Also at Imperial College, London, United Kingdom

[96] Also at Institute of Nuclear Physics of the Uzbekistan Academy of Sciences, Tashkent, Uzbekistan